THE ROLE OF CRUSTAL CONTAMINATION AT THE BUTCHER RIDGE IGNEOUS COMPLEX, ANTARCTICA

By

Mark Alan Shellhorn

Submitted in Partial Fulfillment
of the Requirements for the Degree of
Master of Science in Geology

New Mexico Institute of Mining and Technology

Socorro, New Mexico

July 1982

Abstract

The Butcher Ridge Igneous Complex (BRIC) of the Ferrar Dolerite Group exhibits a greater chemical diversity than that previously recorded in Ferrar Supergroup rocks. Compositions range from tholeiitic basalt through to rhyolite. White Apron Spur represents the most complete stratigraphic section at the BRIC, grading from massive basalt through high-K andesite, high- K dacite, and well layered high-K rhyolites and finally back into massive basalt. Vitrophyres are common in the high-K dacites and high-K rhyolites.

Major element analyses show systematic variations on oxide variation diagrams. Vitrophyric samples deviate slightly from this trend and show relative enrichment in Na_2O and depletion in K_2O compared to their crystalline counterparts. Trace element analyses consistently exhibit systematic variations on the basalt through high-K andesite compositions. Plateau like variations are commonly displayed for the high-K dacite and high-K rhyolite compositions. Rare earth eelement (REE) patterns exhibit light REE enrichment relative to the heavy REE, and display increasing Eu anomalies with increasing SiO_2 concentration.

Whole-rock $\delta^{18}O$ values range from +3.08 to +10.3 per mil and exhibit an overall crude positive variation with SiO_2 concentration. $\delta^{18}O$ values for plagioclase separates average

+0.5 to +1.5 per mil higher than corresponding whole rock values. Strontium compositions exhibit initial $^{87}Sr/^{86}Sr$ ratios from 0.71021 to 0.71569 in the basalt through high-K andesite compositions, and 0.71493 to 0.71608 in the high-K dacite through high-K rhyolite compositions.

Geochemical data suggest that two separate petrogenetic processes occurred. Samples of the basalt, high-K basaltic andesite, and high-K andesite rock types exhibit chemical variations which are consistent with a mixing model between a basalt end member and a component derived by melting of crustal material. The basalt end member is assumed to have an initial $^{87}Sr/^{86}Sr$ ratio of about 0.709 and a Sr concentration of 100 ppm. The calculated elemental composition of this end member is consistent with average tholeiites as well as other basic Ferrar Supergroup rocks. The Sr isotope composition of the contaminant was derived by the intersection of the mixing line with a trend defined local Paleozoic basement rocks on an initial $^{87}Sr/^{86}Sr$ ratio verses 1/Sr plot. The intersection indicates an initial $^{87}Sr/^{86}Sr$ ratio of 0.7153 and a Sr concentration of 322 ppm for the contaminant. The mixing relation at the BRIC is unique and supports the hypothesis of an enriched mantle source of the basalt end member. The contaminant shows a different composition than previously interpreted suggesting that the crustal material is different from that contaminating Ferrar Supergroup rocks elsewhere.

Samples of the high-K dacite and high-K rhyolite groups exhibit elemental and isotopic compositions requiring an origin by melting or partial melting of crustal material. The similarity of these compositions to local granites suggests that they were probably the source. REE data indicate that fractionation of some mineral phase may be accompanying the melting process. Vitrophyres associated with the high-K dacites and high-K rhyolites exhibit alkali variations indicative of secondary hydration, and are not consistent with elemental trends shown by the other samples. However, the vitrophyres are considered to be part of the same petrogenetic process.

Acknowledgments

I wish to express special thanks to Dr. Philip R. Kyle, without whom I could not have completed this study. His guidance and understanding are most appreciated. I would like to thank Bob Osburn, Dr. Charles Chapin, and Dr. David Norman for critically reviewing the manuscript, Dr. John R. Bowman for assisting in the oxygen isotope analyses, Dr. Bob Pankhurst for performing the Rb-Sr isotope analyses, Dr. Gunter Faure for supplying samples from the Carlyon Granodiorite, and Steve Marshak for furnishing unpublished reports on the field geology at the Butcher Ridge Igneous Complex.

I would also like to thank Nancy McLaughlin for compiling the manuscript on to the Dec-20 computer, and researchers at the Ohio State University Nuclear Research Laboratory for assistance in the neutron activation analyses.

Finally, I would like to thank the members of the VXE-6 air squadron for making the project possible.

This research was funded through National Science Foundation Grants DPP-7721590 and DPP-7920316.

TABLE OF CONTENTS

LIST OF FIGURES

Chapter Five

LIST OF TABLES

LIST OF PLATES

CHAPTER ONE. INTRODUCTION

Introduction

The Ferrar Supergroup (Kyle et al., 1981) is widespread along the Transantarctic Mountains of Antarctica and consists of tholeiitic basalt lava flows, dolerite sills and dikes, and gabbroic layered intrusions. Strontium isotope analyses of the basalt lava flows (Faure et al., 1974, 1982) and the dolerite sills and dikes (Compston et al., 1968) showed them to be characterized by initial $^{87}Sr/^{86}Sr$ ratios of 0.7095-0.7113 which are anomalously high for basaltic rocks (Faure and Powell, 1972, Faure, 1977). Compston et al. (1968), examined several possible models that could cause such high $^{87}Sr/^{86}Sr$ ratios and proposed crustal contamination to be most probable.

Following the work of Compston et al. (1968), Faure et al., (1974, 1982) tried to demonstrate quantitatively that crustal contamination was responsible for variations in both the major element chemistry and the high $^{87}Sr/^{86}Sr$ ratios, in several suites of basalt flows. Thereafter, Kyle (1980) following suggestions by Brooks and Hart (1978), proposed that the anomalous initial $^{87}Sr/^{86}Sr$ isotopic ratios were the result of a heterogeneous mantle source. Thus a major controversy arose concerning the petrogenesis of the basalt rocks in the Ferrar Supergroup, were they the result of crustal contamination or were they derived from an enriched mantle source.

During the 1978/79 Austral summer field season the Butcher Ridge Igneous Complex (BRIC) was briefly visited by Kyle et al., (1979). Existing geologic maps (Grindley and Laird, 1969) indicated the area consisted of Ferrar Dolerite, even though it had not been previously visited. Instead Butcher Ridge was found to consist of strongly deformed and layered igneous rocks many of which were glassy. Chemical analyses (Kyle et al., 1981) of the rocks ranged from basalt to rhyolite. $^{40}Ar/^{39}Ar$ incremental age spectra (Kyle et al., 1981) showed that the body was 175 Ma. old and fell within the 179±7 Ma. age range of the Ferrar Supergroup, thus indicating a Jurassic age of emplacement. This was the first known occcurence of salic rocks within the Ferrar Supergroup although such evolved rocks occur within the Karoo rocks of similar age in Southern Africa.

Purpose of Investigation

The field relations of the BRIC rocks proved to be extremely complex and at this time there is no clear understanding of the mode of emplacent of many of the mapped units. In order to obtain a new perspective on the rocks it was decided to examine their geochemistry and evaluate their petrogenesis. Although this approach is contrary to the usual sequence of investigation, it was justified on the grounds that, once the petrogenetic relatonships were established they would provide a new perspective in which to view the field relationships.

This study is primarily geochemical with emphasis on the oxygen isotope geochemistry. The principle aims were to: 1)chemically and isotopically characterize the nature of the rocks; 2) propose working models for their petrogenesis and evaluate in detail the role of crustal contamination in their genesis; and 3) determine the extent and nature of deuteric alteration and possible effects of ground water. Sampling for isotopic and geochemical analyses was concentrated at White Apron Spur, which was the most complete secton exposed, and was believed to be representative of the geology of the BRIC.

The BRIC seemed an ideal place to evaluate the extent of crustal contamination because; 1) the rocks showed greater chemical diversity than was known from elsewhere in the Ferrar Supergroup; 2) since many of the rocks at the BRIC were salic, crustal contamination would exhibit a much more visible signature in them; and 3) due to the chemical variability of the BRIC rocks, they allowed a contrast with the chemically monotonous basalt lava flows that had been previously analyzed (Faure et al., 1974, 1982). Thus, the BRIC is believed to be unique, in that it may represents a working model for the petrogenesis of the Ferrar Supergroup.

Discussion of the mode of emplacement and other field relations will be presented elsewhere (Kyle and others, in preparation).

Field Work

During the 1980/81 Austral summer field season the BRIC was visited with the intent of gaining a clear understanding of the mode of emplacement and the accompaning field relations. In the course of the investigations, the BRIC was mapped at a scale of 1:5000 on a 20-meter contour interval topographic base map. Four sections were measured and over 400 samples were systematically collected. Sections that were measured and sampled for analyses were those showing greatest exposure and reasonable accessibility.

Access to the BRIC was by LC-130 ski-equipped aircraft of the U.S. Navy VXE-6 Squadron. Field work was conducted on foot and using snowmobiles out of two remote tent camps over a period of about $3^{1}/2$ weeks.

CHAPTER TWO. FIELD GEOLOGY

Introduction

The BRIC ($79^{o}12'S$ and $155^{o}50'E$) is located in the Transantarctic Mountains approximately 280 kilometers southwest of McMurdo Station (Fig. 1). Bounded on the west by the Polar Plateau, Butcher Ridge is situated at the head of the north arm of the Darwin Glacier which discharges ice from the Polar Plateau into the Ross Ice shelf. Published geologic maps (Grindley and Laird, 1969) indicate that this area is composed of rocks belonging to the Ferrar Dolerite Group which falls within the Ferrar Supergroup (Fig. 2).

The BRIC displays the best exposures toward the east with maximum relief averaging about 600 meters. The lower areas are generally covered by ice-cored moraine, while the higher regions consist of ice-sculptured cliffs which pass downward into steep scree slopes encompassing the maximum relief. The average elevation at the BRIC is about 1800 meters and the highest peak is Butcher Boys Peak at 2125 meters.

Regional Geology

Basement Complex

The Butcher Ridge Igneous Complex lies within the geographic area designated as South Victoria Land. The oldest rocks within the area between the Byrd and Mulock Glaciers (Fig. 2), are a granitic batholith complex

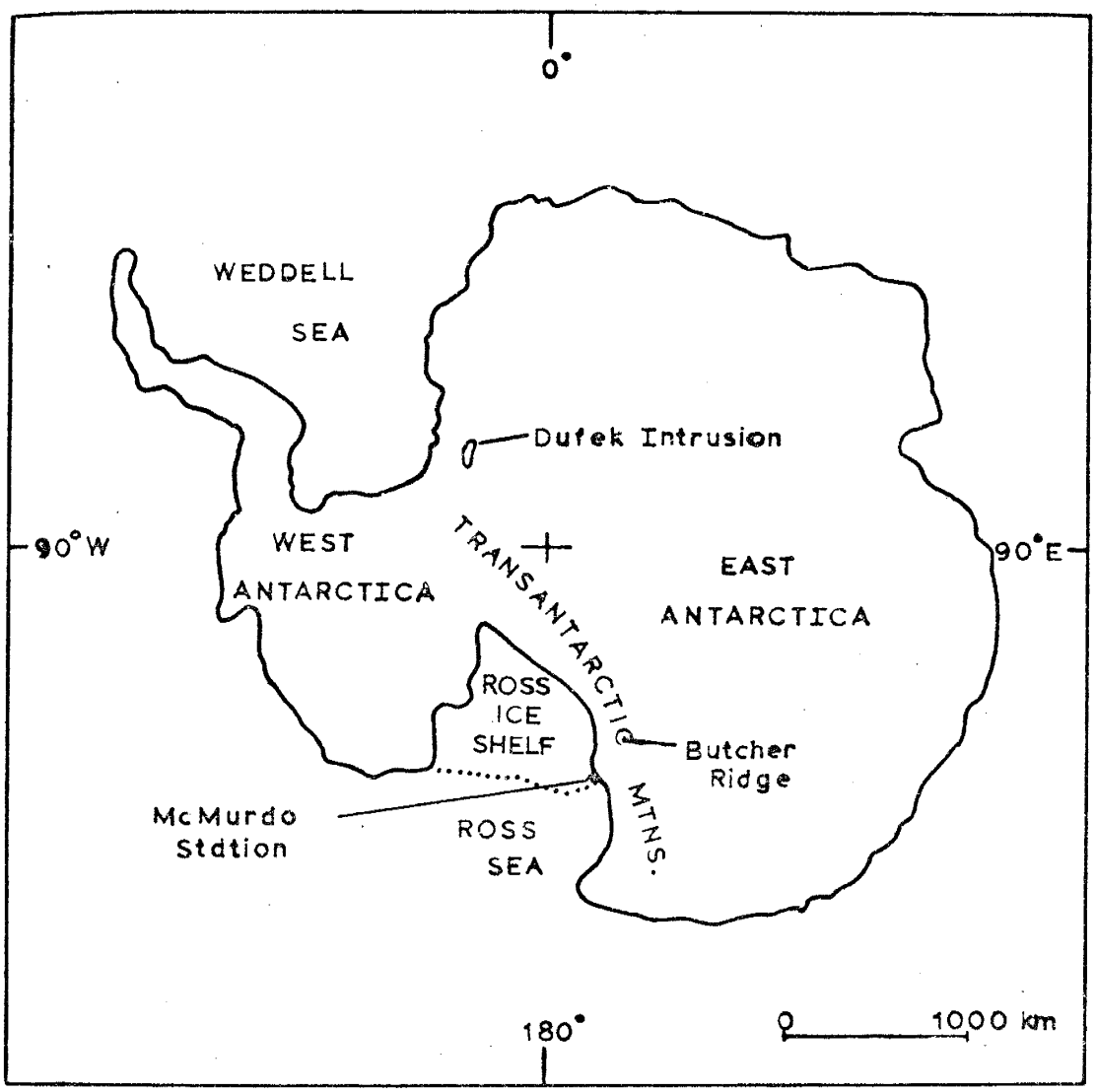

Figure 1: General location map of Antarctica.

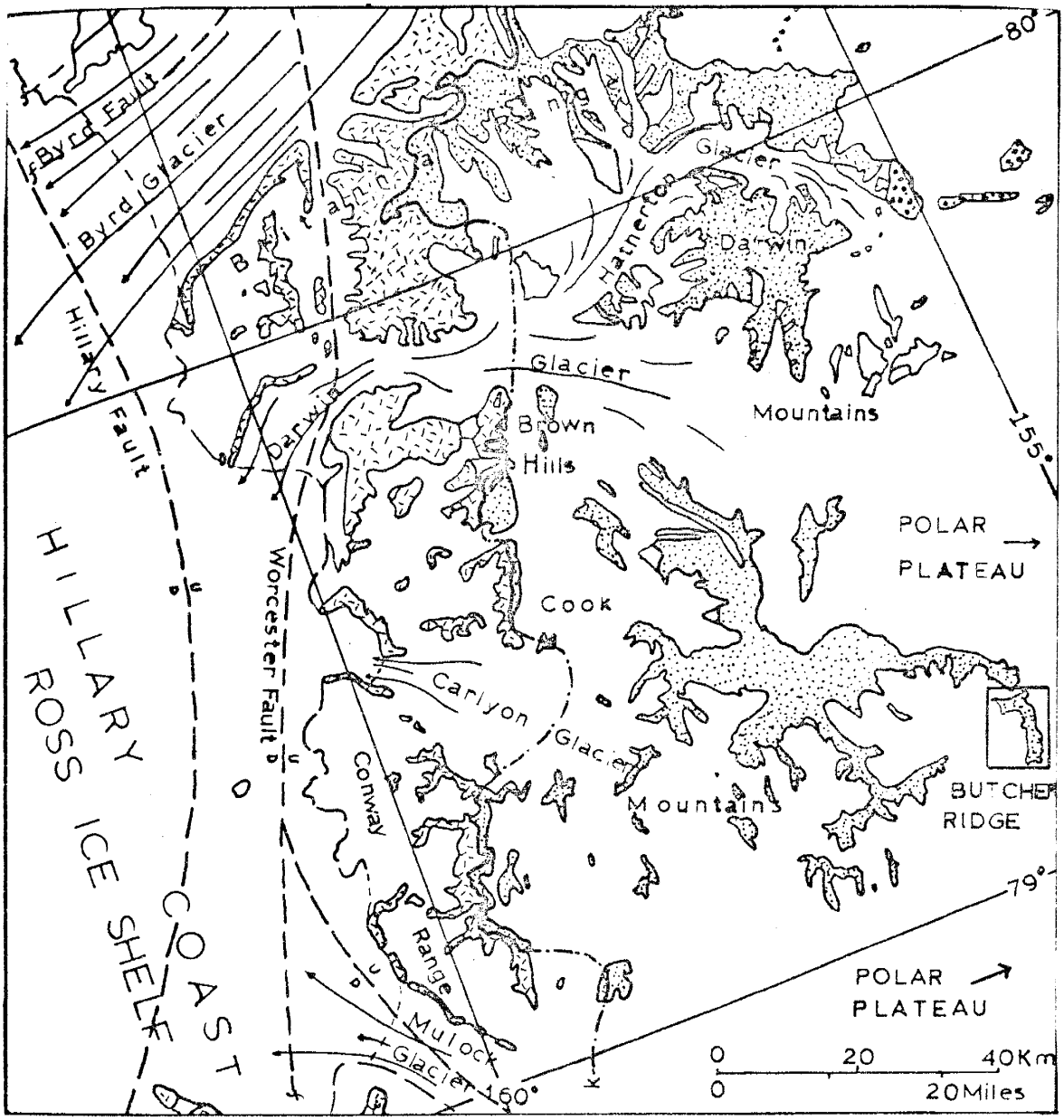

Figure 2: Regional geology map for areas surrounding the BRIC, between the Byrd and Mulock Glaciers (Grindley and Laird, 1969).

consisting of lower Paleozoic (Grindley and Laird, 1969) granites, metasediments and dikes. Several periods of intense folding are recorded in the metasediments, while the entire complex is capped by a nearly level erosion surface known as the Kukri Peneplain. All the granitic basement rocks in this area are a part of the Granite Harbour Intrusive Complex: a name given to all plutonic and hypabyssal intrusives that invade sediments of the Ross System of Harrington (Harrington, 1958), and are older than the Kukri Peneplain (Gunn and Warren, 1962).

These basement rocks have been subdivided (Haskell et al., 1965) into an earlier, coarse-grained granitic to granodioritic suite, a later, finer-grained granitic suite, and basic to intermediate dike rocks and pegmatites. In the Darwin Glacier area the coarse-grained suite has been subdivided into the Carlyon Granodiorite and the Mt. Rich Granite, the fine-grained suite is called the Hope Granite.

Carlyon Granodiorite

The Carlyon Granodiorite is the most widespread in the area of the Brown Hills (Fig. 2) and extends from Bastion Hill to the Ross Ice Shelf (Felder, 1980). This pretectonic unit is medium-to coarse-grained, porphyritic, strongly to moderately foliated, sometimes gneissic, and ranges in composition from granodiorite to granite (Haskell et al., 1965). The modal composition typically contains as much as

35% quartz, 30% andesine, 15-20% orthoclase, 5-10% biotite, and 5-10% hornblende (Haskell et al., 1965).

Strontium isotope ($^{87}Sr/^{86}Sr$) analyses (Felder, 1980) based on seven samples from the Brown Hills area (Fig. 2), yielded a whole rock isochron age of 568±54Ma. with an initial $^{87}Sr/^{86}Sr$ ratio of 0.7121±0.0011. $^{40}Ar/^{39}Ar$ weight average plateau ages obtained on biotite and hornblende yielded a range of ages from 500 Ma. to 540 Ma. (Felder, 1980). The scatter in dates obtained from the mineral separates is believed to mark the time of closure following the metamorphism associated with the Ross Orogeny. The Carlyon Granodiorite is considered to be the earliest intrusive rocks in the area. It probably formed by anatexis of downwarped sediments.

Mt. Rich Granite

The Mt. Rich Granite is far less abundant than the Carlyon Granodiorite. It occurs in a parallel belt lying to the north of, and grading into, the Carlyon Granodiorite (Haskell et al., 1965). This pretectonic to syntectonic unit (Haskell et al., 1965), is medium-to coarse-grained, non-foliated to weakly foliated, and sometime porphyritic, ranging in compositon from granodiorite to granite (Felder, 1980). The average modal composition is 30% quartz, 20% orthoclase, 20-30% plagioclase, up to 15% microcline, up to 5% hornblende, 5-7% biotite, and 2-3% sphene (Felder, 1980).

Strontium isotope ($^{87}Sr/^{86}Sr$) analyses (Felder, 1980) based on six samples yielded a whole rock isochron age of 593+238 Ma., but showed a large uncertainty (+40%) and is not considered reliable. $^{40}Ar/^{39}Ar$ weight average plateau ages obtained on biotite and hornblende separates yielded a similar age range (500-540 Ma.) to that of the Carlyon Granodiorite. Thus the Mt. Rich Granite experienced a similar cooling history, their ages were considered to represent a lower limit (Felder, 1980). Due to the regional nature of the forces associated with the Ross Orogeny, the non-foliated character of the Mt. Rich Granite requires that it be somewhat younger in age. Felder (1980) suggest an age slightly younger than the mineral date of 527 Ma.

Hope Granite

The Hope Granite has a restricted distribution in the Darwin Mountains. It occurs in a body six km wide that encompasses the Blanks Peninsula and the Bowling Green Plateau. This post-tectonic unit is a medium-grained, equigranular microcline granite (Haskell et al., 1965). Modal analyses (Haskell et al., 1965) shows as much as 25% quartz, 50% microcline, 10% orthoclase, 10% oligoclase, 5% biotite, and 5% garnet.

Strontium isotope ($^{87}Sr/^{86}Sr$) analyses based on six samples of leucocratic granites (Felder, 1980) yielded a whole rock isochron age of 484±6 Ma. with an initial $^{87}Sr/^{86}Sr$) ratio of 0.7119±0.0006. It was noted by Felder

that the samples analysed were not in agreement texturally or compositionally with descriptions given by Haskell et al., (1965). $^{40}Ar/^{39}Ar$ weight average plateau ages on one biotite separate gave a date of 543±6 Ma., but was considered unreliable due to a large degree of alteration in the sample (Felder, 1980). Therefore, the date of 484±6 Ma. is considered the best age for the Hope Granite, and is compatible with its occurrence as cross-cutting dikes in the Carlyon Granodiorite.

Metasedimentary Rocks

In the Darwin Mountains area, metasedimentary rocks consist of quartz-biotite-hornblende schists and metaquartzites (Haskell et al., 1965). Metasedimentary rocks occur in small bodies completely surrounded by and passing gradationally into coarse-grained granitic rocks (Felder,1980).

Dikes

Dikes intrude both the granitic rocks and the metasedimentary rocks in the Darwin Mountains and are of three general types. Fine-grained garnetiferous leucrocratic granitic rocks often intrude coarse-grained granites. Dikes of lamprophyre (augite-biotite kerstetites) and hornblende meladiorites intrude all of the basement rocks (Haskell et al., 1965). Finally, coarse-grained

quartzo-feldspathic pegmatites cut all the granitic rocks and dikes (Haskell et al., 1965).

Beacon Supergroup

Sedimentary rocks of the Devonian-Triassic Beacon Supergroup (Grindley and Laird, 1969) rest unconformably on the Kukri Peneplain cut on the basement complex (Warren, 1962). Sedimentary rocks occur throughout most of the region and locally reach as much as 330 meters thick (Askin et al., 1971). The complete stratigraphic section exceeds 1000 meters and consists predominantly of quartzose sandstones with thin beds of tillite, shales, and coals.

Ferrar Supergroup

Rocks intruding the basement complex and the overlying Beacon Supergroup sedimentary rocks belong to the Ferrar Supergroup. Comprised of basalt lava flows (Kirkpatrick Basalt Group), dolerite (diabase) sills and dikes (Ferrar Dolerite Group), and intrusive rocks of the Dufek intrusion (Forrestal Gabbro Group), the Ferrar Supergroup extends from North Victoria Land to the Pensacolo Mountains, spanning some 3000km of the Transantarctic Mountains (Fig 3). Covering an area of $1.0 \times 10^5 km^2$, conservative estimates indicate the Ferrar Supergroup occupies a volume of $5.0 \times 10^5 km^3$ (Kyle et al., 1981).

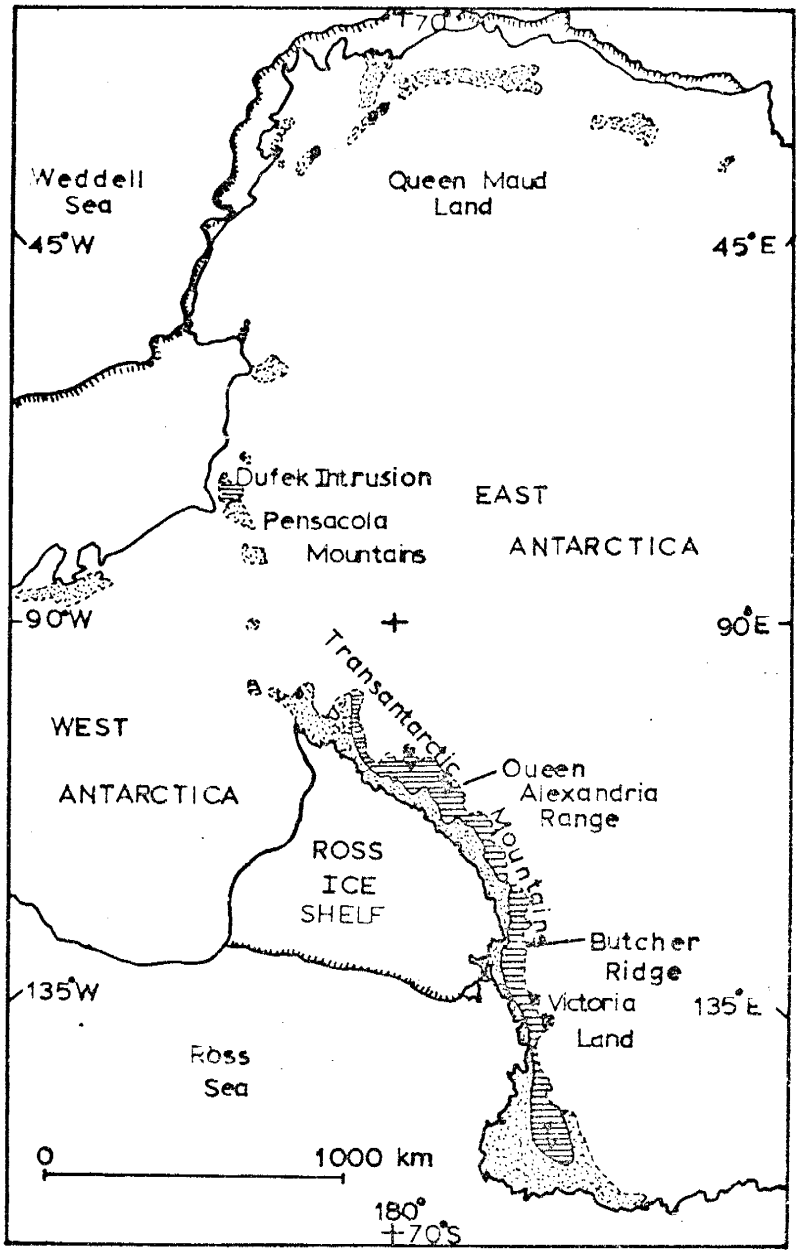

Figure 3: Geologic map of Antarctica showing distribution of the Ferrar Supergroup and associated bedrock (Kyle et al., 1981).

Kirkpatrick Basalt Group

Jurassic tholeiitic basalt lava flows of the Kirkpatrick Basalt Group occur throughout the Central Transantarctic Mountains, South Victoria Land, and North Victoria Land. These flood basalts are scattered remnants of a once much more extensive volcanic plateau whose preserved thickness reaches a maximum of 1400 meters in North Victoria Land (Elliot, 1974). Petrographically, the basalts are typical tholeiites exhibiting little variation in mineral composition, with labradorite, augite, and pigeonite as the principal minerals, accompanied by iron oxides and varying amounts of glass or quartzo feldspathic mesostasis (Elliot, 1972).

Major oxide analyses (Faure et al., 1974) indicate several differences compared to typical continental and oceanic tholeiites. Analyses on representative samples collected at Storm Peak in the Queen Alexandra Range (Fig. 3) show higher concentrations of SiO_2 (56,6%), K_2O (1.29%), total iron as FeO (11.57%), and H_2O + (1.62%) and lower concentrations of Al_2O_3(12.92%), MgO(3.44%) and CaO(7.91%). The TiO_2 content (1.28%) is compatible to that of continental tholeiites. Initial strontium isotope $^{87}Sr/^{86}Sr$ analyses (Faure et al., 1974) range from 0.7094 to 0.7133, with an average of 0.7112+0.0013, and a Rb/Sr ratio of 0.47, all of which are high for rocks of basaltic compositon.

Ferrar Dolerite Group

The Ferrar Dolerite Group, consisting of Jurassic dolerite (diabase) sills and dikes, are the most widespread Ferrar Supergroup rocks. These rocks occur from North Victoria Land to the Pensacola Mountains (Fig. 3). Sills are the most common mode of emplacement and reach up to 1000 meters in thickness (Gunn and Warren, 1962), and average 150-200 meters in thickness (Elliot, 1974). Ferrar Dolerites sills are extensive throughout the region between the Byrd and Mulock Glaciers (Fig. 2). Within the area of the Darwin Mountains, the Ferrar Dolerite occurs as two main sills, one intruding the basement and one at or near the basement-Beacon contact.

A study of variations in phases, mode, and element concentrations (Gunn, 1966) through representative sills show them to belong to at least three separate types; namely, olivine tholeiite, pigeonite tholeiite, and hypersthene tholeiite. Large sills often show vertical changes in the proportions of mineral constituents and differences in mineral composition suggesting differentiation from an originally homogeneous tholeiitic magma (Gunn and Warren, 1962; Gunn, 1966; Hamilton, 1965). Trace element analyses, particularly the rare earth elements, (Kyle, 1980) also support the differentiation model.

Strontium isotope ($^{87}Sr/^{86}Sr$) analyses (Kyle, 1980) obtained from sills of the Ferrar Dolerite Group and from correlative sills in Tasmania show initial strontium isotope ratios ranging from 0.7089 to 0.7153 with a mean of 0.7115±0.0012. This is similar to the ranges observed in the Kirkpatrick Basalt Group. The Rb/Sr ratios of the Ferrar Dolerite Group vary widely probably as a result of differentiation (Kyle, 1980).

Forrestal Gabbro Group

The Forrestal Gabbro Group of the Dufek intrusion consists of a differentiated stratiform mafic igneous complex of Jurassic age, (Ford, 1976) and is located in the Northern Pensacola Mountains (Fig. 3). Aeromagnetic surveys indicate that the intrusive complex occupies a minimum area of 50,000 km^2 with a conservative thickness estimate of 8-9 kilometers (Behrendt et al., 1981). The main body consists of well layered pyroxene gabbro that contains abundant cummulate magnetite in the higher levels (Ford, 1976). Texturally, the rocks are cumulates made up of variable amounts of settled plagioclase, Ca-rich pyroxene, and Ca-poor pyroxene (Ford, 1976). Structurally, the rocks form a layered sequence which is similar to a sequence of sedimentary strata and is capped by a 300 meter thick layer of granophyre (Ford, 1976).

The intrusive complex is subdivided into four formations, in ascending order they are Walker Anorthosite, Aughenbaugh Gabbro, Saratoga Gabbro, and Lexington Granophyre (Ford, 1976). Only a 3.5 km thickness of the Forrestal Gabbro Group is exposed, and is split into two units. The Walker and Aughenbaugh form a 1.8Km-thick section in the Dufek Massif, and the Saratoga and Lexington form a 1.7km-thick section in the Forrestal Range.

Strontium isotope ($^{87}Sr/^{86}Sr$) analyses revealed that samples of the layered mafic rocks are uniform in isotope composition with an initial $^{87}Sr/^{86}Sr$ ratio of about 0.709. Within the granophyric section, initial $^{87}Sr/^{86}Sr$ ratios systematically increase with height and have a maximum value of 0.714 near the roof (C. Hedge personal commun. in Kyle et al., 1981).

Radiometric Ages and Tectonics

Incremental $^{40}Ar/^{39}Ar$ age determinations and conventional K/Ar dates on rocks from the Kirkpatrick Basalt Group, Ferrar Dolerite Group, and the Forrestal Gabbro Group (Kyle et al., 1981) give a best age estimate of 179±7 Ma. Initial $^{87}Sr/^{86}Sr$ ratios are all high and show complete overlap between all three groups (Kyle et al., 1981). These results indicate that all three groups are coeval and were erupted over a short period of time. From their coeval nature, and the fact that the eruptive data falls within the time span of the Karoo magmatism in Southern Africa, it is

apparent that the rocks of the Ferrar Supergroup are associated with the initial fragmentation of Gondwana.

Voluminous tholeiitic rocks like those composing the Ferrar Supergroup are usually associated with extensional tectonics. In sharp contrast to this is the location of the Ferrar Supergroup rocks over the Ross and Bearmore Orogenic belts which predate the Gondwanian fragmentation (Elliot, 1974). Therefore, the best analogy to the tectonic setting of the Ferrar Supergroup is a situation somewhat similar to that of back arc spreading (Fig. 4) within a continental plate (Elliot, 1974).

Such a tectonic environment presents numerous available mechanisms by which to generate the unusual geochemistry exhibited by Ferrar Supergroup rocks. Based on the elevated values of initial $^{87}Sr/^{86}Sr$ ratios, their similar average age value over 3,000km, and their large volume, Kyle (1980) proposed mantle origins for the Ferrar rocks in spite of their high Sr ratios. Likewise, positive correlations between initial $^{87}Sr/^{86}Sr$ ratios, strontium concentrations, and major oxide components have been used to reinforce a mixing hypothesis of mantle derived basalt and granitic crustal rock (Faure et al., 1974).

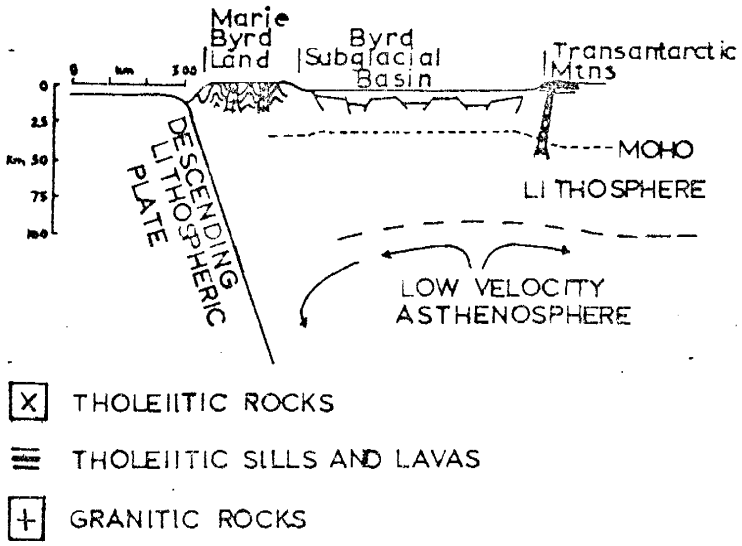

Figure 4: General tectonic setting of West Antarctica and the Transantarctic Mountains (Elliot, 1974).

Butcher Ridge Igneous Complex

Introduction

The BRIC is composed of Jurassic igneous rocks considered to be 179±7Ma. old (Kyle et al., 1981). They are believed to all be high level (hypabyssal) intrusives and are therefore assigned to the Ferrar Dolerite Group. At this time no formal stratigraphic names have been applied to any of the BRIC units, thus it was necessary to describe the units based on gross field characteristics. In the following discussion, the field terminolgy is retained even though it differs somewhat from the chemical classification.

Lithologies and Map Units

Five principal lithologies were recognized at the BRIC with the most complete section exposed at White Apron Spur (Fig. 5). Within White Apron Spur, as well as throughout the BRIC, approximately 70% of the exposure is andesite, 15% is rhyolite, 5% is glass (vitrophyre), 5% dolerite, and 5% sandstone or carbonaceous shale of the Beacon Supergroup. The crystalline rocks (basalt, andesite, rhyolite, and dolerite) are weathered to a dark rusty grey color with rhyolite outcrops slightly lighter in color. The glass bodies, dolerites, and xenoliths will be discussed later.

Principal field criteria for distinguishing between rhyolite and andesite units were based on the presence or absence of pyroxene and plagioclase crystals. Rhyolites contained abundant large plagioclase phenocrysts and no pyroxene, whereas andesites contained abundant pyroxene but no plagioclase. In both units, phenocrysts averaged about 2mm in length. Both andesites and rhyolites were locally vesicular and contained abundant xenoliths.

All exposures of andesite and rhyolite exhibited layering, of which three types were classified as: 1) diffusely layered to massive, 2) well layered, and 3) well layered with distinctive vitrophyric glass layers. Each of the different types of layering were distinguished as mappable units (Marshak, 1980). Thus a total of 8 maps units were distinguished including the glass bodies, mappable xenoliths, dolerite dikes and sills, Quaternary moraine, and crystalline rocks (Marshak, 1980). Figure 5 lists the field terms used in the preliminary mapping of the BRIC.

Contact Relations and Stratigraphic Sequence

As a result of lateral gradations, the vertical sequence of units varies at different locations. In the region of greatest variability (White Apron Spur), the base of the section is diffusely layered andesite (Da_C), overlain conformably by well-layered andesite (La), which is

succeeded by rhyolite with vitrophyres (Rg). This is overlain by layered andesite which is disconformably covered by diffusely layered andesite (Da_A) (Fig. 5). This sequence of units is not continous throughout the entire BRIC, but does exhibit lateral continuity over several hundered meters.

Contacts between the units were located only approximately in many cases; however both conformable and disconformable contacts were mapped. Conformable contacts occur between the layered andesite unit (La) and diffusely layered andesite units (Da_B or Da_C). Most of the other contacts between units at White Apron Spur as well as the entire BRIC are disconformable in the sense that the layering on the opposite sides of the contact is not parallel. These abrupt boundaries are not associated with breccia or gouge zones, and the lack of weathered surfaces between layers is evident throughout.

Layering

Layering at the BRIC is the most pervasive feature. Individual layers are continuous for a minimum of 0.5 km and a maximum of 2 km, with more than 100 distinct layers visible on some cliff faces. The nature of the layering, like the composition of individual units, is variable depending on locality.

Layering in the diffusely layered andesite at White Apron Spur and throughout the BRIC units is perceivable only by subtle color contrasts. Layering boundaries are diffuse and contrasting differences between layers could not be recognized in hand specimen. However, distinct color and textural differences exist between layers within the well layered andesites. The lighter layers are composed of fine-grained andesites containing disseminated 1 cm diameter glass blebs; the darker layers contain a higher proportion of the glass blebs which appear to exhibit an immiscible relationship with the matrix. Contacts between these layers are gradational with both types averaging 2-3 meters in thickness. Crystalline andesite layers within the layered andesite with glass (Lag) unit contain an even higher proportion of glass blebs than those described above. The layers are 1-3 meters thick and alternate with 0.2-0.3-meter-thick black glass. The glass layers have sharp contacts and are discontinuous along strike.

Layering within the rhyolite unit (Rg) was the most pronounced of all the units observed throughout the BRIC. Three lithologies; crystalline rhyolite, hydrated vitrophyre, and vitrophyre were present. The rhyolite layers are commonly 1-3 meters thick and are separated from one another by layers of vitrophyre surrounded by hydrated vitrophyre, both averaging 0.3 meters thick. The vitrophyre layers and their associated hydrated selvages are not

continuous though and will either pinch out allowing adjacent rhyolite layers to come in contact, or thicken (often up dip) and join together to form larger glass bodies. Rhyolite layers contain irregular color banding in which discontinuous lighter bands with dimensions of 0.5 cm x 5 cm and separated by 1-3 cm stand out in contrast to the darker background. The hydrated glass surrounding vitrophyre are common only to this unit and are cream to rusty tan colored, grainy textured, and contain abundant amygdules. Approximately 17 units of rhyolite, vitrophyre, and hydrated vitrophyre layers were mapped at the White Apron Spur section.

Contacts between layers of well layered rhyolite (Rg) are very irregular and complex. Rhyolite layers grade into hydrated vitrophyre layers, while hydrated vitrophyre layers grade into vitrophyre. In both cases the gradational zone exhibits blobs or streaks of one lithology floating in the other. Both gradiational zones average 1-3 cm in width.

Glass Bodies, Xenoliths, and Dolerites

Besides vitrophyric glass layers within the Rg and Lg units, several irregularly shaped glass bodies of 20 meter diameter or greater occur. All of these bodies are found in various levels of the Rg and Lag units and usually occur in cores of non-symmetric folds. Their general shape is like that of a funnel with a sharp upper limit.

Xenoliths on a variety of scales are very common at White Apron Spur and throughout the BRIC, and consist of sandstone or carbonaceous shale of the Beacon Supergroup. The largest of these occurs east of the area designated The Counter (Fig. 5), and exhibits dimensions of 100 meters high by 200 meters wide. Tabular blocks on the scale of tens of meters occur frequently throughout the diffusely layered andesites. These blocks are usually flat-lying with bedding truncated by the surrounding andesite. The andesite surrounding these blocks is chilled and somewhat finer grained adjacent to the xenoliths. Small scale xenoliths are locally abundant in all the units and range in size from a few centimeters to 3 meters in diameter. Bedding within these xenoliths is usually not parallel to that of the surrounding rocks. Within the White Apron Rg section, a large xenolith of carbonaceous shale, approximately 3 meters across, cross-cuts two complete units of associated rhyolite, hydrated vitrophyre, and vitrophyre layers.

Dolerites are absent from the White Apron Spur section, but they occur elsewhere in relatively sharply bounded dikes and sills which have chilled margins. The dolerite is generally darker than the andesite and coarser grained. The largest exposure is located in the area known as Neil's Face and occurs as a sill approximately 100 meters thick in outcrop (Fig. 5).

structure

Folding affects almost all the units at Butcher Ridge but clearly predates the intrusion of dolerite sills and dikes. Grooved slickensides on the layering within folds were not observed suggesting that folding was not the result of flexural slip. Likewise, the lack of breccia or gouge surfaces along these contacts also indicates ductile rheology during folding. Post emplacment faults were not observed in any of the exposures.

The major structure in the BRIC is a large north-south trending, non-symmetrical anticline located in the area of Starting Point Knob and White Apron Spur (Fig. 5). The hinge area is centered in the unit Rg which locally is chaotically folded with glass bodies occurring in the cores of the folds. Chaotic layering within the core of the anticline is truncated by the overlying contact with diffusely layered andesite (Da_A), the layering in the Da_A does not appear to be involved in the folding. Limbs of this anticline locally attain dips up to 70^{o}.

On a smaller scale, the Rg and Lag units are commonly involved in complex folding. The best examples are on Mutton Spur (north of White Apron Spur), where the layering is arched into 3 anticlines with an amplitude and wavelength averaging several tens of meters. These folds are

non-symmetric, non-cylindrical, have variable plunges, and are often cored by black glass bodies.

Finally, jointing is present in almost all the units observed. Crystalline rhyolite and andesite layers display well developed columnar jointing within each layer. Jointing is always normal to layer boundaries, even in tightly folded units. At some localities the Da_A unit exhibits closely spaced planar joint networks that form complex swirling patterns.

CHAPTER THREE. PETROGRAPHY

Nomenclature

The samples collected from White Apron Spur are similar to the rocks seen throughout the BRIC in that they are fine-grained and glassy. Due to the textural nature of the samples a petrographic classification was not feasible. However, a chemical classificaton based on SiO_2 and K_2O abundances proposed by Peccerillo and Taylor (1976) and modified by Ewart (1979), proved suitable.

Comparison of SiO_2 contents (normalized loss-free) to field data (Fig. 6) indicated that natural chemical divisions existed. The five groups resulting from these divisions are as follows; basalt, high-K basaltic andesite, high-K andesite, high-K dacite and high-K rhyolite. Applying the SiO_2 boundaries from Figure 6 to the K_2O-SiO_2 classificaton scheme described above enabled the rhyolite and dacite groups to be subdivided (Fig. 7). Vitrophyric members of these two groups show marked depletion in K_2O. Although the vitrophyric groupings proposed by the suggested symbols do not always fall within separate categories, they do appear distinctly different, both petrographically and chemically, and thus are considered to be unique assemblages.

The data presented in Figure 7 indicates a total of 7 distinct groupings. Symbols used to describe the chemical units are listed in Table 1. Corresponding field units are

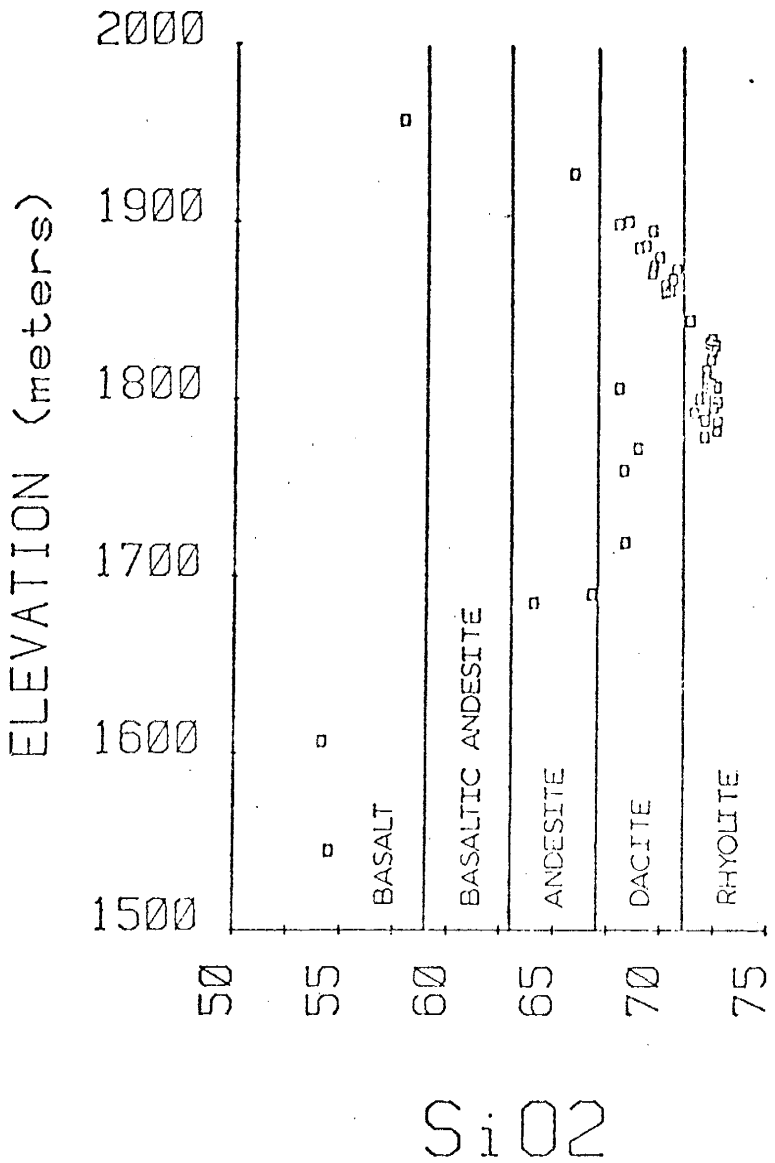

Figure 6: Plot of sample elevation (meters) verses SiO2 content (recalculated to 100% loss-free). Chemical divisions are as follows; basalt (less than 59% SiO2), basaltic andesite (59-63% SiO2), andesite (63-67% SiO2), dacite (67-71% SiO2), and rhyolite (greater than 71% SiO2). SiO2 boundaries are modified after Ewart (1976).

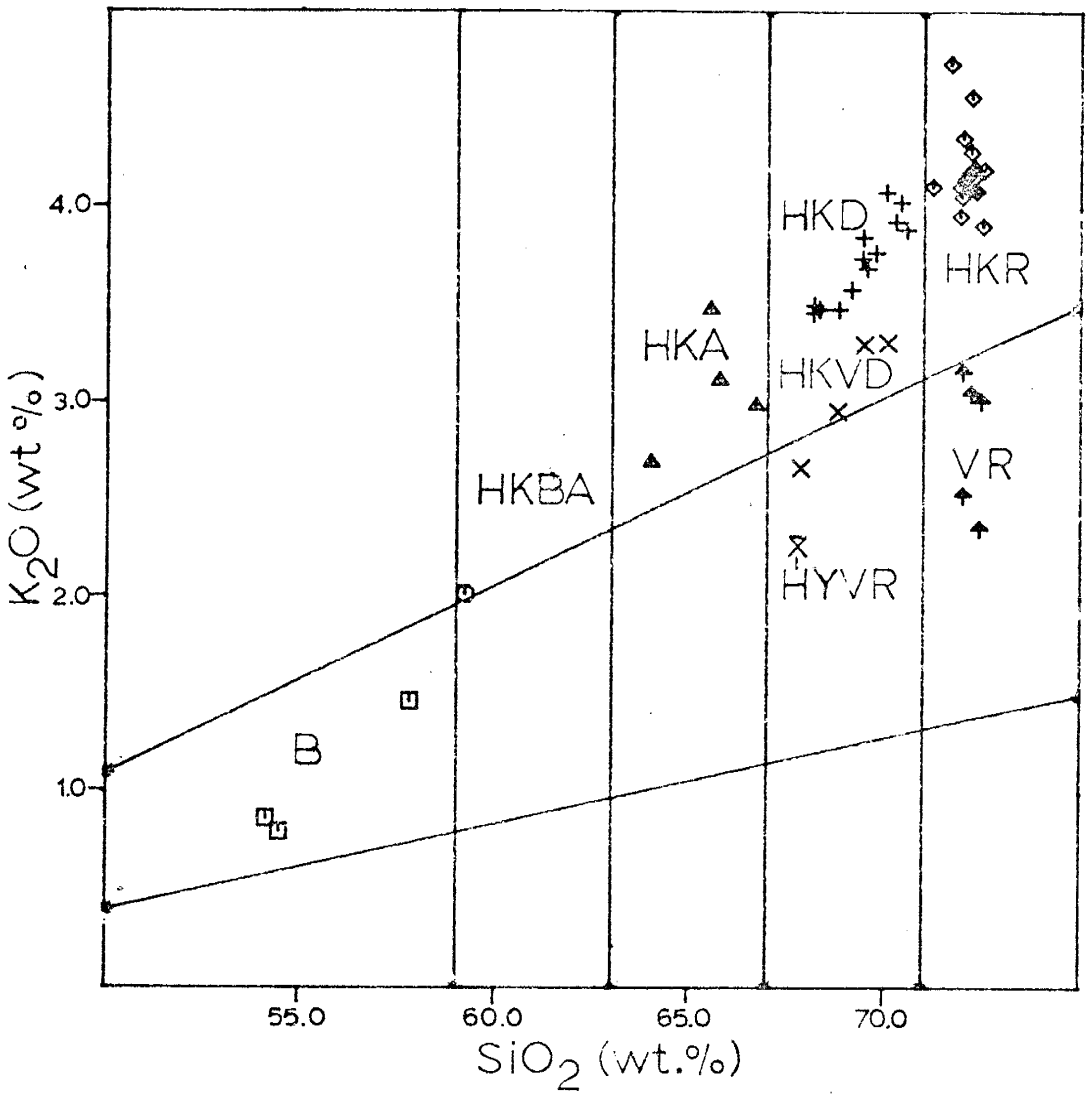

Figure 7: Modified andesite, dacite, and rhyolite classification scheme (Ewart, 1976). All analyses are recalculated to 100% loss-free. See Table 1 for an explanation of the symbols and abbreviations.

Table 1: Explanation of symbols used to describe chemical units and corresponding field units.

CHEMICAL UNITS	FIELD UNITS
- BASALT (B)	DaA + DaC
- HIGH-K BASALTIC ANDESITE (HKBA)	La
- HIGH-K ANDESITE (HKA)	La + DaA
- HIGH-K DACITE (HKD)	La + Lag + Rg + DaA
- HIGH-K VITROPHYRIC DACITE (HKVD)	Rg + DaA
- HIGH-K RHYOLITE (HKR)	Rg
- VITROPHYRIC RHYOLITE (VR)	Rg
- HYDRATED VITROPHYRIC RHYOLITE (HYVR)	Rg

Table 2: Summmary of petrographic character of representative thin sections from the White Apron Spur section of the BRIC.

	Mineralogy				
Rock Type	Cpx	Opx	Fsp	Op	Matrix
Basalt	mp(25)	mp(10)	mp(60)	g	c,sp
Andesite	mp(15),a	mp(8),a	mp(50),x	g	gl(25)
Dacite		mp(20),a	mp(35),x	g,c	gl(35)
Vit. Dacite	mp(2),a	mp(2),a	mp(35),x	g,c	gl(55)
Rhyolite I		mp(10),a	mp(55),x	g,c	gl(30)
II		mp(15),a	mp(70),c,x	g,c	gl(2)
Vit. Rhyolite	mp(1)	mp(5),a	mp(45),x	g,c	gl(45)

Abbreviations:
Minerals: Cpx-clinopyroxene, Opx-orthopyroxene, Fsp-feldspar.
Texture: mp(2)-microphenocrysts, % microphenocrysts estimated.
Mineralogy: a-altered, g-groundmass only, x-xenocrystic
Matrix: c-cryptocrystalline, gl-glassy

also presented to illustrate the broad range of composition which each field unit encompasses. Due to the greater precision with which the chemical units separate the data, the following summaries of each group, as well as individual sample descriptions, are presented on the basis of such a classification. Descriptions of each of the chemical units are given below, and summarized in Table 2. Individual sample descriptions are presented in Appendix 1. Mineral abundances were visually estimated from thin section.

Petrography

Basalt (B)

Two samples from White Apron Spur and one from nearby starting Point Knob (Fig. 5) were examined. They are typically fine-to medium-grained with an overall subophitic texture. The most abundant phenocrysts are plagioclase (60%), clinopyroxene (25%), and orthopyroxene (10%), while minor glass and disseminated opaques also occur. Plagioclase comprises the majority of the phenocrysts phases, and usually occurs as twinned laths which exhibit minor secondary alteration to a material similar to sericite. Plagioclase occasionally exhibits a cryptocrystalline morphology appearing as overgrowths on primary laths and as interstitial material. Clinopyroxene is present as subpoikilitic microphenocrysts and is about one-third the abundance of plagioclase. Clinopyroxene occasionally exhibits twinning and usually shows secondary

alteration to a greater extent than plagioclase. Orthopyroxene occurs as subpoikilitic microphenocrysts and is about half as abundant as clinopyroxene, it shows greater secondary alteration than plagioclase. Glass almost always occurs as an interstitial filling and is significantly altered to a green material that shows remnant spherulitic textures. Opaques are present as microlites within the glass, although some samples show opaques of phenocryst size. Xenoliths of carbonate and alkali feldspar are present in some sections, but minor in abundance.

A representative photomicrograph of the basalt samples is presented in Plate I.

Basaltic Andesite (HKBA)

None of the samples analyzed from White Apron Spur were included in this group. The sample presented in Figure 7 was obtained from Starting Point Knob (Fig. 5), and was not prepared for thin section examination.

Andesite (HKA)

The four andesite samples are fine-to medium-grained and have an overall subintersertal texture. The most abundant minerals are plagioclase (50%), clinopyroxene (15%), and orthopyroxene (8%) while glass and disseminated opaques occur also. Plagioclase is slightly less abundant than that of the basalt samples and is present as mantled laths as well as a variety of cellular morphologies.

Secondary alteration is relatively minor and comparable to that seen in the basalt group. Clinopyroxene is less abundant in this group compared to the basalt group and shows a greater degree of secondary alteration. Orthopyroxene is much less abundant (almost a minor constituent), and like the clinopyroxene shows a greater degree of secondary alteration. Interstitial glass is in much greater abundance in the andesite group (about 4 times as much), and is usually spherulitic in texture. It often contains disseminated opaques and is usually altered to a brownish-green material. Opaques within the interstitial glass are unique in that that they occur as concentrations along glass-grain boundaries. Xenoliths of quartz and K-feldspar of variable size are quite common in the andesite samples. Xenocrysts of slightly altered resorbed plagioclase, possessing epitaxial overgrowths of a cellular nature, also occur in minor abundances.

A representative photomicrograph of the andesite samples is presented in Plate II.

Dacite (HKD)

Thirteen analyzed samples are dacites. All are fine-grained compared to the basalt group and differ in mineralogy. The most abundant minerals are plagioclase (35%) and orthopyroxene (20%) while glass (35%), opaques, and xenolithic material occur also. Plagioclase is about two-thirds as abundant as that in the andesite group and

almost always has cellular morphologies. Minor secondary alteration to a light brown material is present and is about as extensive as that seen in the andesites. Orthopyroxene occurs as microphenocrysts with approximately the same abundance as those seen in the andesites. The orthopyroxene shows extensive secondary alteration to a brownish oxide material. Glass is the most abundant constituent and occurs as an interstitial filling; it is often partly altered to a brownish-green material resembling chlorophaeite. Opaques are minor in abundance and occur only as disseminated grains in glass. Xenoliths are slightly more abundant compared to the andesite and basalt groups. They consist chiefly of highly altered orthopyroxene and plagioclase, and are bimodal in grain size. Like the andesite group, xenocrysts of slightly to highly altered plagioclase possessing epitaxial cellular overgrowths are present, but slightly more abundant than in the andesites.

A representative photomicrograph of the dacite samples is not presented, however, the photomicrograph presented for the vitrophyric dacites in Plate III shows similar features.

Vitrophyric Dacite (HKVD)

Four vitrophyric dacites were analyzed. Vitrophyric dacite was recognized in the field by its obvious glassy texture. Chemical analyses have subsequently indicated that they are chemically distinct compared to the dacites (Fig. 7). The vitrophyric dacites are fine-grained like the

lithoidal dacite samples but differ slightly in mineralogy and texture. They are composed of glass, plagioclase, orthopyroxene, and clinopyroxene while opaques and xenoliths also occur. Glass is the most abundant component (55%). It is usually impregnated with very fine-grained opaques and cryptocrystalline material that concentrates along glass-grain boundaries. The glass is relatively fresh and unaltered compared to that within the dacite samples. Plagioclase exhibits cellular morphologies. Minor secondary alteration to a brownish-green material occurs in the vitrophyric samples. Clinopyroxene and orthopyroxene are only minor constituents and display strong secondary alteration to a greenish-brown material. Xenoliths of plagioclase and highly altered orthopyroxene are equally abundant. Xenocrysts of resorbed plagioclase with epitaxial over-growths are also present but slightly more abundant than the crystalline dacites, and show little or no secondary alteration.

A representative photomicrograph of the vitrophyric dacites is presented in plate III.

Rhyolite (HKR)

Fifteen rhyolites were analyzed. All are fine-grained, and exhibit two textural types, of equal abundance. The first type is significantly more glassy (30% compared to 5%) and contains plagioclase (55%), glass, orthopyroxene (10%), and minor amounts of opaques and xenolithic material.

plagioclase is like that seen in the dacites in that it is commonly cellular in morphology and displays relatively little secondary alteration. Glass is the second most abundant phase and is similar to the dacites in that it is impregnated with microlites of opaques and cryptocrystalline material but does not show concentrations around glass-grain boundaries. Similarly, the glass is relatively fresh and unaltered. Microphenocrysts of orthopyroxene are slightly more abundant than both the orthopyroxene and clinopyroxene of the dacite group. Likewise, extensive secondary alteration is present, but a reddish-brown material is the product in the rhyolite group. Xenoliths are different from those seen in the dacites and are composed chiefly of zeolite, calcite, quartz, and alkali feldspar. Xenocrysts of resorbed and epitaxially overgrown plagioclase are present, however, they are slightly more abundant than in the dacites.

The second type of rhyolite in this group is an equally fine-grained rock but differs texturally from the first type. The most abundant minerals are identical, but abundances and morphology are different. Plagioclase (70%) in this type of rhyolite is by far the most abundant phase being almost half again that of the first type. It differs texturally appearing spherulitic and cryptocrystalline, and composes the majority of the matrix. Orthopyroxene is identical to that of the first type of rhyolite but may be slightly more abundant in some samples. Glass in this type

of rhyolite is at most a minor phase (5%) occurring as an interstitial filling. Xenoliths and xenocrysts are identical to those described above but are about twice as abundant.

Representative photomicrographs of types one and two rhyolites are present in Plates IV and V respectively.

Vitrophyric Rhyolite (VR)

Five of the analyzed samples are vitrophyric rhyolites. Like the vitrophyric dacites, the descriptive textural term was based on field observations. Subsequent major element analyses (Fig. 7) indicate that they differ from the rhyolites. These vitrophyres are fine-grained containing glass (45%), plagioclase (45%), orthopyroxene (2%), clinopyroxene (5%), and opaques while xenoliths and xenocrysts also occur. Glass occurs as a matrix material. It shows relatively no secondary alteraton and is impregnated with microlites of opaques like that of the dacites. Plagioclase occurs as microphenocrysts exhibiting strong cellular morphologies. Orthopyroxene and clinopyroxene occur as microphenocryst that at most are minor in abundance and are relatively free of secondary alteration. Some samples contain veins of zeolites suggesting they are hydrothermally altered. Xenocrysts of resorbed plagioclase possessing epitaxical overgrowths that are usually cellular in morphology are also present and free of alteration.

A representative photomicrograph of the vitrophyric rhyolite samples is presented in plate VI.

Hydrated Rhyolite (HYVR)

One sample was analyzed and is mineralogically identical to the vitrophyric rhyolites, except for extensive alteration of all phases and the presence of an oxide stain throughout the sample.

Petrographic Evidence for Contamination

Two major forms of contamination, aside from the usual secondary alteration and hydrothermal alteration veins, are present at the BRIC. The first, and probably more common of the two, are the presence of xenoliths of varied compostion (Plate IX). Secondly, there are xenocrysts of resorbed plagioclase possessing epitaxial and often cellular overgrowths of differing compositon plagioclase (Plate VIII). Xenocrysts occur in all samples except the basalts, whereas xenoliths are present in all samples.

Xenoliths in the basalts are generally rounded and exhibit a brownish-red alteration zone about their perimeter. Common mineral assemblages of the xenoliths are carbonate, quartz, and alkali feldspar. Most of the xenoliths in this group average a couple of millimeters across and in some samples are abundant enough to be considered a minor constituent.

Within the andesite group, two additional forms of contamination occur. Xenocrysts of resorbed plagioclase possessing epitaxial overgrowths (plate VII) are common and the interior portions of these xenocrysts are dendritic plagioclase exhibiting secondary alteration to a yellowish-green material. These dendritic cores, which are resorption features, are surrounded by an initial non-cellular plagioclase followed by an outer rim of cellular plagioclase, usually consisting of acicular spikes. Similar textures (Hibbard, 1981) have been noted in rocks proposed to be derived from mixing of felsic and mafic magmas. In addition to the xenocrystic plagioclase in the andesites, mantled laths of plagioclase are present. Mantling material in these laths appears to be a combination of quartz and alkali feldspar. Usually the mantling material on these laths is not epitaxial and thus should be considered as possibly formed by syneusis (Dowty, 1980; Stull, 1979).

The dacite group and vitrophyric dacites carry both xenoliths and xenocrysts of the above described resorbed plagioclase. Clear evidence as to the resorption origin of these xenocrysts is evidenced where remnant twinning is present within the dendritic core and is still in optical continuity. Slight alteration is noticeable within the dacite group xenocrysts (Plate VII) but appears relatively absent in the vitrophyric dacites (Plate VIII). Xenoliths within this group are identical to those described in the basalt group with respect to mineralogy, but lack the

typical rim of reddish-brown alteration and rounded perimeter.

The rhyolites and vitrophyric rhyolites possess both xenoliths and xenocrysts. Xenoliths, like those seen in the dacite groups, are typically carbonate with minor amounts of quartz and alkali feldspar. Compared to the basaltic and andesitic groups though the xenoliths average a couple of millimeters larger. Likewise, xenocrysts of resorbed plagioclase with epitaxial cellular overgrowths (plate VIII) are identical to those seen in the dacite groups. Xenocrysts in the rhyolite group and vitrophyric rhyolite group exhibit less secondary alteraton and display remnant twinning confirming a resorpton origin (Stull, 1979).

Crystal Morphologies (Thermal Implicatons)

Up to the middle of the last decade most disequilibrium morphologies of plagioclase, pyroxenes, and olivines, contained in a glassy matrix, were attributed to either quenching of a melt or devitrification (crystal growth out of a glass in the solid state). More recently, experimental crystallization studies simulating cooling histories like those found in nature have brought forth a new spectrum of possible cooling histories which can generate cellular morphologies like those seen in the samples from White Apron Spur. Although the compositions of the samples from White Apron Spur do not correlate exactly with those used in

crystallization experiments, general analogies with respect to overall cooling regimes can tentatively be made. Thus, a speculative comparison of cellular morphologies from each of the rock types is presented below.

Basalt

Spherulitic plagioclase matrix (plate I) is minor in the basalts and is the only evidence of disequilibrium cooling. As a late crystallizing phase, a total quench from the remaining melt is most likely. Crystallization experiments (Lofgren, 1979, 1980) on basalts of comparable plagioclase composition indicate that supercooling over a temperature interval of 285^{o}C produced identical spherulitic textures. Subsequent crystallization runs of supercooling over a temperature interval of as much as 430^{o}C also produced similar textures. Comparisons to spherulitic overgrowths on pre-existing laths were produced by quenching crystal-rich melts from as much as 1050^{o}C. Thus, from the plagioclase morphologies present, supercooling over a temperature interval ranging from approximately 300 to 1050^{o}C is feasible.

Andesite

Disequilibrium cooling within the andesites is evidenced by cellular morphologies and zoning (Plate II) of plagioclase. Cellular morphologies range from skeletal, to dendritic, to spherulitic. Crystallization experiments

using whole rock compositions are not common, thus comparison of crystal morphologies must be made on plagioclase melts that have been supercooled to various degrees. Previous work (Lofgren, 1974, 1980; Lofgren and Gooley, 1977) indicate that dendritic morphologies of comparable plagioclase composition can be produced by supercooling over temperature intervals of approximately 150°C. Skeletal crystal have been reproduced in similar experiments by supercooling the samples over a temperature interval of 100°C (Lofgren, 1974). Relative to the basalt morphologies, the spherulitic morphologies in the andesites were reproduced by supercooling over a temperature interval ranging from 250-1050°C (Lofgren, 1974, 1980).

The range of supercooling temperatures associated with the plagioclase morphologies in the andesites is unlikely to represent one step cooling. Instead, it may be due to an initial small temperature drop followed by a subsequently larger drop that approaches a total quench. This type of temperature cooling history would allow for initial development of microphenocrysts of cellular morphologies as pseudo primary phases followed by quenched spherulitic overgrowths and matrix material.

Dacites and Vitrophyric Dacites

Samples of these groups contain identical plagioclase morphologies to those in the andesite group, except there is morphological evidence suggesting severe nucleation inhibition (Plate III). Since nucleation is a direct function of degree of supercooling (Lofgren, 1974; Swanson, 1977), greater degrees of supercooling would be required to produce such morphologies. As very little work has been performed on the more felsic rocks, direct thermal analogies to individual textures cannot be made. In comparing the dacites to the andesites though, it is apparent that the degree of overall supercooling must have been equal or greater.

Rhyolites and Vitrophyric Rhyolites

In comparison to the dacite groups the rhyolites exhibit the same morphologies indicative of an even greater degree of nucleation inhibition (Plates X). Crystallization experiments on rhyolite glasses (Lofgren, 1971) indicate supercooling over a temperature range of 500-900^{o}C was necessary to produce cellular morphologies similar to those seen in the rhyolites. These temperatures correlate well with the obvious spontaneous nucleation associated with large degrees of supercooling and thus are probably feasible cooling intervals.

Hydrated Vitrophyric Rhyolite (HYVR)

One sample was analyzed and is identical to the vitrophyric rhyolites, except for extensive alteration of all phases and the presence of an oxide stain throughout the sample.

Plate I

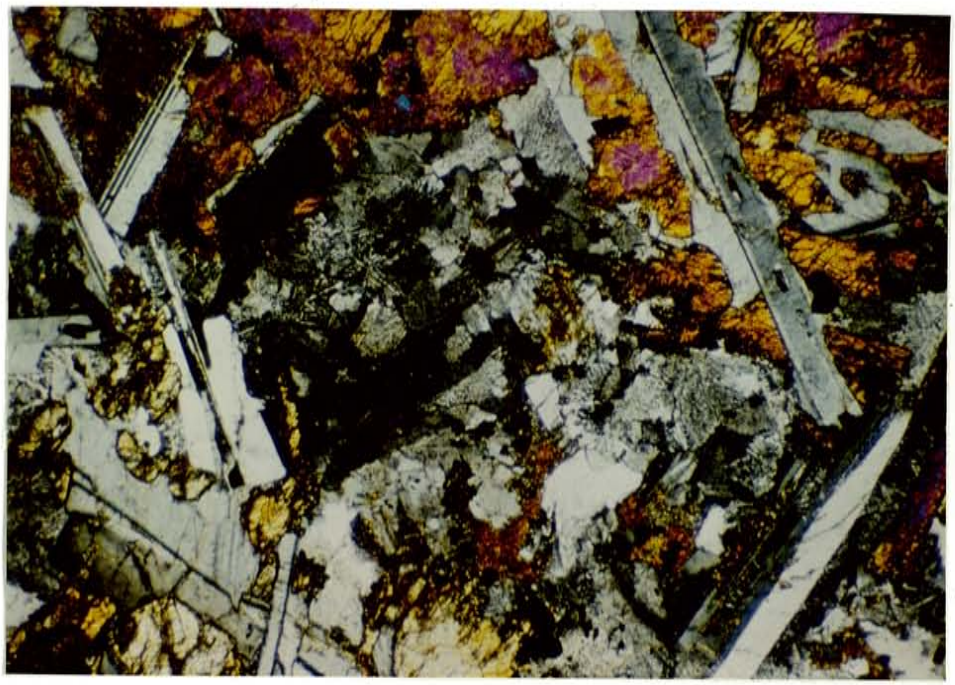

Plate II

Plate I: A fine to medium-grained basalt (80675) with subophitic texture containing phenocryst of plagioclase, and microphenocryst of clinopyroxene and orthopyroxene, with a matrix consisting of cryptocrystalline feldspar and disseminated opaques.

Plate II: A fine-grained andesite (80404) showing a subintersertal texture with microphenocrysts of cellular plagioclase, altered clinopyroxene and orthopyroxene. Matrix is composed of slightly altered glass containing disseminated opaques.

Plate III

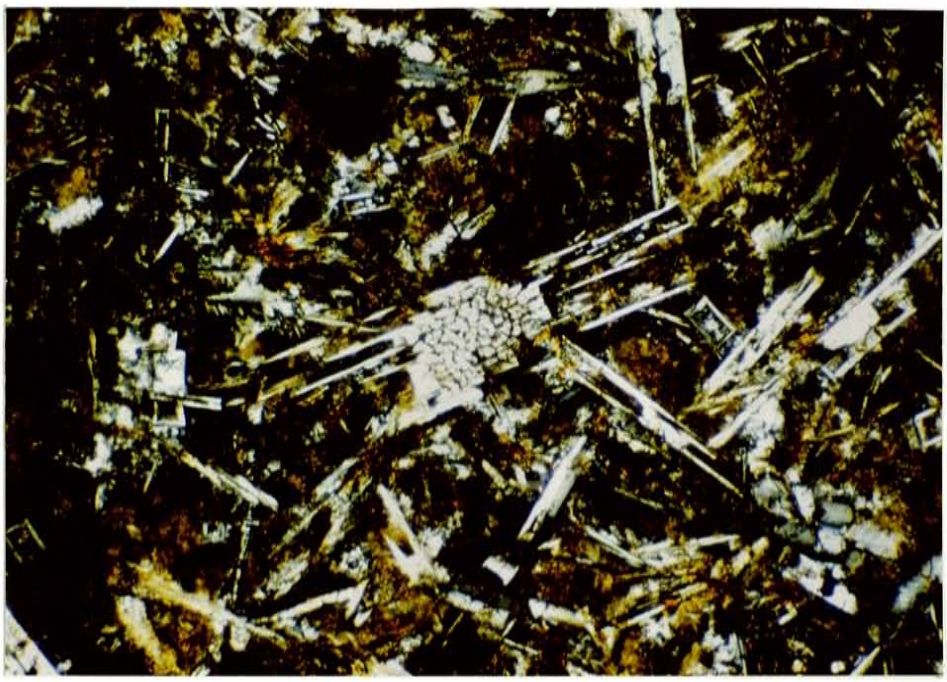

Plate IV

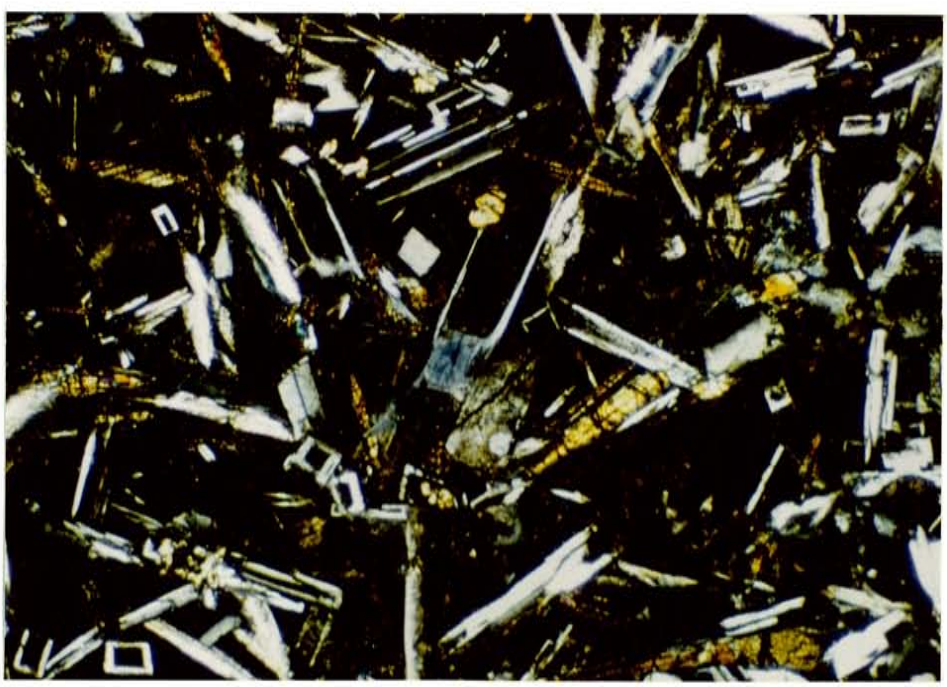

plate III: A fine-grained vitrophyric dacite (80664) containing microphenocrysts of cellular plagioclase, altered clinopyroxene and orthopyroxene. Matrix is composed of fresh glass containing disseminated opaques and cryptocrystalline material.

Plate IV: A fine-grained rhyolite (80306) microphenocrysts of cellular plagioclase and extensively altered orthopyroxene in a glassy matrix containing microlites of opaques and other cryptocrystalline material. Xenocrysts of plagioclase possessing epitaxial dendritic cores surrounded by non cellular rims are common.

Plate V

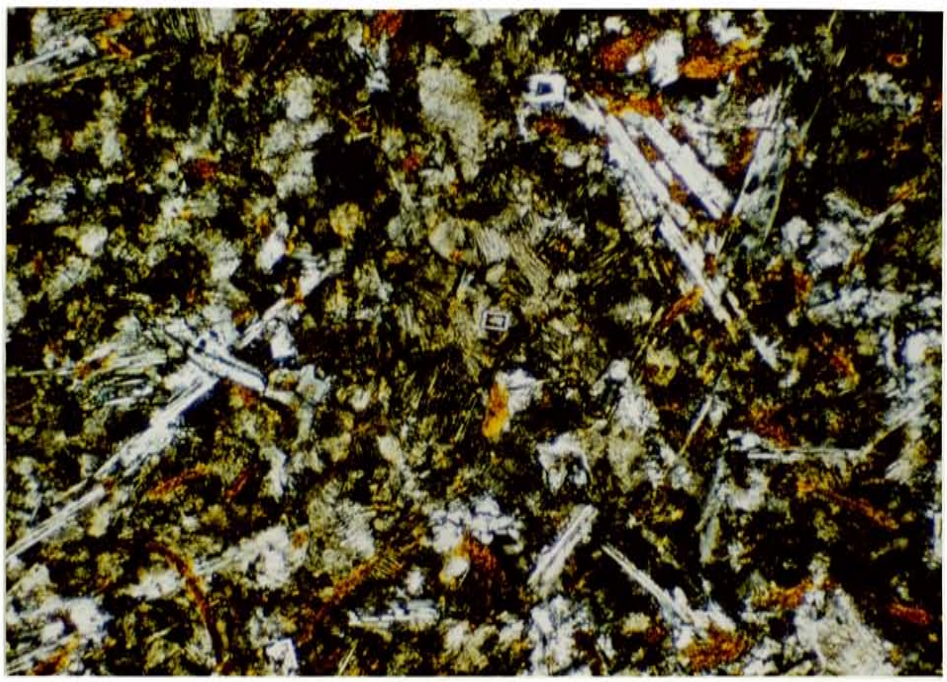

Plate VI

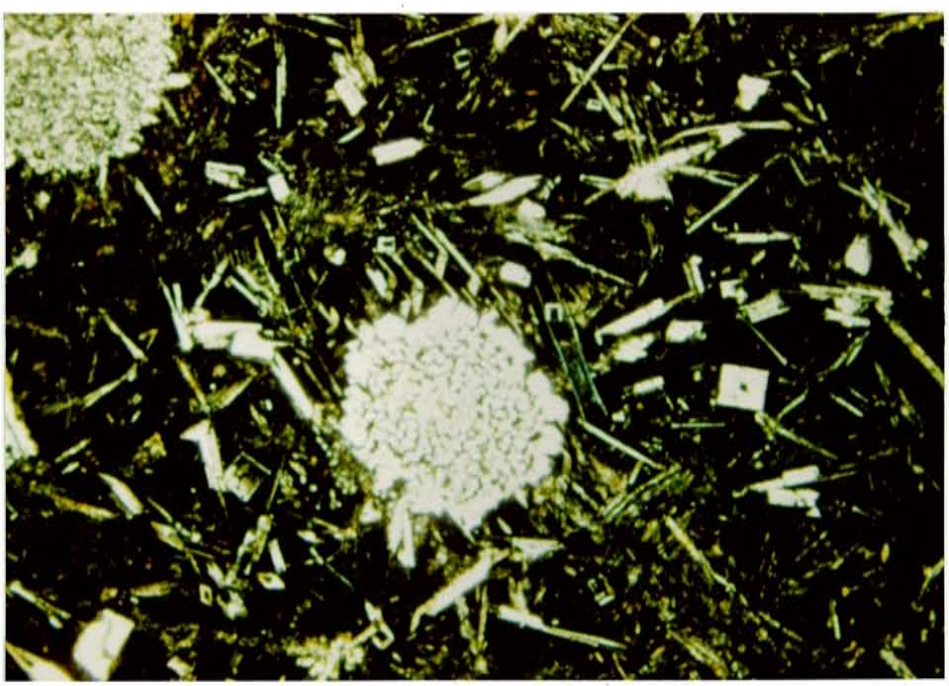

Plate V: A fine-grained rhyolite (80307) containing microphenocrysts of cellular plagioclase and extensively altered orthopyroxene in a matrix of cryptocrystalline feldspar containing disseminated opaques.

Plate VI: A fine-grained vitrophyric rhyolite (80323) containing microphenocrysts of cellular plagioclase, altered clinopyroxene and orthopyroxene in a matrix of fresh glass. The matrix is impregnated with opaques. Xenocrysts of plagioclase possessing epitaxial dendritic cores rimmed by non cellular plagioclase are common.

Plate VII

Plate VIII

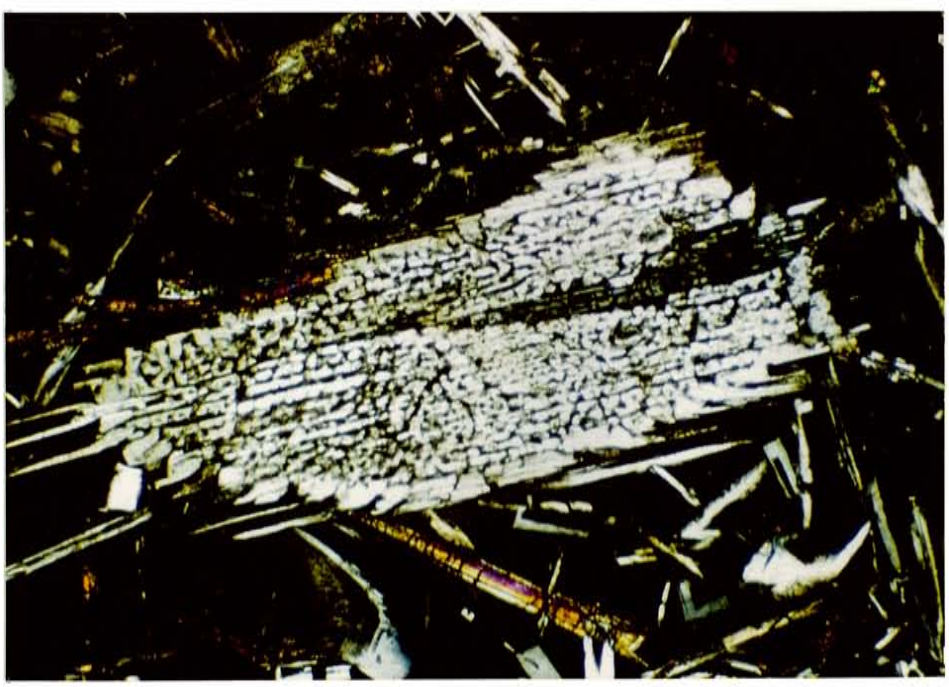

Plate VII: Andesite (80404) containing an altered xenocryst of plagioclase exhibiting a resorbed epitaxial dentritic interior surrounded by non cellular overgrowths displaying quenched rims. Similar xenocrysts are present in the dacite and rhyolite groups.

Plate VIII: Vitrophyric dacite (80664) with a fresh xenocryst of plagioclase exhibiting a resorbed epitaxial dendritic interior which is surrounded by a non cellular overgrowth possessing a rim of acicular spikes. Similar xenocrysts are common to all but the basalt group.

Plate IX

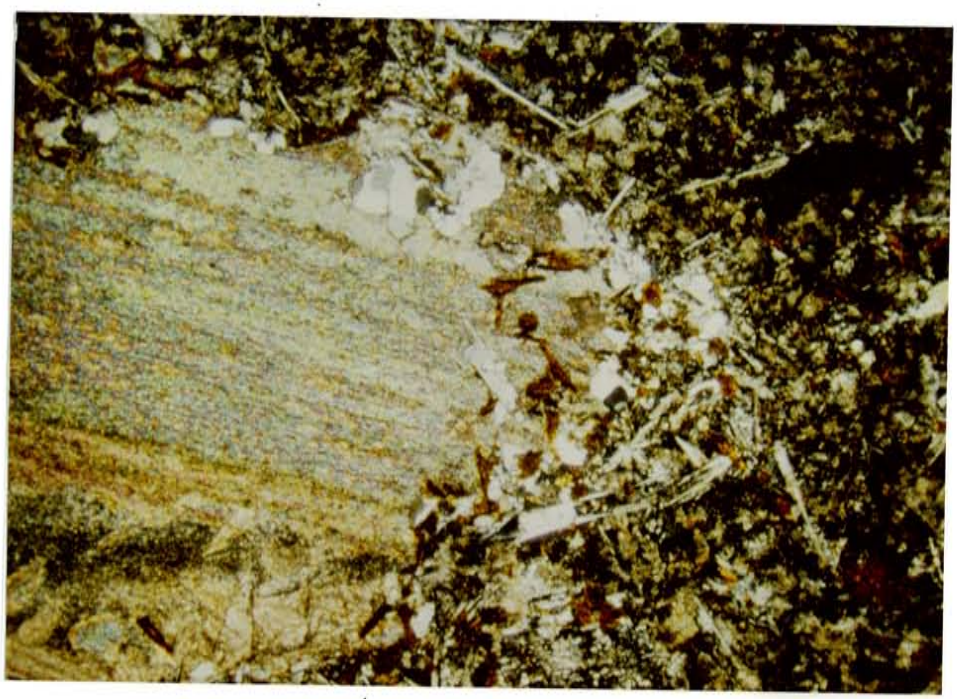

Plate X

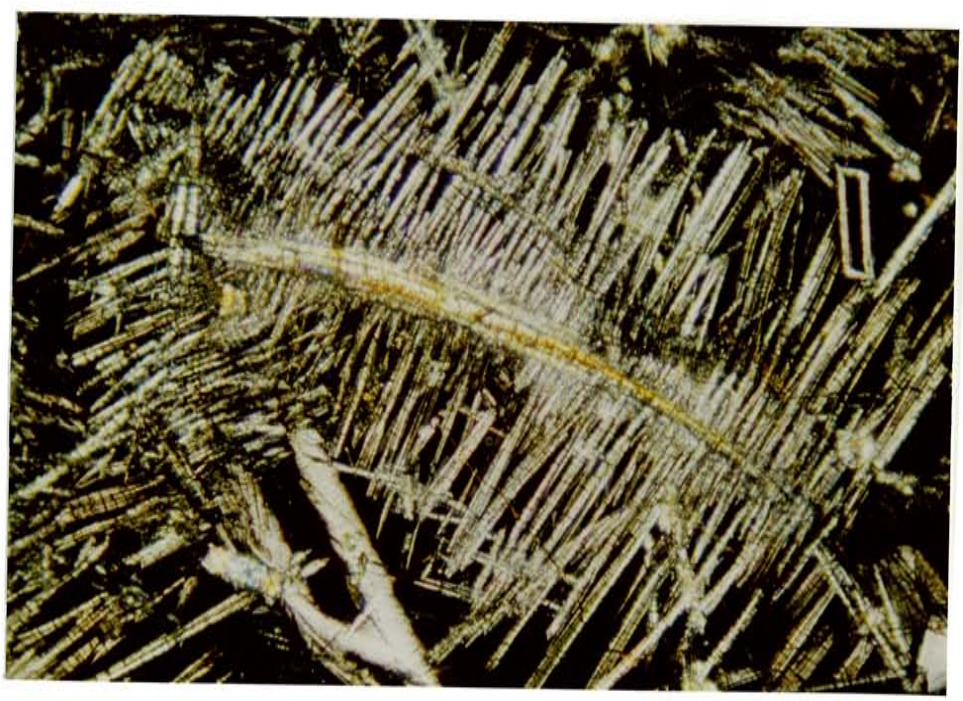

plate IX: Rhyolite (80307) with a xenolith of possible Beacon rock, made up of carbonate rimmed by a bimodal distribution of alkali feldspar and quartz. Xenoliths are sometimes accompanied by significant amounts of zeolite. Xenoliths are common to all the rock types.

Plate X: Vitrophyric rhyolite (80323) with feather or comb texture exhibited by plagioclase laths nucleated on pre-existing 0.2 mm long pyroxene. Such textures are suggestive of supercooling and inhibition of nucleation. They are most pronounced in the more silicic samples and vitrophyres.

CHAPTER FOUR. GEOCHEMISTRY

Introduction

Major element analyses were determined using x-ray fluorescence analysis on 49 samples by Philip R. Kyle at Victoria University of Wellington, New Zealand. Trace elements were determined on 35 samples by instrumental neutron activation analysis (INAA) at the Ohio State University Nuclear Research Laboratory. Brief discussions of the analytical procedures are given in Appendices 2 and 3, respectively. Major element analyses and CIPW norms for average BRIC rock types are presented in Appendix 2; trace element analyses are presented in Appendix 3.

Whole rock Rb-Sr isotope analyses were determined on twenty-three samples by Dr. R.J. Pankhurst at the Institute of Geological Sciences, London, England, using standard procedures (see Appendix 4). Oxygen isotope analyses of nineteen whole-rock samples and eleven mineral separates were made at the University of Utah Stable Isotope Laboratory using standard procedures (see Appendix 4).

Major Element Chemistry

The major element data are plotted using Harker variation diagrams (Fig. 8) (Harker, 1909) with SiO_2 concentration chosen as the abscissa due to its wide variation. Harker variation diagrams are typically used to illustrate evolutionary trends in cogenetic suites of

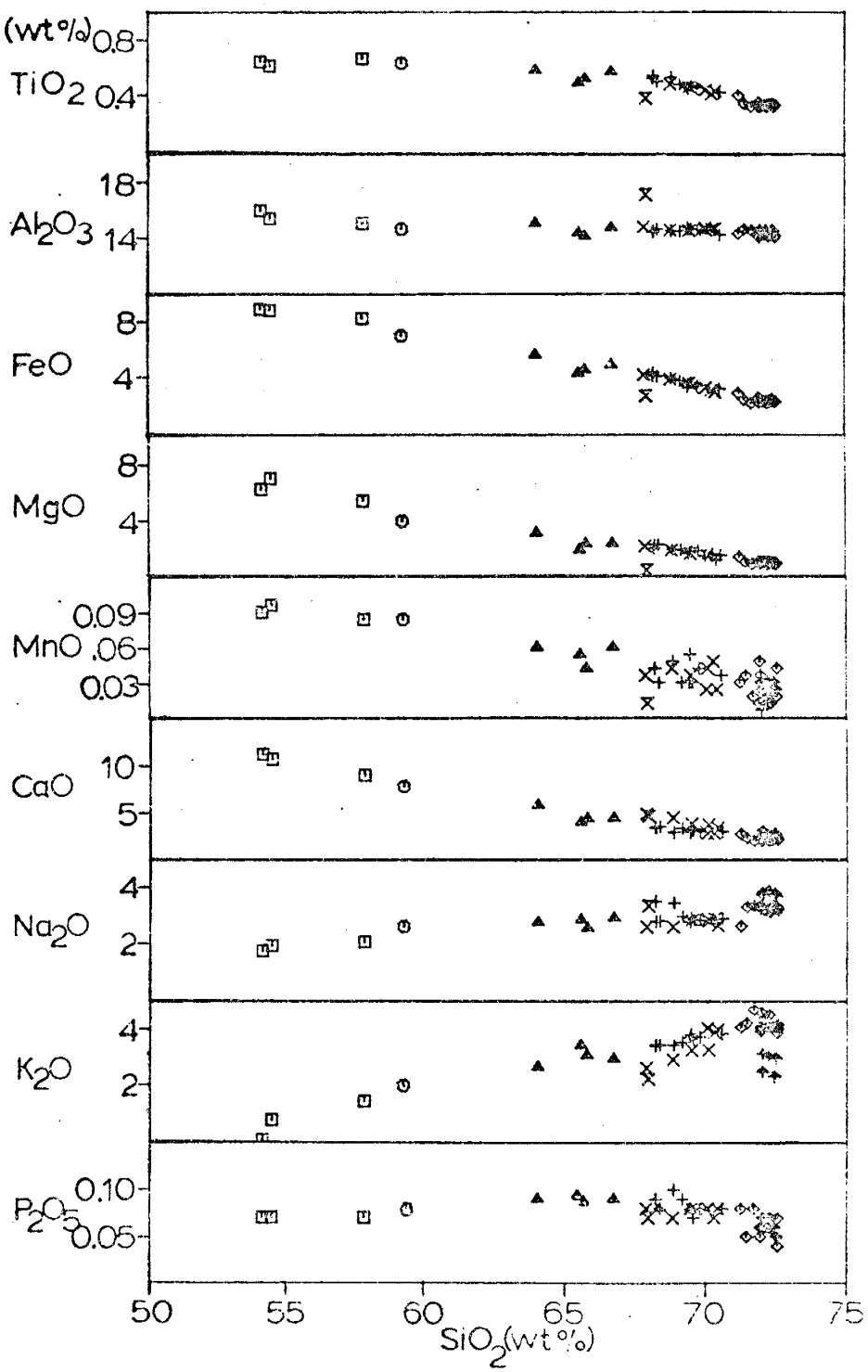

Figure 8: Major element variation diagrams. All analyses are recalculated to 100% loss-free.

igneous rocks (Cox et al, 1980). Normally systematic variations are interpreted as a result of crystal fractionation (Cox et al., 1980). Variation diagrams will also produce systematic variations when a combination of assimilation and fractional crystallization occurs (McBirney, 1979). In order to distinguish the affects of contamination it is usually necessary to use isotope geochemistry. Therefore petrogenetic interpretations cannot be based solely on variation diagrams.

Because of varying degrees of alteration and hydration, analyses have been normalized to 100% loss-free with total iron as FeO (indicated by FeO*) (see Appendix 2).

Silicon

The SiO_2 content ranges from 54.1% in the basalt group to 72.5% in the high-K rhyolite group (Fig. 8). The silica content displays gaps between 54% and 57%, and 58 and 64%. These are presently considered to reflect the limited number of analyses in contrast to the relatively clustered patterns exhibited for compositions of 57 to 73% SiO_2. The basaltic andesite sample is not from White Apron Spur, thus increasing the gap to 57 to 64%.

CIPW norms for average BRIC rock types indicate that all the rock types are saturated with respect to silica. Corrundum occurs in the norms of the HKD, HKR, and VR groups, suggesting saturation with Al_2O_3. BRIC samples

display an increase of Na-rich plagioclase with increasing SiO_2. Diopside, hypersthene, magnetite, and ilmenite decrease with increasing SiO_2 and are most abundant in the mafic compositions.

Ordinate Elements

Linear trends are seen on the variation diagrams for TiO_2, CaO, Na_2O, and P_2O_5. The variations are not continuous, but consist of two segments with different slopes. The segments correspond to SiO_2 variations of 54-68% and 68-73%, and suggest that two separate petrogenetic processes may be operating.

TiO_2, FeO*, MgO, and CaO show a negative correlation with SiO_2 concentrations, with the FeO*, and MgO correlations being continuous throughout the entire SiO_2 range. Lack of significant scattering in the data suggests that loss or gain of these major elements due to alteration is minor. MnO also shows a negative correlation with SiO_2 content, but displays a greater degree of data scatter. This scatter is due to analytical error.

The Al_2O_3 pattern is effectively flat or decreasing slightly. The concentrations of P_2O_5 appear to remain constant in relation to the SiO_2 content up to 68%, where they exhibit a negative correlation. Some of the scatter in the P_2O_5 is analytical.

The concentrations of Na_2O and K_2O differ from the rest of the major elements in that they increase with increasing SiO_2 content. Futhermore, the VR group displays significant relative enrichment in Na_2O while both the VR and HKVD groups exhibit depletion in K_2O in contrast to the general trend.

Sample 80314 is a hydrated (10% loss) vitrophyric rhyolite and consistently deviates from the major element trends shown by other samples.

Trace Element Chemistry

Trace element data are presented on Harker variation diagrams (Fig. 9), with SiO_2 as the common abscissa. Like the major element plots, more than one petrogenetic interpretation can be derived from systematic variations in trace element relative to SiO_2 concentrations. Five trends are recognizable in the trace element plots. Most elements show little variaition about the distinctive trend lines, indicating that secondary alteration has not affected the data significantly.

Scandium and chromium exhibit negative covariation to SiO_2. Scandium decreases throughout the whole SiO_2 range. The chromium trend flattens above 68% SiO_2 and is nearly level. All the remaining elements exhibit positive covariations with SiO_2. Rubidium, barium, and strontium exhibit strong positive correlations with SiO_2 abundances.

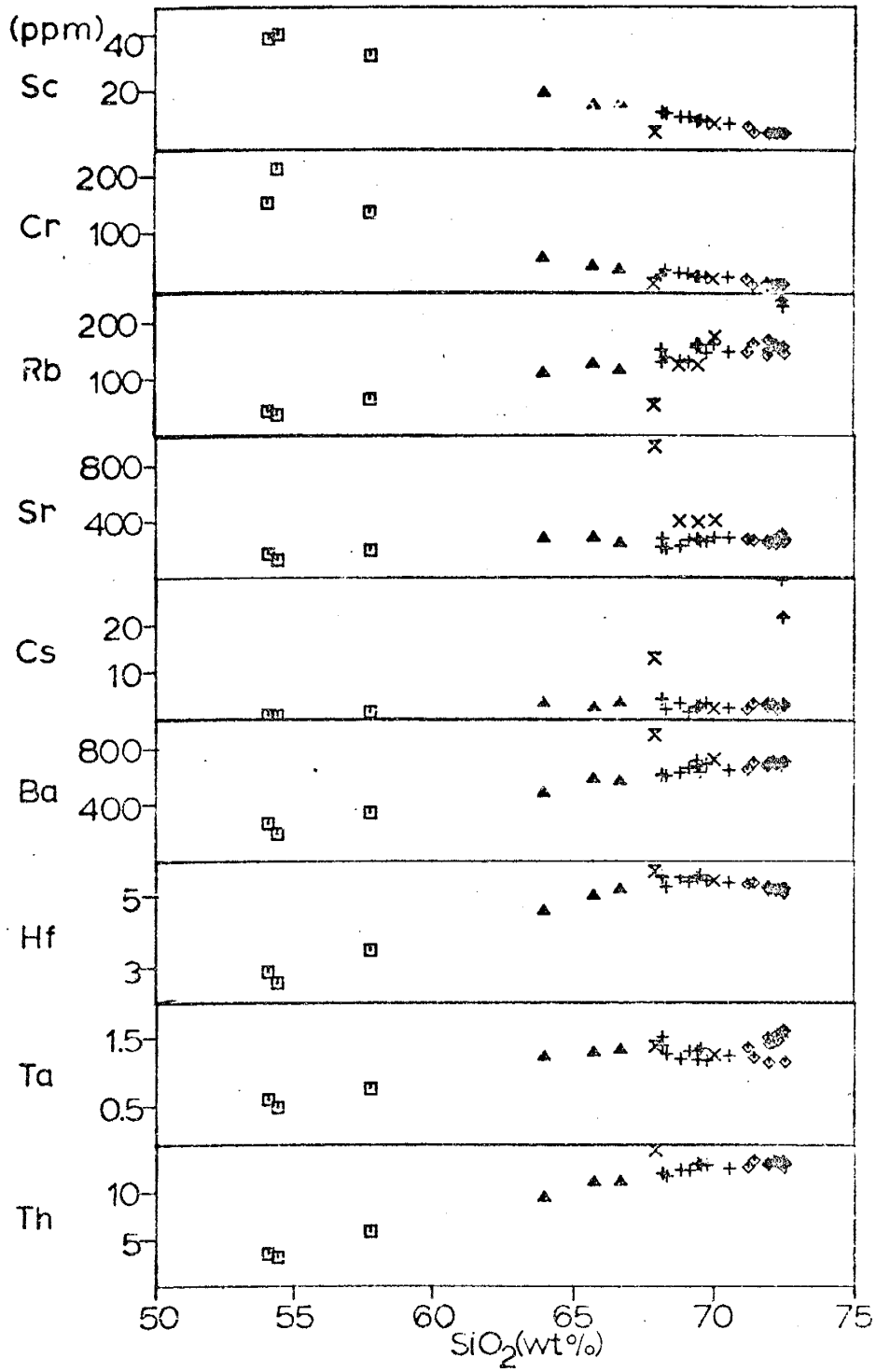

Figure 9: Trace element variation diagrams. SiO2 concentrations are recalculated to 100% loss-free.

Rubidium contents in the VR samples are distinctly higher than shown by the main trend. Cesium shows little variation above 64% SiO_2. Strontium in the HKVD group is enriched relative to the other samples. Cesium is extremely high in the VR group.

Tantalum and thorium covariations with SiO_2 display positive variations up to 68% SiO_2, but appear to plateau from there on. Tantalum shows some scatter from 68% SiO_2 on. Thorium exhibits no such deviations and shows little scatter. Hafnium increases markedly from 54% to 68% SiO_2, and then decreases with increasing SiO_2 content.

The hydrated vitrophyric rhyolite sample (80314) exhibits a clear deviation from the overall trend in all but the hafnium and tantalum plots. Strong depletions are seen in concentrations of scandium, chromium, and rubidium where strong enrichments are seen in strontium, cesium, barium, and thorium.

Rare Earth Chemistry

The rare earth elements (REE) comprise the fourteen elements from lanthanum to lutetium. Often they are subdivided into two groups, the light rare earth elements (LREE) lanthanum to samarium, and the heavy rare earth elements (HREE) europium to lutetium. Seven REE were analyzed by INAA including; lanthanum (La), cerium (Ce), samarium (Sm), europium (Eu), terbium (Tb), ytterbium (Yb),

and lutetium (Lu). The data are displayed using chondrite-normalized plots (Masuda, 1962, Coryell et al., 1963) and were normalized to corresponding Leedy chondrite REE abundances (Table 3) of Sun and Hanson (1976) (Fig. 10A-E).

REE Patterns

All the samples display significant REE enrichment relative to chondrite (Fig. 10-A); the LREE are enriched relative to the HREE. The basalt group has the largest variations in REE contents, with Lu showing an increase relative to other HREE. All of the samples have negative Eu anomalies. The negative Eu anomaly increases with increasing REE enrichment.

The high-K andesite patterns (Fig. 10-B) are similar to the basalt patterns but show a larger degree of LREE enrichment. La ranges from 82 to 94 times chondrite abundances. HREE do not display as much of an increase compared to the LREE, as Lu ranges 12 to 14 times chondrite abundances. In contrast to the basalt patterns, Lu does not exhibit an anomalous enrichment. Compared to the basalt patterns it appears that only the LREE have been significantly enriched. Similarly the negative Eu anomaly increases with total REE enrichment. The high-K andesite patterns appear to display less variation compared to the basalt patterns.

Table 3: Chrondrite normalization values of Sun and Hanson (1976).

Chrondrite Normalization Values

Element	Chrondrite ratio
La	0.315
Ce	0.813
Sm	0.192
Eu	0.0722
Tb	0.049
Yb	0.208
Lu	0.0323

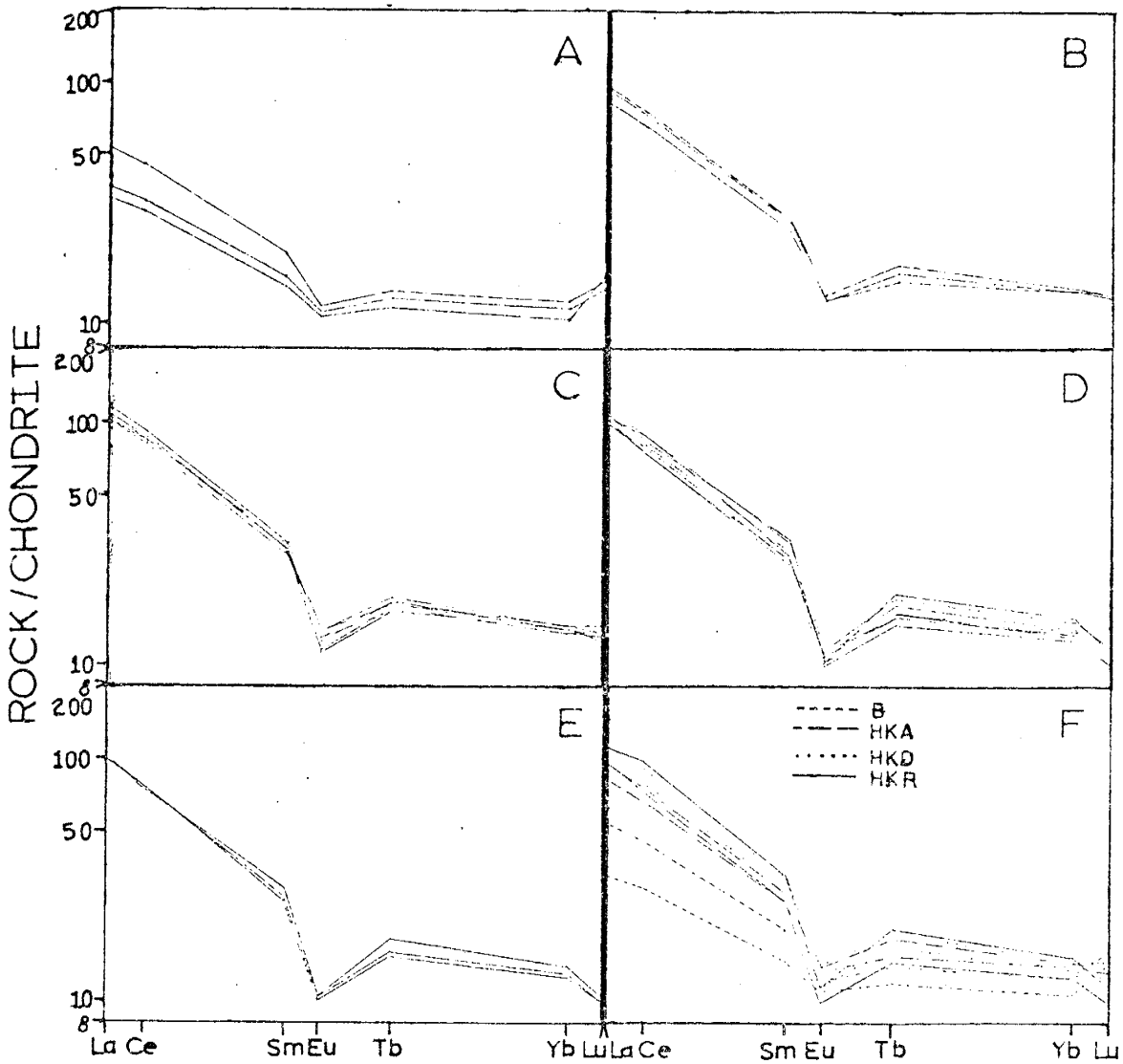

Figure 10 A-F: Chrondrite normalized REE plots. Sample data have been normalized to Leedy chrondrite values of Sun and Hanson (1976) (Table 3). REE patterns for figures are as follows; A-basalt (B), B- high-K andesite (HKA), C-high-K dacite (HKD), D- high-K rhyolite (HKR), E- vitrophyric rhyolite (VR), and F-corresponding rock type envelopes.

The high-K dacite patterns (Fig. 10-C) are quite similar to the high-K andesite patterns in the HREE but show greater LREE enrichment. La ranges from 98 to 112 times chondrite abundances and is significantly higher than the high-K andesite samples. Lu ranges from 12 to 14 times chondrite abundances and is identical to the the high-K andesite abundances. Likewise, the high-K dacite pattern lacks any significant anomalous Lu enrichment compared to the basalt patterns. The negative Eu anomaly is slightly larger, but actual Eu abundances are about the same compared to the basalt and high-K andesite abundances. In comparison to the high-K andesites, the high-K dacite patterns appear to have only been modified by LREE enrichment while exhibiting tighter patterns.

High-K rhyolite patterns (Fig. 10-D) practically overlap the high-K dacite patterns. La ranges from 98 to 111 times chondrite and falls within the range for the high-K dacite patterns. In contrast though, Lu ranges from 9.5 to 11 times chondrite, thus exhibiting an anomalous depletion. Likewise, a significant negative Eu anomaly is present; it is larger due to both LREE enrichment and a depletion in overall Eu abundance.

The vitrophyric rhyolite patterns (Fig. 10-E) are identical to the high-K rhyolite patterns. Both samples fall inside the high-K rhyolite envelope (Fig. 10-F)

Rock group envelopes (Fig. 10-F) indicate that increasing SiO_2 content through the high-K dacite group is accompanied by significant LREE enrichment and an increasing negative Eu anomaly. This trend appears to peak with the high-K rhyolite envelope, which encompasses the high-K dacite and most of the high-K andesite envelopes throughout the LREE, and most of the HREE. A prominent gap exists between the basalt envelope and the high-K andesite envelope, and is probably a reflection of sampling rather than a distinct boundary in chemistry. An anomalous enrichment of Lu in the basalt and depletion of Lu in the high-K rhyolite contrasts the remaining rock types.

Rb-Sr Chemistry

Initial $^{87}Sr/^{86}Sr$ ratios were determined using a decay constant for ^{87}Rb of $1.42 \times 10^{-11} yr^{-1}$ and an age of 179±7 Ma. (Table 4). $^{87}Rb/^{86}Sr$ and $^{87}Sr/^{86}Sr$ whole rock ratios are plotted on a standard isochron diagram (Fig. 11) and produce two distinct trends. One trend consists of the HKD, HKVD, HKR, and VR groups, the other consists of the B, HKBA, and HKA groups.

Isochrons have been fitted to various combinations of the data using weighted regression analysis (Table 5). Only a combination of the HKVD and VR samples produce a whole rock isochron that falls within the 179±7 Ma. age range accepted for the Ferrar Supergroup rocks (Kyle et al.,1981). This isochron is believed to be fortuitous as data will be

Table 4: Rb-Sr data for the Butcher Ridge Igneous Complex, Antarctica.

Sample	RB	SR	87RB/86SR	87SR/86SR	(87SR/86SR) INIT
80631	23.5	123	0.673+7	0.71192+7	0.71021+8
80394	32.4	121	0.778+8	0.71275+7	0.71077+8
80675	58.2	169	0.998+5	0.71502+7	0.71248+9
79014	80.0	220	1.058+5	0.71538+7	0.71268+9
79021	129.0	279	1.345+5	0.71913+7	0.71569+10
80404	118.0	263	1.302+7	0.71810+7	0.71479+10
80673	128.0	261	1.421+7	0.71822+7	0.71460+10
80403	135.0	244	1.604+8	0.71987+7	0.71579+11
80326	144.0	251	1.664+8	0.71963+7	0.71540+11
80419	161.0	279	1.675+8	0.71999+7	0.71573+11
80672	137.0	226	1.763+9	0.71954+7	0.71505+12
80418	175.0	399	1.273+6	0.71858+7	0.71534+10
80664	125.0	388	0.933+5	0.71770+7	0.71533+9
80668	125.0	395	0.915+5	0.71726+7	0.71493+9
80306	159.0	300	1.535+8	0.71994+7	0.71603+11
79036	174.0	258	1.746+7	0.72041+7	0.71595+11
80324	170.0	262	1.876+9	0.72083+7	0.71605+12
80325	167.0	266	1.817+9	0.72065+7	0.71603+12
80410	152.0	294	1.501+8	0.71955+7	0.71573+11
80315	178.0	263	1.960+10	0.72107+7	0.71608+12
80323	261.0	343	2.203+11	0.72088+7	0.71527+13
80313	252.0	326	2.246+11	0.72111+7	0.71539+14
80314	51.5	1110	0.134+1	0.71658+7	0.71624+7

*- Initial values were calculated at 179±3.5 Ma. using a decay constant of 1.42×10^{-11} yr^{-1}. All errors are calculated at two sigma.

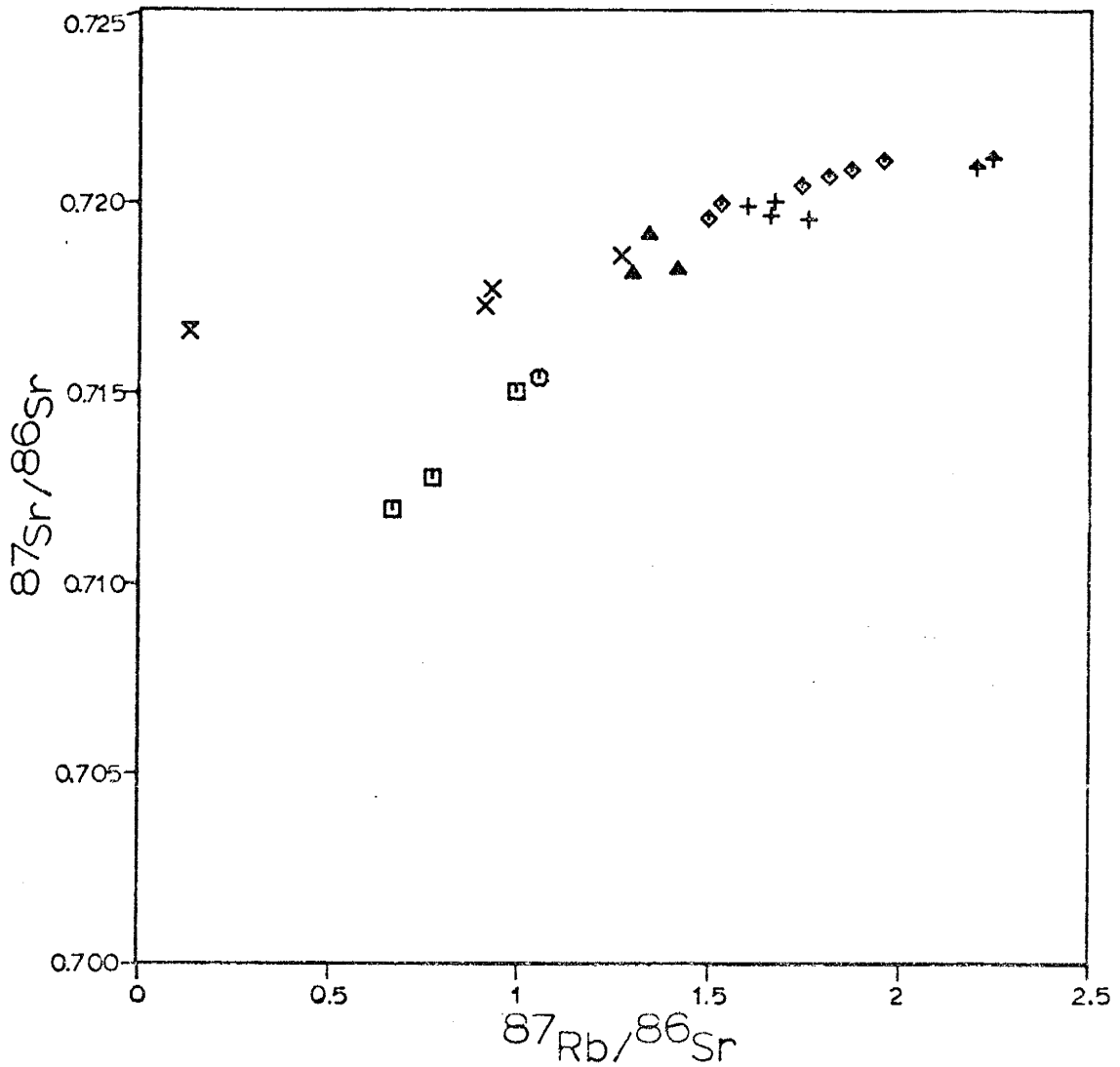

Figure 11: Whole-rock Rb-Sr isochron for samples from the White Apron Spur and Starting Point Knob sections of the BRIC. See Table 1 for an explanation of symbols.

Table 5: Isochron based on weighted regression analysis for different sample combinations. Reciprocals of squares of analytical errors used for weighting.

Rock Types	N	Slope	Intercept	Del	r	Age(Ma.)
B,HKBA,HKA	7	0.0086	0.7062	1	.998	600.1±19.3
HKVD,HKD,HKR,VR	16	0.0034	0.7144	6	.996	236.6±8.6
HKD,HKR	10	0.0035	0.7142	3	.991	248.5±16.6
HKVD,VR	5	0.0025	0.7152	0	.986	175.7±17.0

N- Number of samples in combined rock types.
Del- Number of samples not fitting calculated isochron, and subsequently not included in estimation of the isochron.
r- Correlation coefficient.

presented to suggest that these samples have have undergone significant alteration. Three other isochrons have been obtained (Table 5) however, these all yield ages considerably older than that accepted for the BRIC rocks and the Ferrar Supergroup. These isochrons must represent ficticous isochrons. Their implications on the petrogenesis of the BRIC is presented in the following chapter.

Plots of Sr concentrations versus major, trace, and rare earth elements (Fig. 12) consistently exhibit a linear relationship between samples in the B, HKBA, and HKA groups (Table 6). A plot of initial $^{87}Sr/^{86}Sr$ ratios against $^{1}/Sr$ concentrations displays a similar correlation (Fig. 13,). These variations are indicative of simple two component mixing between the basalts and a more salic component.

The HKD, HKVD, HKR, and VR groups display markedly different variations on standard mixing diagrams and the Sr-element plots compared to the B, HKBA, and HKA trends described above. A crude linear trend is present on the initial $^{87}Sr/^{86}Sr$ versus $^{1}/Sr$ plot showing near constant Sr ratios. They show Sr concentrations that are higher and lower than those of the HKA samples, where the trends appear to connect. In the Sr-element plots, the data is usually clustered about the HKA samples. However, linear trends in MgO, Sc, Cr, Eu, Tb, Yb, and Lu are present. These trends commonly connect to the HKA end of the B-HKBA-HKA linear trend. Within the MgO, Sc, and Cr plots, progression from

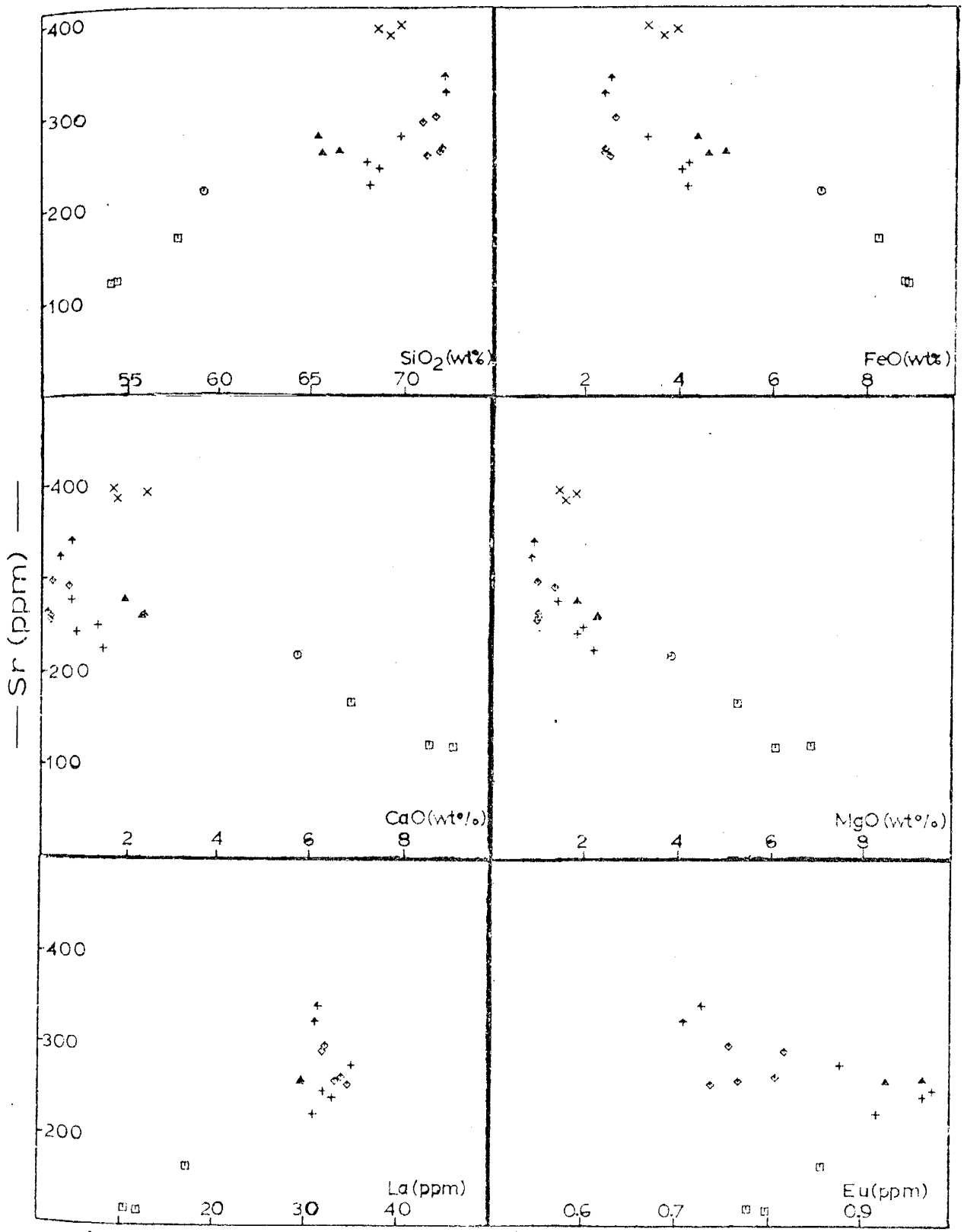

Figure 12: Plots of select major and trace elements versus Sr concentrations. See Table 1 for an explanation of symbols.

Table 6: Statistical correlations of linear regressions for plots of elements versus Sr.

Element	Mixing Line Equation	N	R2
SiO2	(Sr)M = 44.512 + 0.0783(SiO2)	7	0.94
TiO2	(Sr)M = 0.751 - 0.0007(TiO2)	7	0.61
Al2O3	(Sr)M = 16.614 - 0.0079(Al2O3)	7	0.80
FeO*	(Sr)M = 12.789 - 0.0294(FeO*)	7	0.95
MnO	(Sr)M = 0.215 - 0.0004(MnO)	7	0.80
MgO	(Sr)M = 10.337 - 0.0304(MgO)	7	0.98
CaO	(Sr)M = 16.700 - 0.0456(CaO)	7	0.97
Na2O	(Sr)M = 1.035 + 0.0068(Na2O)	7	0.93
K2O	(Sr)M = -1.209 + 0.0161(K2O)	7	0.98
Sc	(Sr)M = 61.212 - 0.1730(Sc)	5	0.99
Cr	(Sr)M = 312.814 - 1.0278(Cr)	5	0.92
Cs	(Sr)M = -1.036 + 0.0153(Cs)	5	0.91
Ba	(Sr)M = -66.471 + 2.4476(Ba)	5	0.97
La	(Sr)M = -5.494 + 0.1340(La)	5	1.00
Ce	(Sr)M = -6.618 + 0.2573(Ce)	5	1.00
Sm	(Sr)M = 0.800 + 0.0171(Sm)	5	0.99
Eu	(Sr)M = 0.656 + 0.0011(Eu)	5	0.96
Tb	(Sr)M = 0.389 + 0.0018(Tb)	5	0.95
Yb	(Sr)M = 1.844 + 0.0042(Yb)	5	0.92
Lu	(Sr)M = 0.591 - 0.0007(Lu)	5	0.95
Hf	(Sr)M = 0.652 + 0.0171(Hf)	5	0.99
Ta	(Sr)M = -0.070 + 0.0053(Ta)	5	0.98
Th	(Sr)M = -3.546 + 0.0559(Th)	5	1.00

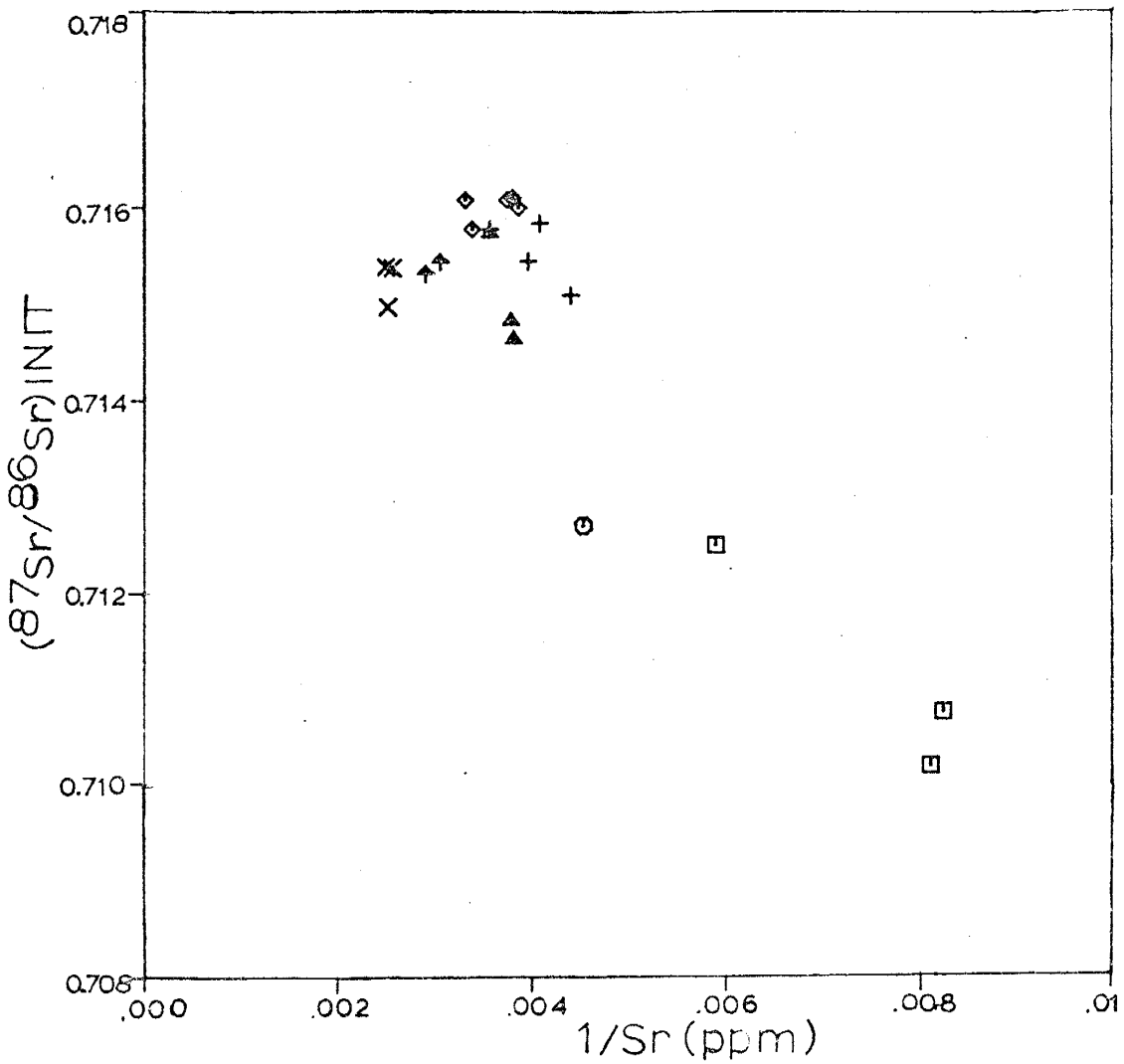

Figure 13: Mixing diagram showing samples from the White Apron Spur and Starting Point Knob sections of the BRIC. Mixing between isotopically distinct results in linear trends. See Table 1 for an explanation of symbols.

the HKD to the HKR groups is accompanied by an increase in Sr content, while Eu, Tb, Yb, and Lu show decreasing Sr concentrations. The variations suggest that these samples can not be part of the simple mixing implied for the B-HKBA-HKA trend, they must originate from a source with higher initial $^{87}Sr/^{86}Sr$ ratios.

Discussion (Oxygen Isotope Systematics)

Oxygen is by far the most abundant element in igneous rocks and in liquid, solid, and gaseous phases that are important in magmatic phenomena. Its three stable isotopes ^{16}O, ^{17}O, and ^{18}O possess slight chemical and physical variations which cause temperature dependent-fractionation extending up into magmatic temperatures. Oxygen isotope fractionation allows inferences to be made about equilibrium temperature of crystallization. Crustal and mantle-derived rocks have distinct oxygen isotope compositions which allows the evolutionary history of magmas, such as assimilation, partial melting, and occasionally its origin to be discerned.

A compilation of common $\delta^{18}O$ values for igneous rocks by Epstein and Taylor, (1967), Taylor (1968), and Hoefs (1973), indicate that gabbros, basalts, and anorthosites have very similar values ranging from +5.5 to +7.4‰ and are indistinguishable from most andesites, syenites, and trachytes (Faure, 1977). Granitic rocks and pegmatites have

higher and more variable values, ranging from +7 to +13‰ (Faure, 1977).

Variations in the oxygen isotope composition of igneous rocks are brought about by a variety of mechanisms. In relation to the types of rocks seen in the Ferrar Supergroup and the limitations of analyses constrained by the rocks, not all processes effecting oxygen isotope compositions are relevant to this discussion. Assimilation of country rock, interaction with meteoric groundwaters or magmatic waters, and fractional crystallization are probably the most important.

Assimilation of crustal rocks by mantle derived melts involves incorporation of rocks commonly having higher $\delta^{18}O$ values. The extent to which the ^{18}O content and thus the $\delta^{18}O$ value of the original magma changes is hard to predict. Assimilation of crustal material involves several variables: ^{18}O content of the country rock, ^{18}O content of the magma, the extent of crystal fractionation, and the temperatures of the magma and country rock. Equally important are the effects of dehydration and decarbonation (Hoefs, 1980). The effects of assimilation on oxygen isotopes has been modelled by Taylor (1980) and DePaolo (1981), who suggested that the most significant increases in $\delta^{18}O$ values are in the more mafic constituents while leveling off of the $\delta^{18}O$ values occurs in the more silicic members.

Interaction of igneous intrusions with meteoric ground waters has been examined in considerable detail by Taylor (1971, 1974b, 1977, 1978). The interaction and transport of meteoric water through hot igneous intrusive rocks has been shown to produce a depletion of $\delta^{18}O$ in the igneous rock by as much as 10‰ to 15‰ (Hoefs, 1980). Numerous cases have been well documented; the Skaegaard intrusion in Greenland, portions of the Sierra Nevada batholith in California, and the Coast Range batholith in British Columbia are to name just a few.

Taylor (1974) suggests that intrusive rocks exhibiting abnormally low $\delta^{18}O$ values due to interaction between igneous rocks and meteoric waters are: (1) emplaced into highly jointed volcanics that are permeable to ground water movement; (2) commonly depleted in ^{18}O in the feldspars to a greater degree than other coexisting minerals with the feldspars exhibiting a turbidity or cloudiness; (3) display alteration of primary pyroxenes and olivines to amphibole, chlorite, Fe-Ti oxides, and/or epidote; (4) contain mariolitic cavities; (5) display intergrowths of turbid alkali feldspar and quartz. Hoefs (1980) subsequently suggested that absence or minor occurrences of these features in low $\delta^{18}O$ rocks implies that the hydrothermal alteration occurred at very high temperatures. Contamination by hydrothermal alteration requires large amounts of heat to convectively drive meteoric waters through a plutonic complex (Taylor, 1974).

In contrast to the changes in ^{18}O content from interaction with ground water, high temperature isotopic reactions with an aqueous phase such as a brine produced as a product of differention will elevate the ^{18}O concentrations of the rock and thus its $\delta^{18}O$ value (Taylor, 1974; Faure, 1977). The elevated $\delta^{18}O$ values of magmatic water are a result of the continous isotopic exchange with silicates in the magma (Hoefs, 1980). The origin of the water from degassing of lower crust, upper mantle, or from recycled meteoric water is of no significance, as magmatic temperatures will allow total silicate-liquid exchange. Probably the best example of such a mechanism is evidenced by the $\delta^{18}O$ value variations from the Muskox intrusion (Epstein and Taylor, 1967).

Fractionation between liquid and solid phases is a temperature-dependent process. At relatively high temperatures, fractionation is small and plays a minor roll in influencing the oxygen isotope compositions of rocks (Hoefs, 1980). Therefore, the intrusive/extrusive mode of emplacement plays a significant function in the role of fractionation, particularly in the mafic constituents (Taylor, 1968a; Anderson et al., 1971). Fractionation between mafic plutonics and their volcanic equivalents differ by about a factor of two and are possibly due to retrograde exchange or post-crystallization exchange reactions of plutonic rocks with a fluid phase (Hoefs, 1980). Small differences in $\delta^{18}O$ values between phenocrysts

and groundmass in volcanics and chilled intrusives imply attainment and freezing of equilibrium at magmatic temperatures (Hoef, 1980).

The tendency of silicate minerals to concentrate ^{18}O is directly related to their chemical compositions. Since different compositions imply differing physiochemical properties, partitioning of oxygen isotopes accompanies any transition or transformation. A large number of analyses by Epstein and Taylor (1967) have been reduced to give the following ranking of ^{18}O concentration in decreasing tendency: quartz, alkali feldspar, calcite, intermediate plagioclase, anorthite, pyroxene, hornblende, biotite, chlorite, ilmenite, and magnetite.

At magmatic temperatures the partition coefficient of oxygen between plagioclase and a magmatic liquid approaches unity, thus the oxygen isotope composition of plagioclase phenocrysts varies within narrow limits suggesting equilibration of oxygen with the parent magma. The $^{18}O/^{16}O$ ratio of the feldspar should closely approximate the melt from which it crystallized (Taylor and Epstein, 1962; 1963). In gabbroic rocks, plagioclase is thought to be about 0.3 to 0.5‰ richer than the melt while in granitic rocks, plagioclase is thought to be about 0.2 to 0.4‰ lower than the melt (Taylor, 1968).

Pyroxene and magnetite exhibit a lesser tendency to concentrate ^{18}O and have values lower than the melt from which they crystallized. This effect is enhanced at lower temperatures. Upon rapid cooling of a magma, the $^{18}O/^{16}O$ ratios of the pyroxene should be slightly lower than the whole rock, while magnetite will be significantly lower. Care should be taken in evaluation of magnetite $\delta^{18}O$ values as magnetite is removed from magmas by magnetic properties and its oxygen compositions are probably not consistent with the associated crystallizing phases.

Rapidly quenched, supercooled glass should represent the $^{18}O/^{16}O$ ratios of the silicate-melt phases from which the crystallizing phases where derived. However, rhyolitic glasses with H2O contents greater than 0.5-1.0 weight per cent do not in general have $^{18}O/^{16}O$ ratios similar to their coexisting feldspar phenocrysts (Taylor, 1968). Analyses of several glasses (Taylor, 1968) demonstrate that simple hydration does not totally explain the observed isotopic compositons of the glass and coexisting mineral phases.

Oxygen Isotope Chemistry

The $^{18}O/^{16}O$ ratio normalized relative to SMOW for whole-rock and mineral separate analysis from the BRIC, along with four whole-rock analyses of the Carlyon Granodiorite and Leucocratic Granite, are listed in Table 7.

Table 7; Oxygen isotope data from the Butcher Ridge Igneous Complex, Antarctica and surrounding areas.

		DELTA ^{18}O				
Sample	Type	Whole Rock	Plag.	Pyx.	Glass	Magnetite
80631	B	+3.08		+2.3		
80394	B	+6.0	+5.9			+1.75
80675	B	+5.99				+3.05
79021	HKBA	(+10.5)				
80404	HKA	+6.4				
80673	HKA	+8.0	+9.5			
80403	HKA	+8.8				
80326	HKD		+7.6			
80419	HKD		+8.7			
80672	HKD	+8.94	(+9.7)			
80418	HKVD	+10.1				
80664	HKVD	+7.8				
80668	HKVD	+9.1				
80306	HKR	+7.2				
80324	HKR	(+8.82)		+8.8		
80325	HKR	+10.0				
80410	HKR	+9.5				
80315	HKR	+10.2				
80323	VR	+9.42		+10.9		
80313	VR	+6.8			+9.2	
80314	HYHKR	+10.3				
B-78-9	GRANITE	+10.1				
B-78-14	GRANITE	+9.6				
B-78-33	GRANITE	+9.3				
B-78-34	GRANITE	+9.5				

All analyses are reported in parts per mil and normalized with respect to SMOW. Samples listed in parentheses represent low yields (<94%) during extraction and are susceptable to fractionation. These values should be viewed with some speculation. Repeated runs on low yield samples are listed in column 2. Samples B-78-9 through B-78-33 are from the Carlyon Granodiorite, B-78-34 is from the Leucocratic Granite of the Brown Hills, Antarctica (Felder,1980).

Whole-rock oxygen isotope analyses of samples from the BRIC range from; +3.08‰ to +6.0‰ in the B group, +6.4‰ to a questionable +10.5‰ in the HKA group, +8.8‰ to +8.94‰ in the HKD group, +7.8‰ to +10.1‰ in the HKVD group, +7.2‰ to +10.2‰ in the HKR group, and +6.8‰ to +9.42‰ in the VR group. The hydrated sample (80314) yields a whole-rock value of +10.3‰, which is the highest $\delta^{18}O$ value recorded for any whole-rock sample.

An apparent non-linear but systematic positive variation exists between the whole-rock $\delta^{18}O$ value and SiO_2 abundance in the samples of the B, HKA, HKD, and HKVD groups (Fig. 14). Whole-rock $\delta^{18}O$ values within the HKR and VR group seem to deviate from this crude trend and exhibit a large variation ranging as low as +7.2‰ and as high as +10.2‰.

$\delta^{18}O$ values for plagioclase separates range from +5.9‰ in the B group to +10.9‰ in the VR group. In contrast to the whole-rock $\delta^{18}O$ values, plagioclase $\delta^{18}O$ values do not display a systematic variation with whole-rock SiO_2 concentrations. In the B group, the $\delta^{18}O$ value of plagioclase closely resembles that of the whole-rock value (sample 80394). Likewise, sample 80324 of the HKR group shows a similar correlation. All remaining pairs of plagioclase and whole-rock $\delta^{18}O$ values indicate that plagioclase separates consistently yield higher (+0.76‰ to +1.5‰) $\delta^{18}O$ values than the whole-rock analyses.

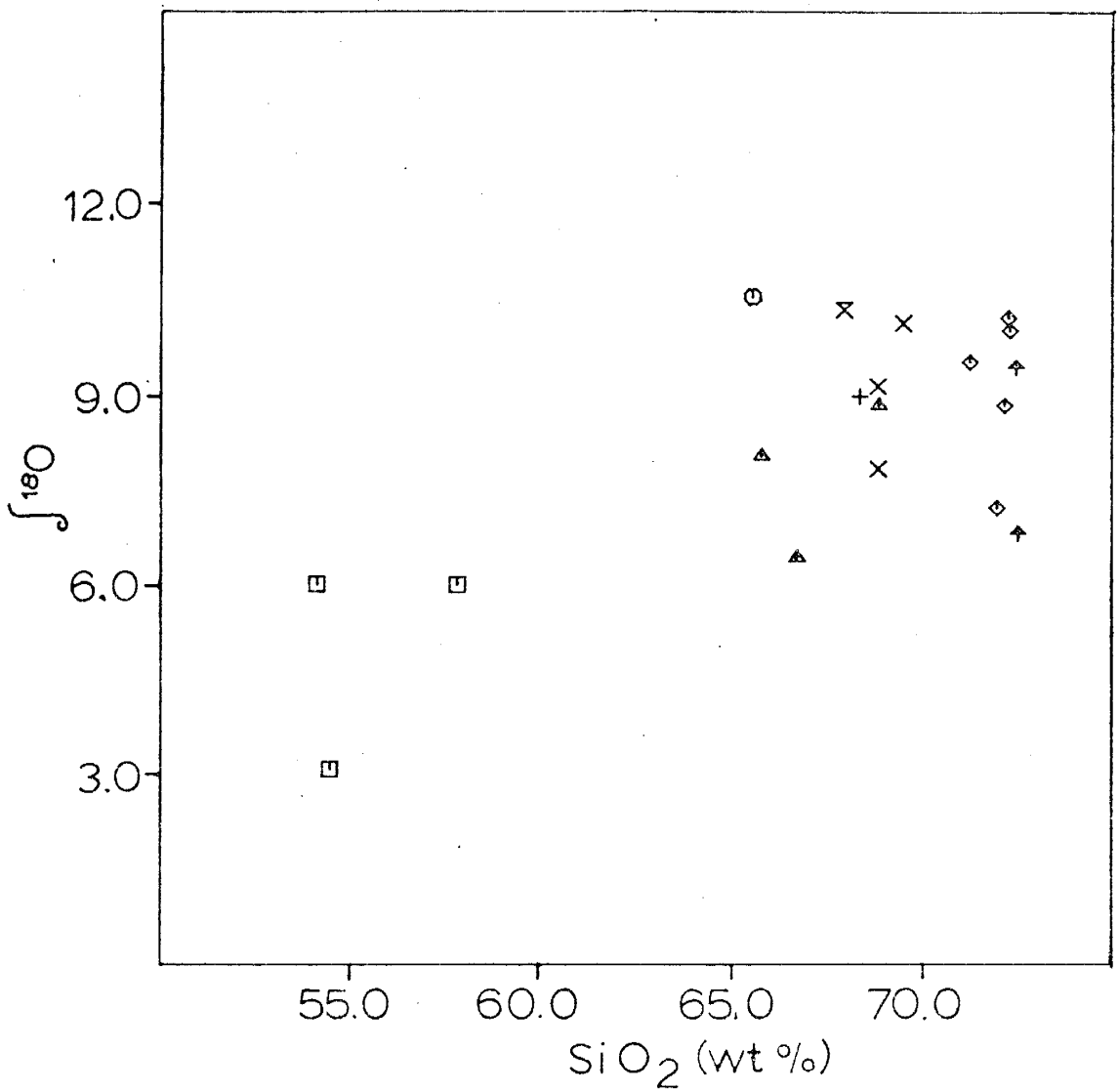

Figure 14: Plot of Delta-18 values versus SiO2 concentrations for samples of the White Apron Spur and Starting Point Knob sections. See Table 1 for an explanation of symbols.

One pyroxene separate analyzed from sample 80631 of the B group yielded a $\delta^{18}O$ value less than that of the corresponding whole-rock analysis. Likewise, one glass separate, of petrographically fresh glass, was analyzed (sample 80323) and produced a $\delta^{18}O$ value less than that of the corresponding whole-rock analysis. Two mineral separates of Mg-Fe oxide were analyzed (samples 80394 and 80675) yielding markedly lower $\delta^{18}O$ values than the whole-rock values.

Finally, in a plot of initial $^{87}Sr/^{86}Sr$ ratios versus $\delta^{18}O$ values, two trends are apparent (Fig. 15). The lower trend, consisting of samples from the B, HKBA, and HKA groups exhibit a positive variation between initial $^{87}Sr/^{86}Sr$ ratios and whole-rock $\delta^{18}O$ values. However, the upper trend consisting of samples from the HKD, HKVA, HKR, and VR groups, displays a linear variation with almost constant initial $^{87}Sr/^{86}Sr$ ratios.

Evaluation of Data

Samples 80631, 79021, 80313, and 80314 are not considered representative of their original oxygen isotope compositions. Samples 80631 and 80313 lie considerably below the range in average values for rocks of similar composition, and are probably contaminated with meteoric ground water. The pyroxene separate analysis on sample 80631 supports this interpretation. Sample 80314 exhibits a

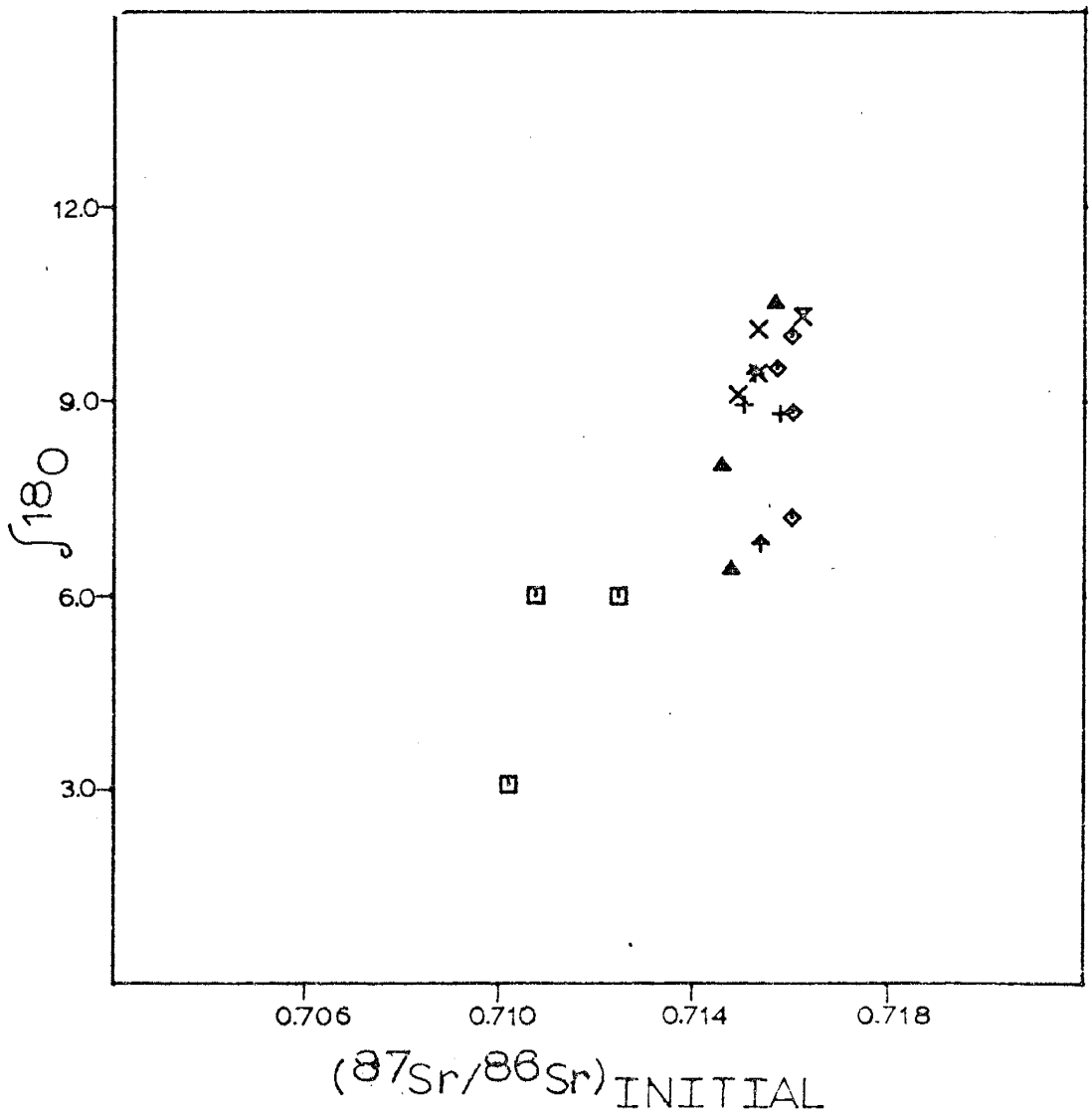

Figure 15: Combined Delta-18 and initial Sr ratio mixing mixing diagram after Taylor (1980). See Table 1 for an explanation of symbols.

high loss on ignition suggesting considerable hydration. Magmatic water (brines) produce the opposite effect of groundwater, such a process may explain variations produced in sample 79021. n light this evidence the above described samples have been excluded from the following discussion.

$\delta^{18}O$ values of the B, HKBA, and HKA groups show a systematic positive variation when plotted against initial $^{87}Sr/^{86}Sr$ ratios (Figure 14,). Recent work by Taylor (1980), Faure (1980), and James (1981) suggest that such variations are the result of assimilation of crustal rocks. Crystal fractionation of mineral phases could not account for the range of $\delta^{18}O$ values (+6.0-+8.8‰) or the systematic change in initial Sr ratios. The agreement of the +6.0‰ value of the basalt sample (80394) with values accepted for mantle-derived rocks suggests that it may represent a composition close to the basaltic end member. A plagioclase separate from this sample indicates almost no variation from the whole-rock value, suggesting that little or no contamination is present and that rapid cooling from magmatic temperatures has occurred. A plagioclase separate from the high-K andesite has a higher $\delta^{18}O$ than the whole rock values which is greater than can be explained by fractionation. The difference therefore is probably the result of contamination.

Samples of the HKD, HKVD, HKR, and VR groups exhibit a trend in Figure 14 of increasing $\delta^{18}O$ values, whereas the initial $^{87}Sr/^{86}Sr$ ratios show only minor variations. $^{87}Sr/^{86}Sr$ ratios, in contrast to $\delta^{18}O$ values, do not change significantly during partial melting or differentiation. The $\delta^{18}O$ values of these groups are quite similar to the values given for some local basement rocks (Table 6) and would suggest that if differentiation was the maior process, then it would have to be imposed on a melt derived from crustal rocks.

A suggested relationship between the local granites and granodiorites and the processes described above is examined more closely in the following chapter.

Discussion (Vitrophyres)

One of the main problems in intrepretating the geochemistry from the BRIC is to determine whether or not the vitrophyres represent pristine magmatic material. Previous investigations (Lipman, 1965) of glassy rocks indicate that obsidians, pitchstones, and vitrophyres are easily alterated after deposition, and that the degree of alteration may increase with time. This also seems to be the case for the vitrophyres of the BRIC.

Vitrophyres from both the HKVD and VR groups exhibit several unique geochemical characteristics. Compared to the HKR group, the VR group is enriched in Na_2O, Rb, and Cs and

depleted in K_2O. The HKVD group shows enrichment in CaO and Sr relative to the HKD group. The types of alteration affecting glassy parts of extrusive volcanic bodies and shallow intrusive bodies are produced by four main processes; leaching by ground water, secondary devitrification, secondary hydration, and primary crystallization (Lipman, 1965). Leaching by ground water has been shown to deplete glasses relative to crystalline rock in SiO_2 and Na_2O while enriching them in Al_2O_3 (Lipman, 1965 and Noble, 1965). The lack of such variation in SiO_2 and Al_2O_3 in the BRIC vitrophyres appears to suggest a minimal roll of leaching as an effective variable in their development.

Secondary devitrification occurs during and after the cooling of a magmatic body, and is due to the thermodynamic metastability of glasses below their melting temperatures. Numerous analyses on pairs of glassy and crystalline rocks (Lipman, 1965) suggest that relative to their crystalline counterparts, glasses display alkali enrichment in Na_2O and depletion in K_2O. Such variations are quite similar to those seen in the vitrophyres from the BRIC, thus offering a possible mechanism by which to account for the BRIC vitrophyre alkali variations.

Major conflicts arise in application of secondary devitrification as the controlling process for the BRIC vitrophyre alkali variations. Petrographic inspection of

the vitrophyres reveals fresh and unalterd glass suggesting that secondary devitrification has been at most minimal. Although the crystalline HKR samples do exhibit apparent devitrified textures in the groundmass, opposite alkali variations would arise if secondary devitrification were present, and would not produce variations consistent with current data. Likewise, secondary devitrification of the crystalline rocks would markedly change the consistent isotope data currently displayed.

Secondary hydration is a time and surface area dependent process, it commonly occurs in volcanic rocks of Tertiary age and older (Ross and Smith, 1955; Boyd, 1961). Rhyolite glasses containing more than a few tenths of a percent of water have frequently displayed effects of secondary hydration at or near surface temperatures and pressures (Ross and Smith, 1955; Friedman and Smith, 1958). Initially secondary hydration causes glasses to become depleted in Na_2O and enriched in K_2O relative to their non-hydrated counterparts (Lipman, 1965; Aramaki and Lipman, 1965; Noble, 1967; and Lipman et al., 1969). During prolonged hydration removal of Na_2O will continue, but K_2O will cease to be enriched and start to be removed (Noble, 1967).

As the BRJC vitrophyres are much older than Tertiary , and have most likely been subjected to secondary hydration, their alkali variations do not correspond to previously

documented work (Lipman, 1965; Aramaki and Lipman, 1965; Noble, 1967; and Lipman et al., 1969). If the vitrophyres and their crystalline counterparts were intially subjected to primary crystallization (Lipman, 1965), then the original alkali variations would have supposedly exhibited depletion in Na_2O and enrichment in K_2O. Prolonged secondary hydration would then deplete the Na_2O and K_2O concentrations of the vitrophyres relative to the HKR samples. Na_2O variations still do not correspond to those exhibited by the vitrophyres. The processes invoking alkali variations must not be a simple application of the above described processes.

The higher loss on ignitions of the vitrophyres compared to the HKR samples suggests that secondary hydration must have been a significant factor in the BRIC vitrophyre development. The relative depletions in K_2O indicate the hydration was prolonged. Rb concentrations violate this assumption though. The enrichment of Rb in the vitrophyres relative to the HKR samples is opposite to variations in K_2O. Rb is chemically similar to K and substitutes into K bearing mineral lattice sites. Thus Rb variations should mimic K_2O variations. Likewise, Cs concentrations should paralell K_2O because it is also similar in chemical properties. These discordant variations are currently not explanable.

Sr concentrations show slight enrichment in the HKVD group compared to the HKD samples. As Sr substitutes readly for CaO in plagioclase, the slight enrichment of CaO in the HKVD samples is expected. Likewise, the increasing negative Eu anomaly exhibited by the more salic groups indicates that plagioclase is prominent as a crystallizing phase and available for Sr substitution. Thus alkaline earth element concentrations appear to behave more consistently than the alkali elements.

Sample 80314 has a 10% loss on ignition and was probably subjected to prolonged secondary hydration. The 10% loss on ignition of this sample accounts for the depleted alkali variations. Thus, hydration is considered to be the plausible mechanism for causing its loss/gain in alkalis and high Rb concentrations. Similar to the VR group though, Cs increases, which is opposite to what would be expected. Again no interpretations are available for this anomalous behavour. Alkaline earth variations for this sample do behave coherently and are consistent with modification by secondary hydration.

Although some significance could be placed on the presence of xenocrystic and xenolithic material as a possible factor in altering alkali chemistry, petrographic evidence indicates that no one rock type contained abnormal concentrations of xenocrysts. Since the vitrophyres exhibit geochemical variations not explanable by conventional

alteration models, their dissimilarity with respect to their crystalline counterparts must be the result of a more complex alteration involving secondary hydration as a major process. It is concluded from these variations that the vitrophyres of the BRIC do not represent pristine magmatic material, thus their production of isochrons which produce an acceptable age is simply fortuitus. Consequently, the vitrophyres have not been included in subsequent isotope modelling.

CHAPTER FIVE. PETROGENESIS

Introduction

Isotope plus major and trace element data suggests that at least two major physical processes were operating in the genesis of the BRIC rocks. Samples of the B, HKBA, and HKA groups exhibit linear relationships on Harker variaton diagrams for almost all of the elements analyzed. Linear relatonships are also shown between Sr and all the elements analyzed, between initial $^{87}Sr/^{86}Sr$ ratios and $^{1}/Sr$ concentrations, and between $\delta^{18}O$ values and Sr ratios. These relations imply that simple two component binary mixing between basalt and an assimilated crustal component (Faure, 1977; Faure et al., 1974) is responsible.

In contrast, the HKD, HKVD, HKR, and VR groups do not display clear elemental and isotopic variations suggestive of simple two component mixing. The near constant high initial $^{87}Sr/^{86}Sr$ ratios are accompanied by a systematic increase in the $\delta^{18}O$ values suggesting that the rocks were derived by either; 1) a mantle-derived basalt assimilating unusually large quantities of crustal material coupled with fractionation of some mineral phase, or 2) remelting of crustal material in various degrees with assimilation of small amounts of basaltic material, and possibly fractionation of some mineral phase. The latter model is believed to be most feasible because of the high initial

$^{87}Sr/^{86}Sr$ ratios and the similar $\delta^{18}O$ values to the local basement rocks.

Petrogenesis of the B, HKBA, and HKA Rock Types

Binary Mixing

Samples within the B, HKBA, and HKA groups show clear geochemical evidence of binary mixing of a basaltic component and a salic component. Using the linear relation between initial $^{87}Sr/^{86}Sr$ ratios and $^{1}/Sr$ concentrations (Fig. 13), end members have been calculated using assumed values of initial $^{87}Sr/^{86}Sr$; the procedure is described in Appendix 5. A straight line was fitted to the seven data points by least-squares regression, and produced a correlation coefficient of $r^2=.904$ suggesting an excellent fit of the data to the line. The equation of this line is:

$$\left[^{87}Sr/^{86}Sr\right]_M = 0.7183 - 0.9728\left[^{1}/Sr\right]_M$$

Two initial $^{87}Sr/^{86}Sr$ values have been assumed for the basaltic end member namely, 0.704 and 0.709; the corresponding Sr concentrations are 68 and 104 ppm respectively.

These values were chosen in light of a controversy concerning the isotopic nature of the mantle source for the Ferrar Supergroup. Faure et al., (1972, 1974, 1979) had originally suggested that the initial $^{87}Sr/^{86}Sr$ ratios of "normal" mantle averaged about 0.704. Hoefs et al. (1980) also suggested that the initial $^{87}Sr/^{86}Sr$ ratios of the

source was as high as 0.709, but that extensive crustal contamination had occurred. Kyle (1980) following a hypothesis of a heterogeneous mantle proposed by Brooks et al. (1976) and Brooks and Hart (1978), suggested that the initial $^{87}Sr/^{86}Sr$ ratio of the mantle source for the Ferrar Supergroup may have been as high as 0.711. Using oxygen and initial ($^{87}Sr/^{86}Sr$) data on sequence of Kirkpatrick Basalt Group flows Kyle et al., (1982) suggested the source was at least 0.709 or higher.

For the salic end member, the initial $^{87}Sr/^{86}Sr$ ratios of some local Paleozoic basement rocks were calculated at 180 Ma. and then plotted with the BRIC samples on a standard mixing diagram (Fig. 16). The intersection between the granite trend and the BRIC mixing line represents a possible contaminant. The Sr isotope composition of the intersection gives an initial $^{87}Sr/^{86}Sr$ ratio of 0.7153, and a Sr concentration of 322 ppm. This composition is in contrast to those usually assumed by Faure (1981), Faure et al. (1982), being significantly lower (0.7153 compared to 0.720). Likewise, the Sr concentrations are considerably higher than the values (200 ppm) proposed by Faure for the contaminant.

Other elements were determined for the end members from plots verses Sr concentrations by the method described in Appendix 5, plots for selected elements are shown in Figure 12. Statistical data on the correlations between Sr and

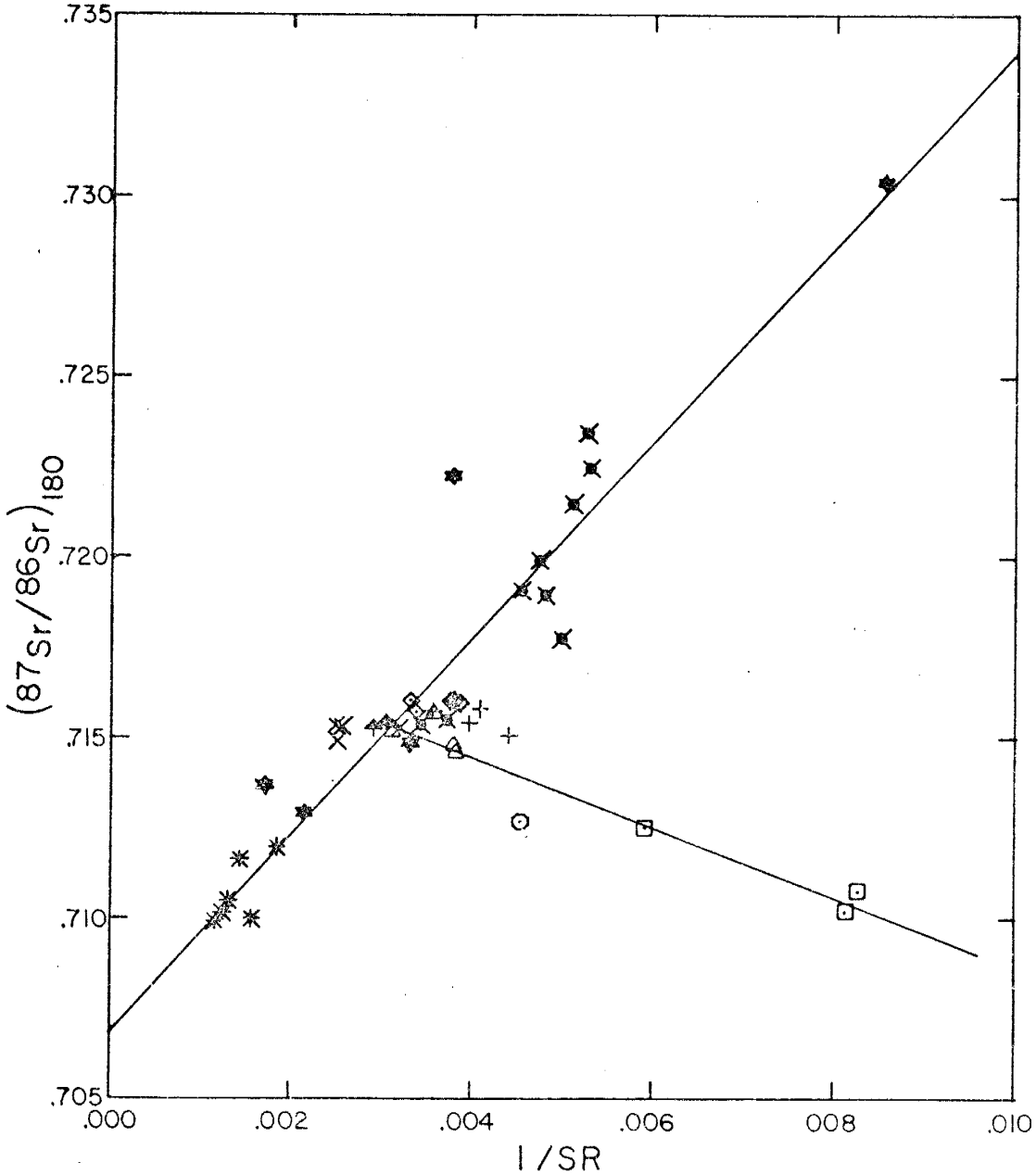

- Basalt
- High–K Basaltic Andesite
- High–K Andesite
- High–K Dacite
- High–K Vitrophyrite Dacite
- High–K Rhyolite
- Vitrophyric Rhyolite
- Mt. Rich Granite
- Leucocratic Granite
- Carlyon Granodiorite

Figure 16: Mixing diagram for samples of the BRIC and local Paleozoic basement rocks.

other elements are given in Table 6. The calculated basalt end member compositions, an average tholeiite (Manson, 1967), and a high MgO chilled margin from a Ferrar Dolerite sill (Kyle personal commun., 1982) are presented in Table 8 for comparison.

Basalt End Members

Calculated compositions for the basalt end members are strikingly similar to those given by Manson (1967). However the 0.709 end member exhibits a better correlation with respect to MgO, CaO, and Na_2O concentrations. In contrast, the 0.704 end member shows better correlation with the chilled margin of a Ferrar Dolerite sill, thought to be a possible primitive composition for the Ferrar Supergroup. Thus, major element compositions do not appear to constrain the more favorable composition. However, trace element concentrations, especially that of Sr, do place constraints on the range of compositions.

The compositions suggested by Faure et al. (1974,1979), and averages presented by Manson (1967), imply that a Sr concentration of 68 ppm for the 0.704 end member is excessively low. Faure noted that basalts of approximately 100 ppm Sr were unusually low compared to other Ferrar Supergroup rocks. Thus it would appear that the 0.704 end member represents unreasonable elemental compositions and isotopic compositions to be consistent with the binary

Table 8; Calculated concentrations for B-HKBA-HKA mixing line end members. An average tholeiite (1) (Manson, 1967), and a high MgO chilled Ferrar Dolerite sill (2) margin are given for comparison with the calculated basalts. An average of eight Carlyon Granodiorite (3) samples (Felder, 1980) is presented for comparison with the calculated contaminant.

End Member Compositions

	Basalt		1	2	Contaminant	3
87Sr/86Sr0	0.704	0.709	---	---	0.7153	0.7188
SiO2	49.78%	52.59%	51.1%	51.42	69.66%	69.15%
TiO2	0.70	0.67	1.6	0.48	0.51	0.54
Al2O3	16.08	15.79	16.2	15.97	14.08	14.43
FeO*	10.79	9.73	10.4	8.15	3.31	4.16
MnO	0.18	0.17	0.17	0.14	0.07	0.07
MgO	8.27	7.17	6.2	8.68	0.54	0.99
CaO	13.60	11.96	9.9	11.35	2.02	3.75
Na2O	1.50	1.74	2.5	1.40	3.21	2.84
K2O	-0.11	0.47	0.7	0.13	3.99	2.70
Total	100.79	100.29	98.77	0.03	97.39	98.63
Sc (ppm)	49.45	43.22	---	---	5.52	---
Cr	242.9	205.9	---	---	-18.4	---
Rb	---	---	---	---	---	---
Sr	68	104	---	---	322	227
Cs	0.002	0.55	---	---	3.88	---
Ba	144	188	---	---	722	---
La	3.62	8.44	---	---	37.66	---
Ce	10.88	20.14	---	---	76.23	---
Sm	1.96	2.58	---	---	5.31	---
Eu	0.73	0.77	---	---	1.02	---
Tb	0.51	0.57	---	---	0.95	---
Yb	2.13	2.28	---	---	3.18	---
Lu	0.54	0.52	---	---	0.36	---
Hf	1.78	2.40	---	---	6.12	---
Ta	0.29	0.48	---	---	1.63	---
Th	0.26	2.27	---	---	14.46	---

mixing model. The 0.709 end member poses reasonable major and trace element compositions which define an acceptable end member. The whole rock and mineral $\delta^{18}O$ values of BRIC basalt sample (80394) are +6.0‰ and +5.9‰ respectively, suggesting that it is probably very close to the mantle composition.

The relative weight percentages of the contaminant (f values) in each of the mixing line samples (Table 9) calculated for both basaltic end members, indicates that the amount of contaminant especially in the HKA samples is unusually high. In light of this data, it appears that the basalt end member may have a Sr isotope composition significantly higher than 0.709. Therefore the basalt sample (80394) might be representative of uncomtaminated mantle-derived basalt. The f values calculated using the initial $^{87}Sr/^{86}Sr$ ratio of sample 80394 as the basalt end member give more plausible values. In consideration of these data, it would appear that even an initial $^{87}Sr/^{86}Sr$ ratio of 0.709 is too low for the basalt end member in the B-HKBA-HKA mixing relation, and that a ratio as high as 0.7108 may be more suitable.

Salic End Member

The calculated composition for the granite end member is compared with the average chemical analyses of eight Carlyon Granodiorite samples (Table 8). The average composition of these local Paleozoic basement rocks was

Table 9; Percent of contaminant (f) for samples of the B-HKBA-HKA mixing trend. Contaminant for each case has an initial 87Sr/86Sr ratio of 0.7153, and a Sr concentration of 322 ppm.

(87Sr/86Sr)0	Rock Type	0.704	0.709	0.7108
80394	B	.21	.08	.00
80631	B	.21	.09	.01
80675	B	.40	.31	.24
79014	HKBA	.60	.56	.49
80404	HKA	.77	.76	.71
80673	HKA	.76	.75	.70
79021	HKA	.84	.83	.79

chosen on the basis that the Carlyon was the most abundant rock type in the area, and that the average of the analyses would help to minimize chemical variability normally found in granitic intrusions.

The calculated end member has a higher K_2O and lower FeO, MgO, and CaO contents than the average Carlyon Granodiorite. Isotopic compositions show the calculated end member to possess a significantly lower initital $^{87}Sr/^{86}Sr$ ratio than the averge Carlyon Granodiorite (0.7153 compared to 0.7188), and a higher Sr concentration (322ppm compared to 227ppm). The data suggests that even though the calculated contaminant is similar to the major element composition of the Carlyon Granodiorite, the isotopic data shows marked differences which inhibit the direct use of the calculated contaminant as the salic end member. However, the close relationship between the salic end of the B-HKBA-HKA mixing line and the Paleozoic basement rocks does imply a convincing relation between the two. Considering the variability normally demonstrated in granitic intrusions it is reasonable to assume that the calculated salic end member is a good approximation to the contaminating material.

Implications

The constraints posed on the basaltic end member are in contrast to data and interpretations proposed by Faure (1981), Faure et al. (1972,1974,1979,1982). The proposed

initial Sr ratios are significantly higher, but exhibit similar Sr concentrations as well as overall elemental compositions. A number of questions are subsequently posed by the BRIC data. 1) Is the lowest initial $^{87}Sr/^{86}Sr$ ratio of the basalt group representative of the mantle or not, 2) What is the variability of the upper mantle with respect to Sr and oxygen isotopes and chemical compositions if the interpretations of a mantle with an initial $^{87}Sr/^{86}Sr$ ratio of 0.709 or greater is accepted, and 3) If the mantle source is 0.709 or higher, how did it get to such a high level.

Previous work by Faure et al. (1972, 1974) on Ferrar Supergroup rocks implied that "normal" mantle-derived basalts were defined by an initial $^{87}Sr/^{86}Sr$ ratio of 0.704 and Sr concentrations approaching 200ppm. At that time elevated Sr ratios were interpreted to be the result of crustal contamination. More recently (Hoefs et al., 1980) proposed that the initial Sr ratios of uncontaminated basalt ranged as high as 0.709. Kyle (1980) had proposed that the chemical variations seen in the Kirkpatrick Basalts analyzed by Faure were the result of differentiation.

The mixing relations shown at the BRIC are quite unique, in that such a model fit to a simple mixing model has not been previously documented. The data constrain the basaltic end member to an initial Sr ratio of at least 0.709, but it may possibly range as high as 0.711. This should be indicative of the upper mantle. The data indicate

the basaltic end member was probably derived from an enriched mantle source such as was suggested by Kyle (1980). This interpretation casts considerable doubt on the models previously proposed for the petrogenesis of the Ferrar Supergroup (Faure, 1982; Faure et al., 1972, 1974, 1979).

Petrogenesis of the Dacites and Rhyolites

Introduction

Several models could account for the chemistry of the dacites and rhyolites, initial $^{87}Sr/^{86}Sr$ ratios suggest that remelting of crustal material is the most plausible. $\delta^{18}O$ values are correlative with local Paleozoic basement rocks and initial Sr ratios exhibit crustal values. The rhyolites and dacites plot close to the salic end member of the binary mixing line. Therefore, the data poses an option for two partial melting models; 1) remelting or partially remelting of crustal rocks to form one batch of magma of dacite composition, which differentiates into a rhyolite composition by crystal fractionation, and 2) varying degrees of partial melting forming two separate batches of magma. Both models require contamination as seen by the presence of basic xenocrysts in the rocks. However, this contamination is considered minimal due to the near constant initial $^{87}Sr/^{86}Sr$ ratios. Regardless of the origin of the chemistry of the high-K dacite and high-K rhyolite groups, normative mineral compositions indicate the rocks originated at a shallow level. The vitrophyres associated with these groups

have been shown to be altered by some secondary process, but are considered to have a similar petrogenesis to the dacites and rhyolites.

Differentiation Model

REE data exhibit negative Eu anomalies which appear to increase when progressing from the dacites to rhyolites. Such variations could be interpreted to be the result of fractionation, of feldspar, and could also account for the systematic increase in $\delta^{18}O$ values. Inherent to this model however, is the necessity for constant initial $^{87}Sr/^{86}Sr$ ratios. Student ALT-test indicated that the initial Sr ratios of the dacites and rhyolites are different at the 99.4% confidence level. If differentiation is the main process affecting a partial melt of dacite composition, then some minor contamination must also occur in order to alter the initial Sr ratios.

Assimilation of country rock has been shown to be related to fractional crystallization (Taylor, 1980; DePaolo, 1981). The latent heat of crystallization during fractionation is used in dissolving and reacting with wall rock. Such a process might be present in the fractionation of a dacite melt ot a rhyolite, and explain the slight difference in the initial $^{87}Sr/^{86}Sr$ ratios. Figure 17 suggests that the data may be compatible with an assimilation-fractional crystallization model. The effect

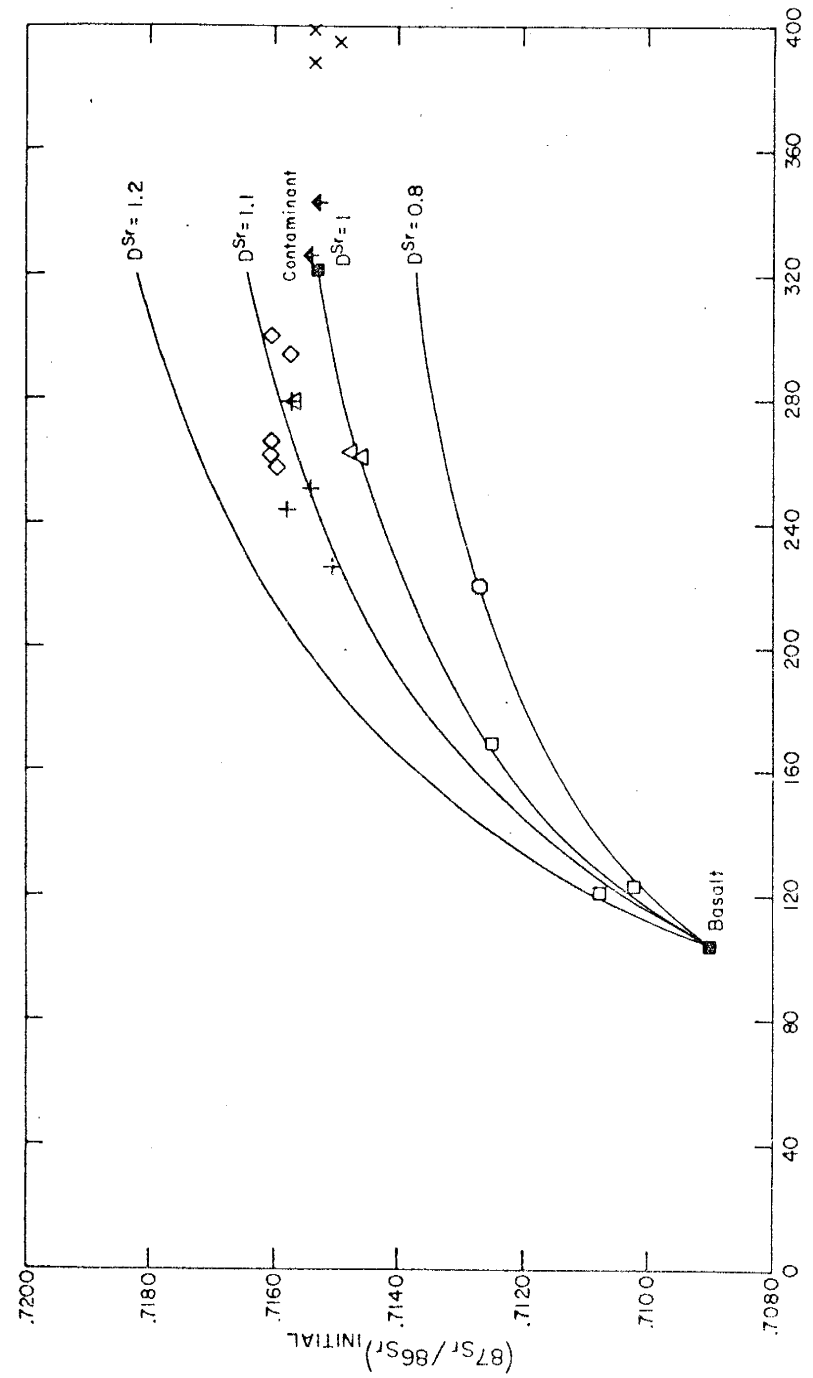

Figure 17: Combined assimilation-fractional crystallization mixing curves (DePaolo, 1981) for samples from the BRIC. Curves are constructed assuming a mass assimilated/mass cystallization ratio of 0.3 (Taylor, 1980), and differing values of the bulk solid/liquid partition coefficient (D) of strontium.

shown on the suggested mixing curve places the data where little change is seen in the initial Sr ratios. Equally possible is the process by which a partial melt of dacite composition is differentiated to form a rhyolite, and contaminated in varying degrees by basic material. Petrographic examination of the dacites showed them to possess basaltic xenocrysts in greater abundance than the rhyolites.

Variable Partial Melting

The Sr isotope compositions of the dacites is significantly different compared to the rhyolites. If these differences are not the result of contamination, which is petrographically present, then the dacites and rhyolites must represent two seperate partial melts with the rhyolites more closely approximating a total crustal remelt.

Comparison of the dacite and rhyolite compositions to the average local basement rocks (Carlyon Granodiorite) indicates these rocks are similar in composition, but not quite suitable as precursors. Differences in initial Sr ratios indicate other processes besides partial melting, such as significant contamination by basic material, would have to be present in order for rocks like the Carlyon Granodiorite to be involved. However, considering the variability normally found in granitic intrusions it is likely that a suitable precursor could exist.

Level of Melting

Figures 18 and 19 for samples of the HKD-HKVD and KHR-VR groups illustrate the normative SiO_2, albite, and orthoclase percentages. In both plots the crystalline rocks cluster about the orthoclase side of the one kilobar isobaric minimum. The one kilobar minimum corresponds to a depth of about 3.5 km. In light of the field relations, this suggests an extremely shallow level of intrusion, and is consistent with the hypabyssal nature of the Ferrar Dolerite Group. The deviation of the HKVD and VR groups from any of the granite minimums is consistent with their altered chemistry.

Implications

The petrogenesis of the dacite and rhyolite groups requires deviation from crustal rocks. The nature of this origin at present can not be discerned, although partial melting of Paleozoic granitic plutonic rocks to yield two separate magmas with minimal basaltic contamination is currently favored by the author. The depth at which these melts formed is significant in the fact that if the depth suggested by the isobaric minimum for melt formation is valid, unusual physical parameters especially with respect to heat must be present. Such information may shed light on the physical processes of not only melting of crustal rocks, but also the processes involved in assimilation.

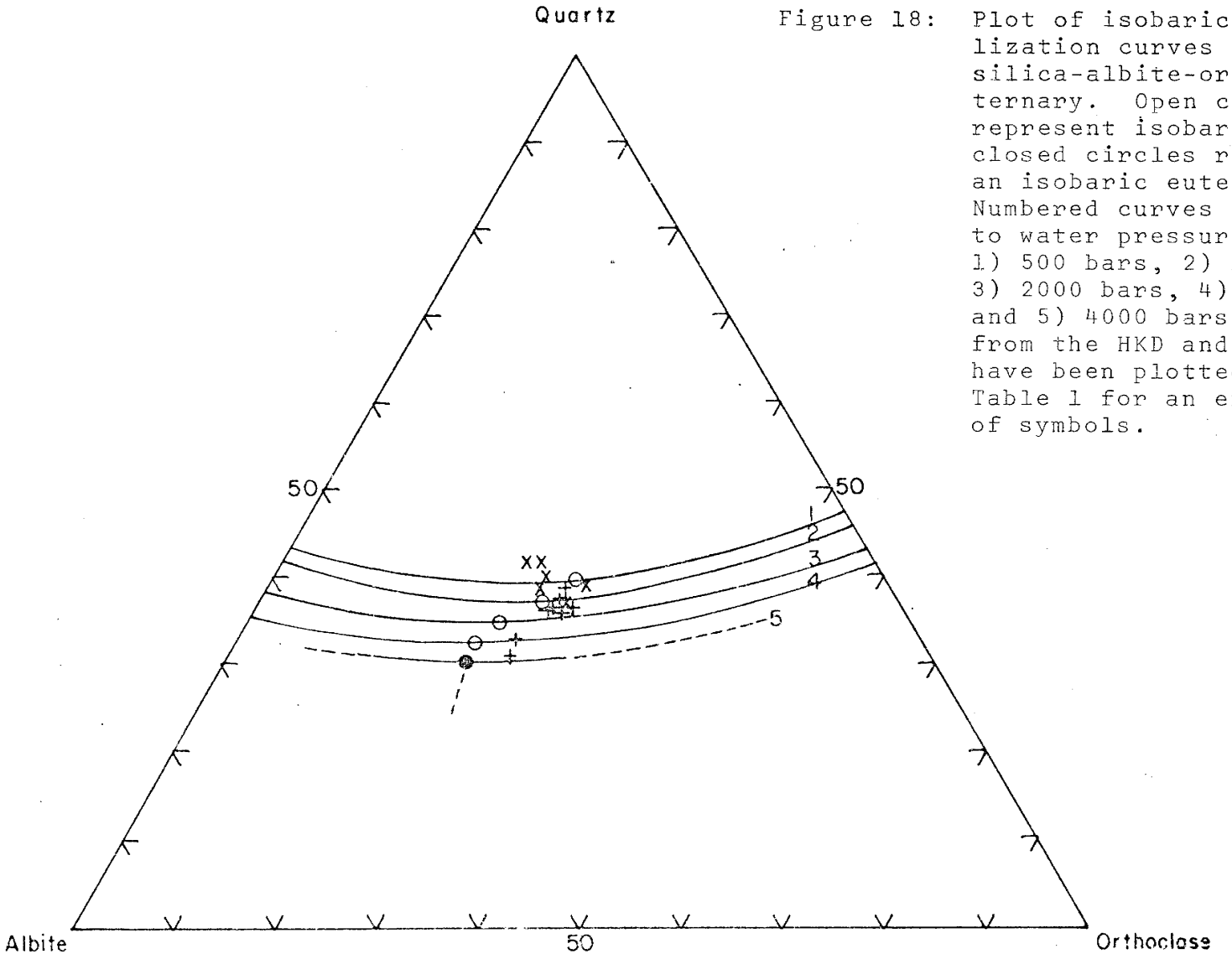

Figure 18: Plot of isobaric crystallization curves in the silica-albite-orthoclase ternary. Open circles represent isobaric minimum, closed circles represent an isobaric eutectic. Numbered curves correspond to water pressures of; 1) 500 bars, 2) 1000 bars, 3) 2000 bars, 4) 3000 bars, and 5) 4000 bars. Samples from the HKD and HKVD groups have been plotted. See Table 1 for an explanation of symbols.

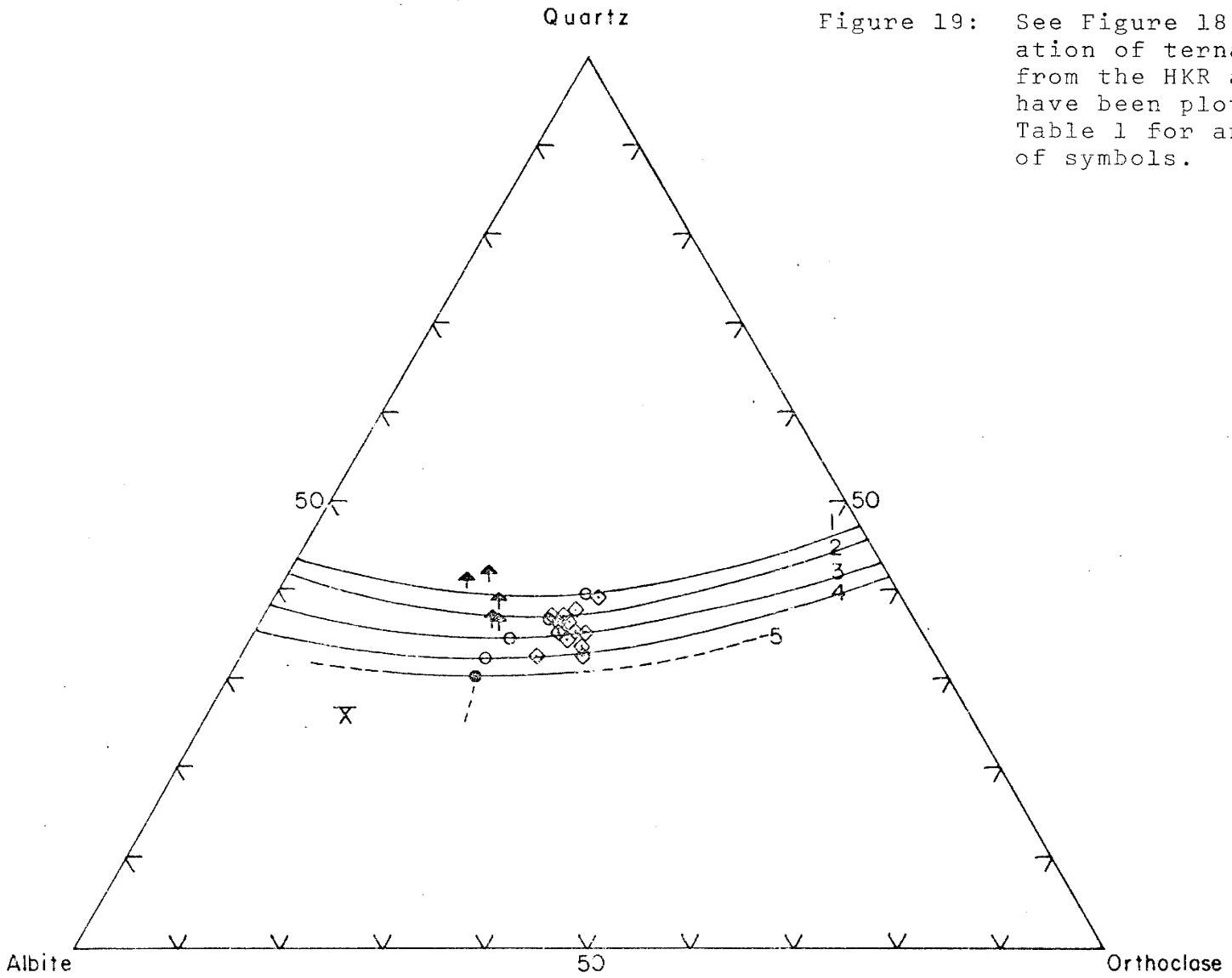

Figure 19: See Figure 18 for explanation of ternary. Samples from the HKR and VR groups have been plotted. See Table 1 for an explanation of symbols.

Trace Element and REE Criteria for Distinguishing Crustal Contamination

Although systematic variations in isotopic ratios are the best criteria for distinguishing crustal contamination, two recent models by Thompson et al. (1982) and Woods (1980) have attempted to use trace element abundances for this purpose. The applications and interpretations of these models have been somewhat speculative (Thompson et al.,1980). Binary mixing at the BRIC is well documented and presents an opportunity to test the models.

Thompson et al. (1982) used REE and other trace element data in an attempt to determine the extent of contamination on Hebridean Palaeocene magmas by Archean sial. Using chondrite normalized trace element plots, Thompson et al. (1982) suggested that the extreme relative depletion of incompatible elements in mantle derived magmas makes them sensitive to the addition of small amounts sial rich in these elements. Contamination of Hebridean Palaeocene magmas affected abundances of Ba, Rb, Th, K, Sr and LREE whilst having negligible affect on Nb, Ta, P, Zr, Hf, Ti, Y, and middle-heavy REE. In addition, Thompson et al. have suggested that some continental basalt suites, such as the Ferrar Supergroup described by Kyle (1980), exhibit crustal signatures in their incompatible element patterns.

Simple mixing as suggested by Faure (1974, 1979, 1980) and contamination of Ferrar rocks in general as suggested by Thompson et al. (1980) should be quite apparent in the BRIC rocks. In a chondrite normalized plot (Figure 20), the rock groups from the BRIC have been averaged and normalized with respect to chondrite (except Rb, K) and plotted on a trace element variation diagram identical to those used by Thompson et al. (1980). Unfortunately, trace element data for local granites and granodiorites were unavailable, thus the average composition for crust (Krauskopf, 1979) is used for comparison.

The patterns displayed in Figure 20 are in agreement with previous interpretations of mixing models. B, HKBA, and HKA group patterns all exhibit a crustal finger print with the B group possessing lower concentrations. Likewise, HKD, HKVD, HKR, and Vr group patterns are almost identical to the average crustal pattern. Except for the B group, all patterns display relative enrichment in Ba, Rb, Th, and, K. Such variatons were suggested by Thompson et al. (1980) to be resultant of sial contamination. However, LREE patterns were inferred to be subject ot similar enrichments, but are not shown in the BRIC patterns. La, Ce, and Sm display relative depletion compared to the average crust (Krauskopf, 1979). Some speculation is maintained though as the average crust is probably significantly different in composition from the contaminant present at the BRIC. In agreement with

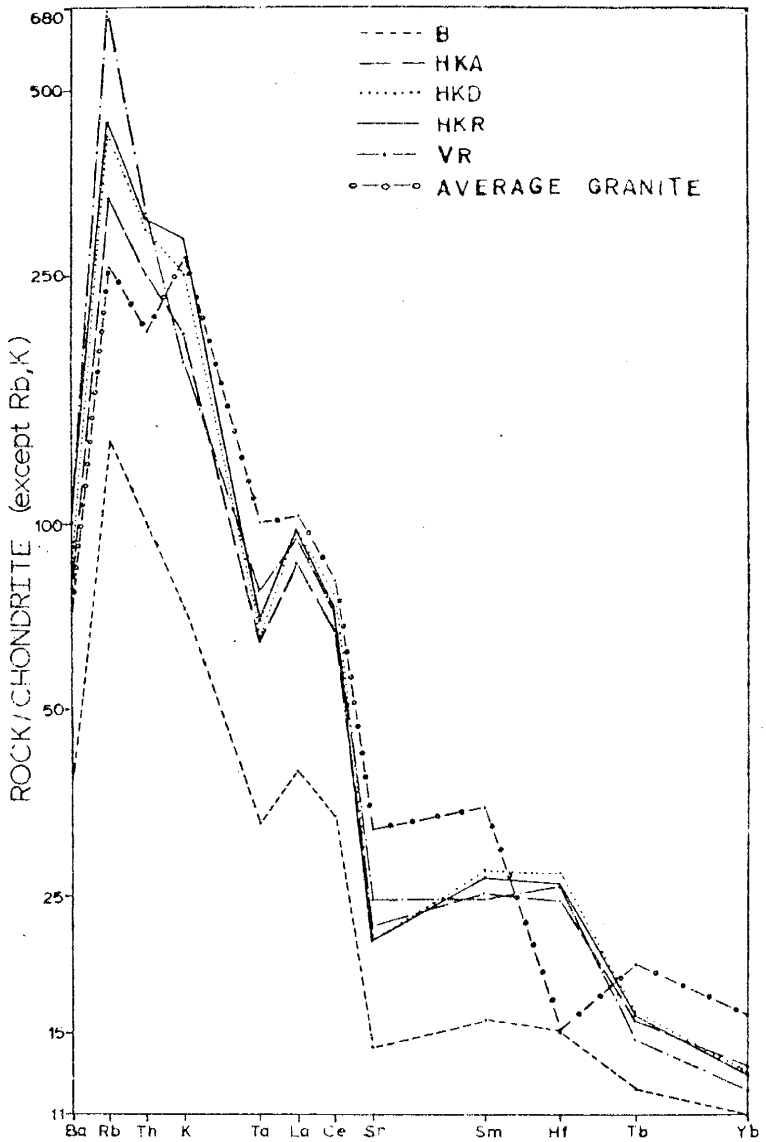

Figure 20: Chondrite normalized incompatible element patterns for samples of the BRIC and average crust (Krauskopf, 1979). Diagram is after Thompson et al. (1982).

observations by Thompson et al. (1980) the HREE and trace elements Ta and Sr do not exhibit as much crustal influence. Hf however, displays a negative correlation with respect to the average crust and may be due to differences in composition of local basement rocks and the average crust.

From Figure 20, it does appear that crustal influence is present in all of the rock groups at the BRIC. However, the exact nature of the process can not be discerned from this diagram. The relative enrichments of certain trace elements suggest that a process similar to that described by DePaolo (1981), where combined assimilation-fractional crystallization (AFC) could account for such a variation. It is clear though that the average crust presented by Krauskopf (1979) does not adequately define the end member from which to define the mixing process. However, the crustal signature displayed by the BRIC groups is significant and supports the model proposed by Thompson et al. (1980). Any further evaluaton of the model and its application to the BRIC samples seems dependent upon trace element and REE data from the Paleozoic granites.

The approach to tectonomagmatic discrimination and crustal assimilation using hygromagmatophile elements proposed by Wood (1980), Wood et al. (1979) implies an ability to discriminate between lower and upper crustal contamination in a variety of tectonic environments. The model is based on a triangular variation diagram of

coordinates Th-Hf/3-Ta. Two noted variations by Wood et al. (1979) which are pertinant to assimilation like that proposed for the BRIC are; 1) silicic magmas plot reasonably close to their basic parents allowing their discrimination, 2) crystal fractionation tends to push the residual liquid towards the Th apex.

Trace element data from the BRIC have been plotted on a "discrimination" diagram similar to that of Wood (1980) and are presented in Figure 21. Wood et al. (1979) suggests that crustal rocks and uncontaminated within plate basalts (WPB) occupy widely seperated fields, thus the diagram can be used to determine whether a particular WPB lava has been significantly contaminated during its passage through the crust. Assuming this information to be valid, one would expect to see a linear variation correlating samples from area B to area D (Figure 21). The data from the BRIC makes no such variation.

Applying the above interpretations for variations in the Th-Hf/3-Ta diagram, the small variation, displayed by the BRIC data would be solely interpreted as crystal fractionation of a calc-alkaline melt. The evidence for simple mixing between a within plate tholeiitic basalt and a crustal contaminant of calc-alkaline character appears overwhelming, and suggest that the model presented by Wood (1980), et al. (1979) does not adequately explain the processes present at the BRIC. However, the implication as

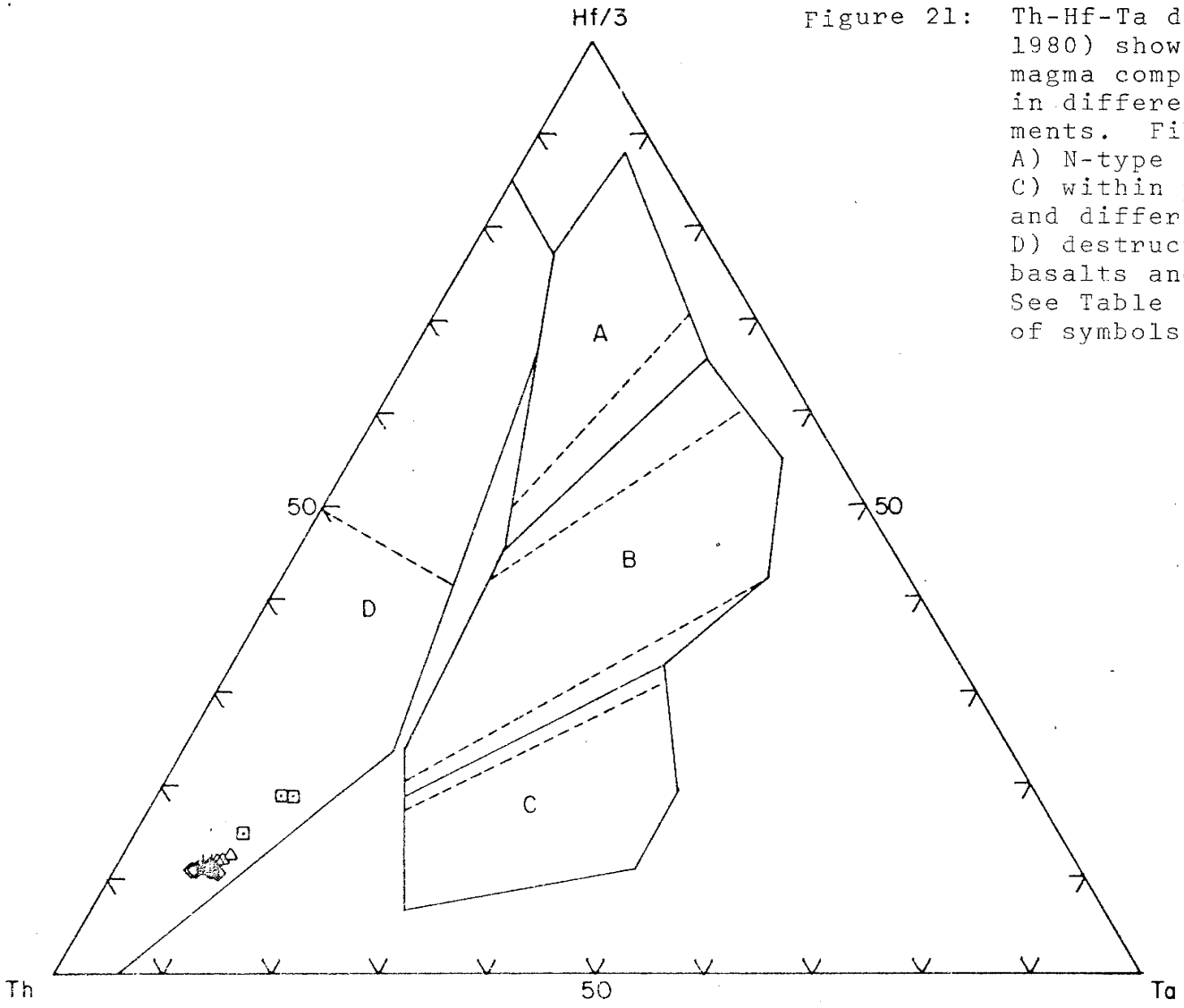

Figure 21: Th-Hf-Ta diagram (Woods, 1980) showing fields of magma composition erupted in different tectonic environments. Fields are as follows; A) N-type MORB, B) E-type MORB, C) within plate alkaline basalts and differentiates, and D) destructive plate-margin basalts and differentiates. See Table 1 for an explanation of symbols.

to fractional crystallization of the more silicic samples, if they are crustal remelts, could have significance.

The data presented in the previous discussion supports this interpretation and thus appears consistent. The fact that the model does not satisfactorally agree with the well defined simple mixing model suggests that its use as a model to define crustal contamination is limited and thus should be applied with caution. Consequently its use in discriminating lower and upper crustal contamination appears restricted to a few cases. Therefore, the use of this model as a tectonomagmatic discriminator is equally speculative. Samples from the BRIC are contained within what Wood (1980) has termed a destructive plate margin. Such a tectonic environment is in contrast to the continental back arc spreading zone currently accepted for Ferrar Supergroup rocks. Therefore, it would appear that this model does not have as broad applications as suggesed by Wood (1980), and is in need of further evaluation.

Mixing within a Regional Viewpoint

Several examples of assimilation by mantle-derived magmas have been presented for rocks of the Ferrar Supergroup (Faure, 1982; et al., 1974; Kyle et al., 1982) as well as the present study. Consequently, a question of how these different examples might be related, arises. Are the proposed contaminants for these contaminated suites of

rocks identical or are they different, possibly reflecting different crustal levels of contamination.

Rb-Sr isotope data from the BRIC, Gorgon Peak (Kyle et al., 1982), Storm Peak (Faure et al., 1974), and Mt Falla (Faure, 1982) clearly show evidence of some crustal assimilation. Mixing lines from each of these areas have been plot Figure 22 in the coordinates of initial $^{87}Sr/^{86}Sr$ ratios and their Sr concentrations. Normally, simple mixing as suggested by Faure (1977) should produce a hyperbolic relation in these coordinates. However, linear-regression analyses listed in Table 10 indicate that the variations fit better to a straight line than a hyperbolic function. Similarly, comparison of the r^2 values indicates a better fit than conventional initial $^{87}Sr/^{86}Sr$-$^{1}/Sr$ diagrams. Kyle et al. 1982 have suggested the unusual linear correlation of $^{87}Sr/^{86}Sr$ vs Sr might be due to data plotting very close to the basalt end member, and the limited range with which the data encompasses.

Aside from the unorthodox approach to interpreting the mixing processes, significant differences between the mixing lines are apparent. A possible interpretation is based on the type of crust involved and possibly the level of contamination. Paleozoic granites and granodiorites are much more common in the areas of the BRIC and Gorgon Peak. Furthermore, previously presented data implies an upper crustal origin for the more silicic members at the BRIC, and

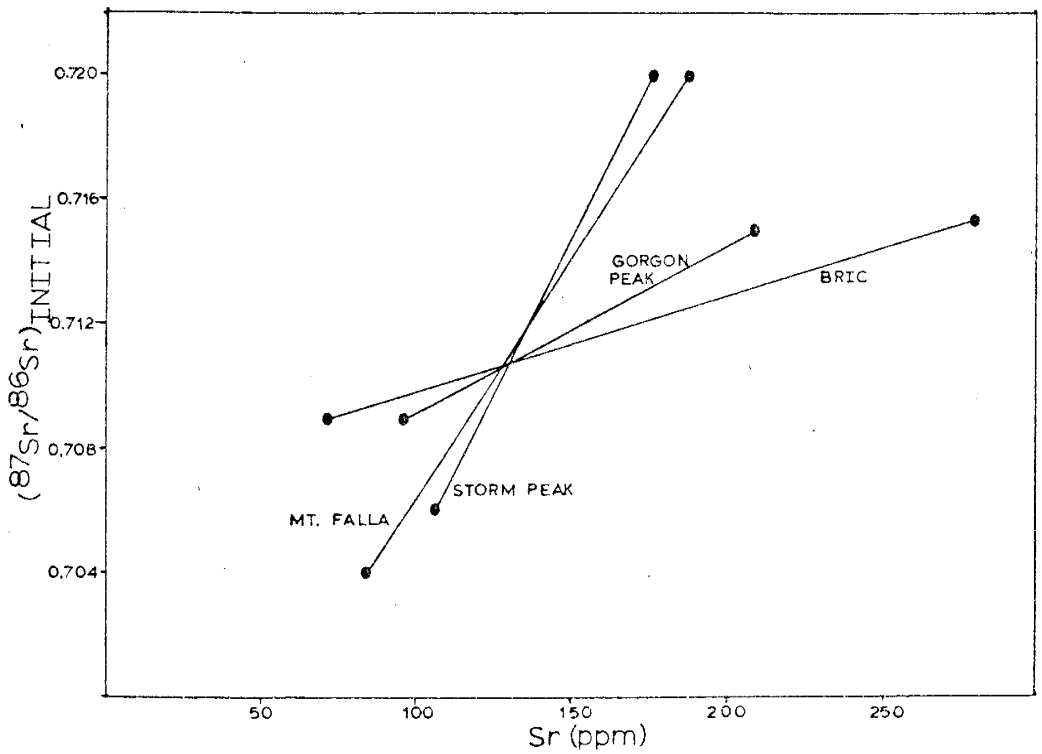

Figure 22: Plot of initial Sr ratios versus Sr concentrations for 4 suites of Ferrar Supergroup rocks believed to show evidence of contamination. See Table 10 for correlation coefficients. Data presented is from; BRIC (present study), Gorgon Peak (Kyle et al., 1982), Storm Peak (Faure et al., 1974), and Mt. Falla (Faure et al., 1982).

Table 10: Statistical comparison of Ferrar Supergroup proposed mixing lines in coordinates of initial Sr ratios and inverse Sr concentrations, and measured Sr ratios.

Initial Sr ratio versus Locality	N	D	1/Sr r	Sr(ppm) r^2
BRIC	7	0	0.904	0.949
Gorgon Peak	15	0	0.84	0.868
Storm Peak	12	3	0.669	0.713
Mt. Falla	14	6	0.662	0.689

N - Number of samples analyzed.
D - Number of samples deleted to produce best fit.
r - Correlation coefficient squared.

for the contaminant. In contrast, Storm Peak and Mt. Falla occur in an area where the basement consists predominantly of Pre Cambrian rocks. Pre Cambrian rocks would exhibit significantly higher initial $^{87}Sr/^{86}Sr$ ratios than the younger Paleozoic granites and granodiorites. The difference in initial Sr ratios might be manifested in the proposed contaminants seen in Figure 22. The implications from this diagram are still speculative, but the potential for discriminating the nature of the crust in mixing models suggested for Ferrar Supergroup rocks seems salient.

Chapter Six. Conclusion

Geochemical analyses of rocks from the White Apron Spur Section of the Butcher Ridge Igneous Complex indicate that several processes were involved in their petrogenesis. The rocks, ranging from tholeiitic basalts through rhyolites exhibit linear variations on oxide variation diagrams which can be interpreted either as a result of differentiation or crustal assimilation.

The mixing hypothesis is verified for the more mafic constituents by linear relations on a standard mixing diagram in the coordinates of initial $^{87}Sr/^{86}Sr$ ratios and the inverse Sr concentrations. Furthermore, the mixing relation is supported by linear relations on Sr-element plots which enable calculations of end member compositions. The more silicic constituents do not fall on this mixing trend and are interpreted to have formed by some other process.

The simple mixing relation manifested by the basalt through high-K andesite compositions define a lower limit for the basalt end member of 104 ppm Sr, and an initial $^{87}Sr/^{86}Sr$ ratio of 0.709. Oxygen isotope analyses of the basalt group samples exhibit $\delta^{18}O$ values slightly higher than those accepted for upper mantle compositions and thus support the calculated end member. The basalt end member element concentration is in agreement with other basalts from the Ferrar Supergroup which have been interpreted to be

the result of crustal assimilation. In light of this data, the constraints placed on end members by the BRIC data appear to be indicative of a heterogeneous mantle source.

The intersection of the mixing line with a linear trend, defined by local Paleozoic granites and granodiorites, located in the region, represents a probable salic end member. The elemental composition derived from such a contaminant defines a composition of 322ppm Sr and an initial $^{87}Sr/^{86}Sr$ ratio of 0.7153. This composition differs significantly from contaminants previously assumed contaminants of Ferrar Supergroup rocks. The close agreement beween the calculated composition of the contaminant at the BRIC and local Paleozioc basement complexes indicates that the difference seen in other Ferrar Supergroup rocks may reflect the age of the contaminant. The higher initial $^{87}Sr/^{86}Sr$ ratios proposed for other Ferrar Supergroup rocks indicate they might be the result of contamination by Pre Cambrian crust. The mixing relations shown by the BRIC data may reflect a shallower level of contamination within the crust, in contrast to a deeper level by the Pre Cambrian crust.

Limited variation in the initial $^{87}Sr/^{86}Sr$ ratios of the high-K dacite and high-K rhyolite group samples indicates they resulted from melting of crustal rocks to form a uniform melt. The deviation of these samples from the B-HKA mixing trend shows they are not part of the

basalt-high-K andesite mixing. Negative Eu anomalies may imply that fractionation of some mineral phase, probably feldspar, is responsible for some of the chemical variations exhibited. The similarity in elemental and isotopic compositions to local granites and granodiorites, and the fact that normative mineral assemblages in the silica-albite-orthoclase system imply a shallow level of formation, suggests an origin from the Paleozoic basement rocks by partial melting possibly accompanied by subsequent fractional crystallization.

The vitrophyres associated with these groups exhibit distinctive alkali and alkaline earth element variations, and trace element variations that suggests they have undergone prolonged secondary hydration, probably by meteoric groundwater. However, some of the variations in trace elements are not consistent with the variations produced by groundwater interaction, nor by any other known process. The vitrophyres are thus considered to have undergone a more complex history of alteration.

Assimilation of country rocks by ascending magmas has been a questionable model for a number of years. The variations exhibited at the BRIC are more consistent with the simple mixing model than any other documented study known at present, and thus represent an example by which to evaluate currently employed models, as well as other rocks of the Ferrar Supergroup.

Current mixing models indicate that simple mixing is not a common process, and that unusual excess heat requirements are necessary for it to occur. Voluminous tholeiitic activity during the Jurassic indicates that additional heat must have been present within the tectonic setting. The areal extent of the BRIC requires that either the volume of mantle-derived basalt be quite large, or that there was significantly higher heat flow than is normally expected. Since no evidence is available to support the elevated crustal temperatures, one must assume that the volume of mantle-derived basalt was quite large. The BRIC might represent the top of a large mafic intrusion such as the Dufek Intrusion.

The mixing relatons and crustal origins exhibited by the BRIC rocks are therefore unique compared to any previous interpretations for Ferrar Supergoup rocks. The above interpretations may help provide insight into mechanisms by which calk-alkaline rocks are generated. Likewise, the consistency with which the BRIC data fit the simple mixing model, and the chemical diversity displayed in comparison to previous work, is suggestive that simple mixing in most instances is evolved under unusual circumstances and does not adequately explain previous interpretations on Ferrar Supergroup rocks. Furthermore, the BRIC data show that assimilation of crustal material can not be modelled using

single systems, such as initial $^{87}Sr/^{86}Sr$ versus $^{1}/Sr$ plot but must incorporate a variety of information including trace elements and oxygen isotopes.

APPENDIX 1: PETROGRAPHIC DESCRIPTONS

Introducton

The following descriptions give detailed descriptions of individual thin sections. Mineral abundances were determined by visual estimates, no modal anlyses were made. Individual mineral compositions (such as an An content of plagioclase) were determined from extinction angles on twinned crystals and thus are only approximations. The most common technique employed was the Michel-Levy method.

As mentioned before, the rocks at the BRIC did not correspond to any formation names already used in the general area. Extrusive names have been retained here for sake of continuity. These names are by no way intended to indicate a mode of emplacement for the rocks at BRIC, but are indicative of the fine-grained and glassy textures seen in the rocks.

Basalts

80631

A fine-grained hypocrystalline subophitic basalt containing plagioclase, clinopyroxene, orthopyroxene, glass and disseminated opaques. Plagioclase occurs as laths and; is subhedral to anhedral, 0.5-1.2 mm in length, comprises 60% of the total rock, exhibits albite twinning and normal zoning, has a composition of An51 (Labradorite), shows secondary alteration to a mottled brown micaceous material and minor sericite, exhibits cellular morphologies (belt-buckle plagioclase) and (sub-fan spherulitic, open). Clinopyroxene (pigeonite) occurs as intergrowths with plagioclase and individual larger subpoikilitic phenocrysts and; is subhedral to anhedral, are 0.1-1.5 mm in length, comprise 25% of the total rock, show extensive secondary alteration to a greenish-brown material (possibly chlorophaeite) and a mottled brown micaceous material.

Orthopyroxene (enstatite) occurs as subpoikilitic intergrowths with plagioclase and smaller individual grains and; is subhedral to anhedral, is 0.1-1.0 mm in lenth, comprises 10% of the total rock, exhibits secondary alteration similar to that of pigeonite. Glass occurs as a brown interstitial filling containing microlites of alkali feldspar and opaques (possible magnetite) and comprises 5% of the total rock.

80394

A medium-grained hypocrystalline subophitic basalt containing plagioclase, clinopyroxene, orthopyroxene, glass, opaques, and minor calcite. Plagioclase occurs as laths and as spherulitic overgrowths, and; is subhedral to anhedral, is 0.2-1.5 mm in length, comprises 60% of the total rock, exhibits albite and carlsbad-albite twinning and normal zoning, has compositon of An54 (Labradorite), shows secondary alteration to sericite, exhibits cellular morphologies ranging from open to closed fan spherulites. Clinopyroxene (pigeonite) occurs as subpoikilitic phenocrysts and; is subhedral to anhedral, is 0.5-1.5 mm in length, comprises 20% of the total rock, is occasionally twinned on 100 and exhibits normal zoning, shows secondary alteration to a greenish-brown material (possibly chlorophaeite), exhibits some degree of prismatic skeletal quench textures. Orthopyroxene (enstatite) occurs as poikilitic phenocrysts and; is subhedral to anhedral is 0.5-3.0 mm in length, comprises 20% of the total rock, shows secondary alteration similar to that of pigeonite. Glass occurs as interstitial spherulites which have many cases altered to a greenish-brown material (chlorophaeite) and contain cryptocrystalline material. Disseminated opaques (magnetite) range up to 0.4 mm across and show dendritic quench textures. Calcite occurs as amygdaloidal fillings up to 0.5 mm across and are usually surrounded by rims of brownish-red alteration.

80675

Similar to 80394 except that the percentage of glass and carbonate is slightly higher and the pyroxenes have more extensive alteraton. Carbonate is present in xenoliths which also contain quartz and alkali feldspar.

Andesites

80404

A fine-to medium-grained hypocrystalline sub-intersertal andesite containing plagioclase, clinopyroxene, orthopyroxene, glass, opaques, and xenoliths. Plagioclase occurs as phenocrysts in both cellular morphologies and normal laths, and; is subhedral to anhedral, ranges 0.1-1.4

mm in lenth, comprises 50% of the total rock, occasionally exhibits Carlsbad twinning and normal zoning, has composition of An54 (Labradorite), shows secondary alteration to a mottled brown material. Cellular morphologies of plagioclase range from skeletal to dendritic to spherulitic forms. Skeletal forms are usually less than 0.5 mm in length. Dendritic forms vary from those filled with glass (tachylyte), to a aggregate of glass and feldspar (plagioclase). Spherulitic plagioclase occurs as overgrowths on previously formed laths. Plagioclase also occurs as spiked laths on larger dendrites which are highly altered. Lath shaped plagioclase exhibit a synneusis type mantled texture in larger grains. Clinopyroxene (probably pigeonite) occurs as phenocrysts and; is subhedral to anhedral, ranges 0.5-3.5 mm in lenth, comprises 15% of the total rock, is extensively altered to a reddish-brown oxide. Orthopyroxene (enstatite) occurs as phenocrysts and; is anhedral, ranges 0.2-2.5 mm in length, comprises 5-8% of the total rock, is altered extensively like pigeonite. Glass occurs as a interstitial filling between grains and within cellular morphologies of plagioclase. It is of the form tachylyte, scattered with cryptocrystalline opaques and possibly feldspars. It also occurs as spherulites and spherulitic overgrowths on plagioclase laths. It comprises up to 25% of the total rock and alters to a brownish-green material (chlorophaeite). Opaques occur principally as cryptocrystalline material within glass, but minor phenocrysts (up to 0.2 mm), probably magnetite, are present. In the cryptocrystalline material opaques seem to concentrate towards glass-grain boundaries, especially those associated with pyroxenes. Xenoliths are rounded, up to 2.0 mm across, and consist chiefly of quartz and K-feldspar. Within in xenoliths both quartz and K-feldspar are bi-modal in size. Some xenoliths also contain altered pyroxene.

80673

Similar to 80404 except that xenoliths are more abundant, and large portions of the rock appear to be covered with a brown oxide. Mantling textures on feldspars are not as prominent in this sample. Percentage of glass is probably only 20%, with a increase in the abundance of pyroxenes.

Dacite

80423

A fine-grined hypocrystalline dacite containing plagioclase, orthopyroxene glass, opaques, and xenoliths. Plagioclase occurs as microphenocrysts and; are anhedral, range 0.1 - 0.9 mm in length, comprise 35% of the total rock, exhibit minor carlsbad twinning and normal zoning, show compostion of An38 (Andesine), show secondary

alternation to a light brown micaceous mateial. Microphenocrysts all exhibit cellular mophologies ranging from skeltal to dendritic to acicular to spherulitic. Spherulitic plagioclase occurs both as open fan spherulites and as spherultic overgrowths on pre-exisiting laths. Orthopyroxene (probably bronzite) occurs as microphenocrysts and; are anhedral, range 0.1 - 1.0 mm in length, comprises 15-20% of the total rock, show secondary alteration to a brownish oxide material. Glass occurs prominently as a interstitial material resembling tachylyte. It comprises 35-40% of the total rock, contains cryptocrystalline material (probably feldspar), is altered to a greenish-brown material (probably chlorophaeite), and is often spherulitic. Opaques occur only as disseminated cryptocrystalline material within the glass. Xenoliths are comprised chiefly of highly altered orthopyroxene (probably bronzite) and plagioclase. Plagioclase occurs as microlites and as phenocrysts within the xenoliths. Minor amounts of glass are sometimes present in the xenoliths. In general they are finer grained than the surrounding rock with the border usually composed of microlites of plagioclase. Xenolith size varies from 0.1 mm - 5.0 mm. Bimodal grain size is present within the xenolith as plagioclse occurs as microlites and 0.2 mm xenolith phenocrysts. Medium-grain xenoliths of dendritic plagioclase rimmed by spikes of tabular plagioclase are also prominent. Together these two forms of xenoliths comprise 5-7% of the total rock.

80419

Similar to 80423 except that plagioclase totals about 45% of the rock.

79059

Similar to 80423 except that feldspar and pyroxene are 5-10% more abundant at the expense of glass. Xenoliths are far less abundant.

80663

Similar to 80423 except that pyroxene is slightly more abundant and alteration of glass and pyroxene is of a greater degree.

80665

Similar to 80423 except that glass is 5-10% less abundant, while plagioclase is more prevalent. Alteration of pyroxene is more abundant and xenoliths are not as common.

80669

Similar in mineralogy to 80423 but plagioclase comprises 55-60% of the rock while glass only comprises about 20%. Pyroxenes are almost completely altered to a reddish-brown oxide. Quench textures of plagioclase are not as enhanced as those of 80423.

79055

Similar to 80423 except that pyroxene averages slightly larger grain size and is probably 5-10% more abundant. A different form of xenoliths containing calcite and alkali feldspar are abundant. These xenoliths average 0.5-1.5 mm accross and show little or no evidence of disequilibrium with surrounding material. Some rounded pyroxenes show evidence of resorption. Spherulitic plagioclase appears to be absent.

80672

Similar to 80423 except glass only totals about 15-20% while plagioclase comprises 50-55%. Xenoliths similar to those described in 79055 are abundant.

Vitrophyric Dacite

80418

A fine-grained hypocrystalline vitophyric dacite containing plagioclase, clinopyroxene, orthopyroxene, glass opaques, and xenoliths. Plagioclase occurs as microphenocrysts and; are subhedral to anhedral, range 0.1-1.0 mm in length, comprise 35% of the total rock, rarely exhibit carlsbad twinning, are often normally zoned, exhibit secondary alteration to a greenish-brown material. Microphenocrysts all exhibit some form of cellular morphology ranging from skeletal to dendritic to acicular to spherulitic. Clinopyroxene and orthopyroxene occur as microphenocrysts and; are anhedral, average 0.2 mm in length, comprise 5% of the total rock, exhibit severe secondary alteratin to a greenish-brown material. Glass comprises the matrix and totals 50-55% of the total rock. It is impregnated with disseminated opaques and cryptocrystalline material. Opaques within the glass appear to concentrate near glass-grain boundaries. Pyroxene microlites within glass exhibit a glass corona free of cryptocrystalline material. Opaque microlites in the glass, but a few microphenocrysts (up to 0.1 mm) are present. Xenoliths are similar to those described in 80423.

80664

Similar to 80418 except that xenoliths are less common and zeolite is present as vogue fillings.

80668

Similar to 80418 except grain size indicates a fine-to-medium-grained average applies. Plagioclse is somewhat more abundant at the expense of the glass. Pyroxene might average 5% higher also. Xenoliths and zeolites are slightly more prevalent.

80671

Similar to 80418 except that grain size of feldspar and pyroxene the rock is fine-to-medium grained. Plagioclase is 5-10% more abundant and pyroxene is relatively unaltered compared to other dacite vitrophyres. Orthopyroxene appears to be hypersthene while clinopyroxene appears to be augite.

Rhyolites

80306

A fine-grained hypocrystalline rhyolite containing plagioclase, orthopyroxene, glass, opaques and xenoliths. Plagioclase occurs as microphenocrysts and; are subhedral, range 0.05-1.2 mm in length, comprise 55% of the total rock, occasionally exhibit carlsbad twinning, show both normal and oscillatory zoning, has composition ~ An3 (albite), exhibits relatively little secondary alteration. Almost all of the microphenocrysts of plagioclase exhibit textures indicative of quenching, ranging from skeletal to spherulitic, with spherulitic being the most prominent. Orthopyroxene (probably bronzite) also occurs as microphenocrysts and; are anhedral, range 0.1-1.0 mm in length, comprise 10% of the total rock, show extensive secondary alteration to a reddish-brown material. Glass occurs as the matrix and is relatively fresh but is impregnated with disseminated opaques and cryptocrystalline material (probably alkali feldspar). Glass matrix comprises up to 30% of the total rock. Xenocrystic plagioclase characterized by dendritic shaped resorption textures is abundant (up to 5%) and in many cases retains remnant twinning. Some xenocrysts exhibit epitaxial overgrowths of spiked-dendrite plagioclase. Xenocrysts average 1-3.5 mm across.

80307

A fine-grained hypocrystalline rhyolite containing plagioclase, orthopyroxene, glass, opaques, and xenoliths. Plagioclase occurs as microphenocrysts and; are subhedral

to ahhedral, range 0.05-1.0 mm in length, comprise 60-70% of the total rock, are rarely twinned (carlsbad), exhibit normal and oscillatory zoning, have composition ~ An8 (albite), show relatively little secondary alteration. Plagioclase is usually spherulitic and cryptocrystalline in nature often appearing to compose the majority of the matrix. The microphenocyrsts are present in cellular morphologies usually as spiked-laths and dendrites. Orthopyroxene (probably bronzite) also occurs as microphenocrysts and; are anhedral, range 0.1-1.0 mm in length, comprise 15% of the totl rock, show extensive secondary alteration to a reddish-brown material. Glass occurs as a minor interstitial filling (< 2%) and contains disseminated opaques. Minor occurences of opaques as microphenocrysts up to 0.1 mm are present. Xenoliths of calcite, quartz, feldspar, and zeolite up to 4.5 mm across are present. Xenocrysts of plagioclase identical to those found in sample 80306 are present. Xenoliths and xenocrysts comprise up to 15% of the total rock.

80308

Similar to 80307 except that the amount of xenoliths is greatly reduced.

80315

Similar to 80307 except that veins of zeolite (probably pumpellyite) are present. Zeolite is also seen to rim infillings of vogues that are cored by a red-brown opaque (probably hematite).

79037

Similar to 80306 except that glass is altered in some places to a yellowish-green material.

79046

Similar to 80307.

79050

Similar to 80306 except that glass is slightly more altered to a greenish material (probably chlorophaeite). Plagioclase is more like that in 80307 in texture.

80324

Similar to 80307. Plagioclase is slightly more cryptocrystalline. Glass is usually altered to a greenish-brown material (chlorophaeite). Xenoliths are much less common than 80307.

80325

Similar to 80307.

80410

Similar to 80306 except that pyroxene is slightly more abundant, but is altered to a greater extent. Xenoliths of calcite, quartz, zeolite, and feldspar are absent, but xenocrystic plagioclase is more abundant.

Vitrophyric Rhyolites

80323

A fine-grained hypocrystalline vitrophyric rhyolite containing plagioclase, orthopyroxene, clinopyroxene, glass, opaques, and xenocrysts. Plagioclase is present as microphenocrysts and; are subhedral to anhedral, range 0.1 to 1.0 mm in length, comprise 45% of the total rock, exhibit carlsbad twinning and normal zoning, have compositions ~ An10 (albite), show relatively little secondary alteration. Plagioclase exhibits cellular morphologies (comb-like and spherulitic) indicative of severe quenching. Lesser degrees are evidenced by dendritic and skeletal textures which are also abundant. Orthopyroxene (probably hypersthene) occurs as microphenocrysts and; is subhedral to anhedral, ranges 0.1 to 1.0 mm in length, comprises 5% of the total rock, shows relatively no secondary alteration. Clinopyroxene (probably augite) also occurs as microphenocrysts and; is subhedral, ranges 0.1 to 0.3 mm in length, comprises < 1% of the total rock, and shows relatively no secondary alteration. The matrix is composed of fresh glass which contains disseminated microlites of opaques. Glass comprises 45% of the total rock. Xenocrysts of plagioclase showing resorption textures average 0.1 to 2.0 mm across and comprise ~ 5% of the total rock, with a composition approximately that of Labradorite.

80313

Similar to 80323 except that infillings of zeolite (probably pumpellyite) up to 2.5 mm across are present and comprise 3-5% of the total rock.

79045

Similar to 80323 except that infillings of zeolite like those in sample 80313 are present and are surrounded by rims of a yellowish brown alteration. In addition, veins of zeolite are present with a similar alteration.

Hydrated Vitrophyric Rhyolite

80314

A fine-grained hypocrystalline hydrated rhyolite consisting of plagioclase, orthopyroxene, glass, opaques, and xenocrystic plagioclase. Plagioclase occurs as microphenocrysts and; are subhedral to anhedral, range 0.1 to 0.8 mm in length, comprise 40% of the total rock, exhibit carlsbad twinning and normal zoning, have composition ~ An10 (albite), and show marked secondary alteration to a brownish material. Plagioclase exhibits a variety of cellular morphologies like those in sample 80323. Pyroxene (orthopyroxene) is extremely altered to a yellowish-brown material, and comprises about 15% of the total rock. Glass is present as the matrix material, but is almost always altered to a greenish-brown material. It comprises approximately 35% of the total rock. Veins of zeolite like that in sample 79045 are present. Xenocrysts of plagioclase like those in sample 80323 are also present. A reddish-brown oxide material is present and appears to be concentrated about clusters of microphenocrysts. Opaques (probably magnetite) average 0.1 mm across and are scattered throughout the section.

Appendix 2

Major Element Analyses

Procedure

Major elements were analyzed at Victoria University of Wellington, New Zealand by x-ray fluorescence using the method of Norrish and Hutton (1969). 0.5 grams of sample was fused in a lithium borate flux containing La_2O_3 as a heavy absorber, then analyzed using standard procedures on an automated Seimens SRS-1 x-ray spectrometer. The system was calibrated using a wide range of rock standards from various sources.

Analytical Results

Major element analyses, and values recalculated loss free, are presented in Table A1. CIPW norms calculated for the average concentrations of each of the rocks are presented in Table A2.

Table A1: Major element analysis from the White Apron Ridge section of the Butcher Ridge Igneous Complex.

Sample	80631	80394	80399	80404	80401	80326	80403
Height(m)	1545	1607	1685	1690	1719	1760	1772
Field unit	Dac	Dac	Dac	La	La	Lag	Lag
SiO2	53.86	53.01	62.10	64.25	66.66	66.82	66.91
TiO2	0.61	0.64	0.57	0.56	0.54	0.52	0.52
Al2O3	15.26	15.69	14.74	14.33	14.33	14.28	14.29
FeO*	8.77	8.47	5.55	4.83	4.32	4.32	3.94
MnO	0.16	0.15	0.10	0.10	0.07	0.07	0.08
MgO	6.85	6.03	2.95	2.20	2.15	1.92	1.78
CaO	10.59	11.00	5.63	4.24	3.32	3.30	2.80
Na2O	1.94	1.73	2.73	2.85	2.77	3.48	3.39
K2O	0.79	0.85	2.61	2.87	3.41	3.38	3.37
P2O5	0.07	0.07	0.09	0.09	0.09	0.09	0.10
L.O.I.	1.02	0.96	2.52	2.60	2.39	1.88	2.99
TOTAL	99.92	98.90	99.59	98.92	100.05	99.87	100.17
INAA							
FeO	8.81	8.75	5.40	4.83	4.24	4.19	3.91
Na2O	1.96	1.84	2.86	3.14	3.02	3.41	3.75
			Recalculated to 100%				
SiO2	54.46	54.12	64.00	66.70	68.20	68.18	68.84
TiO2	0.62	0.65	0.59	0.58	0.55	0.53	0.54
Al2O3	15.43	16.02	15.18	14.88	14.67	14.57	14.70
FeO*	8.87	8.95	5.72	5.01	4.42	4.21	4.05
MnO	0.16	0.15	0.10	0.10	0.07	0.07	0.08
MgO	6.93	6.16	3.04	2.28	2.20	1.96	1.83
CaO	10.71	11.23	5.80	4.40	3.40	3.37	2.88
Na2O	1.96	1.77	2.81	2.96	2.84	3.55	3.49
K2O	0.80	0.87	2.69	2.98	3.49	3.45	3.47
P2O5	0.07	0.07	0.09	0.09	0.09	0.09	0.10
Rock type	B	B	HKA	HKA	HKD	HKD	HKD

*- All Fe is calculated as FeO

Table A1: Major element analysis from the White Apron Ridge section of the Butcher Ridge Igneous Complex.

Sample	80306	80307	79033	80308	79035	79036	79037
Height(m)	1778	1782	1786	1787	1793	1797	1800
Field unit	Rg	Rg	Rg	Rg	Rg	Rg	Rg
SiO2	70.18	70.94	70.90	70.69	70.01	69.68	70.80
TiO2	0.35	0.33	0.33	0.33	0.33	0.34	0.34
Al2O3	14.11	13.96	14.00	13.98	14.09	14.41	14.14
FeO*	2.56	2.30	2.31	2.42	2.43	2.44	2.31
MnO	0.08	0.04	0.07	0.06	0.02	0.06	0.02
MgO	0.95	0.87	0.82	0.95	0.95	0.94	0.89
CaO	2.24	2.24	2.09	2.01	2.15	2.20	2.00
Na2O	3.20	3.29	3.22	3.74	3.32	3.27	3.33
K2O	3.85	3.82	3.96	3.98	3.99	4.15	3.99
P2O5	0.05	0.05	0.04	0.06	0.06	0.05	0.06
L.O.I.	1.98	1.96	1.74	1.89	1.94	1.97	1.74
TOTAL	99.55	99.80	99.29	100.11	99.29	99.51	99.61
INAA							
FeO	2.45	2.32	2.27	2.31	-----	2.38	-----
Na2O	3.32	3.39	3.32	3.38	-----	3.45	-----
			Recalculated to 100%				
SiO2	71.93	72.51	72.54	71.97	71.92	71.44	72.34
TiO2	0.36	0.34	0.34	0.34	0.34	0.35	0.34
Al2O3	14.46	14.27	14.32	14.23	14.47	14.77	14.45
FeO*	2.62	2.35	2.36	2.46	2.50	2.50	2.36
MnO	0.08	0.04	0.07	0.06	0.02	0.06	0.02
MgO	0.97	0.89	0.84	0.97	0.98	0.96	0.91
CaO	2.32	2.29	2.14	2.05	2.21	2.26	2.04
Na2O	3.28	3.36	3.29	3.81	3.41	3.35	3.40
K2O	3.95	3.90	4.05	4.05	4.10	4.25	4.08
P2O5	0.05	0.05	0.04	0.06	0.06	0.05	0.06
Rock type	HKR	HKR	HKR	HKR	HKR	HKR	HKR

*- All Fe is calculated as FeO

Table A1: Major element analysis from the White Apron Ridge section of the Butcher Ridge Igneous Complex.

Sample	79045	79046	79048	79049	79050	80323	80324
Height(m)	1810	1811	1817	1821	1828	1830	1832
Field unit	Rg	Rg	Rg	Rg	Rg	Rg	Rg
SiO2	70.03	70.58	70.45	68.49	70.66	68.66	69.96
TiO2	0.31	0.32	0.33	0.33	0.33	0.33	0.33
Al2O3	14.29	14.23	14.25	14.02	14.11	13.98	13.97
FeO*	2.32	2.38	2.34	2.43	2.31	2.40	2.31
MnO	0.03	0.04	0.04	0.01	0.05	0.05	0.03
MgO	0.78	0.88	0.94	0.86	0.89	0.84	0.94
CaO	2.41	2.06	2.16	2.89	2.08	2.62	2.20
Na2O	3.79	3.21	3.19	3.36	3.17	3.63	3.15
K2O	2.95	4.26	4.05	2.40	4.19	2.23	4.04
P2O5	0.07	0.06	0.06	0.07	0.07	0.06	0.06
L.O.I.	3.07	2.05	2.20	4.74	1.98	4.37	2.29
TOTAL	100.05	100.07	100.01	99.87	99.84	99.17	99.28
INAA							
FeO*	-----	-----	-----	-----	-----	2.35	2.38
Na2O	-----	-----	-----	-----	-----	4.02	3.37
Recalculated to 100%							
SiO2	72.21	72.01	72.03	72.00	72.21	72.43	72.13
TiO2	0.32	0.33	0.34	0.35	0.34	0.35	0.34
Al2O3	14.73	14.52	14.57	14.74	14.42	14.75	14.40
FeO*	2.39	2.43	2.39	2.55	2.36	2.53	2.38
MnO	0.03	0.04	0.04	0.01	0.05	0.05	0.03
MgO	0.80	0.90	0.96	0.91	0.91	0.89	0.99
CaO	2.49	2.10	2.21	3.04	2.13	2.76	2.27
Na2O	3.91	3.27	3.26	3.82	3.24	3.83	3.25
K2O	3.04	4.35	4.14	2.52	4.28	2.35	4.17
P2O5	0.07	0.06	0.07	0.07	0.07	0.06	0.06
Rock type	VR	HKR	HKR	VR	HKR	VR	HKR

*- All Fe calculated as FeO

Table A1: Major element analysis from the White Apron Ridge section of the Butcher Ridge Igneous Complex.

Sample	79052	80325	80410	80418	80419	79059	80423
Height(m)	1833	1834	1844	1860	1864	1866	1868
Field unit	Rg	Rg	Rg	Rg	Rg	Rg	Rg
SiO2	70.54	70.51	68.67	66.93	67.11	67.23	66.76
TiO2	0.33	0.34	0.40	0.43	0.43	0.40	0.42
Al2O3	13.93	14.09	13.96	14.05	14.28	14.16	14.06
FeO*	2.38	2.33	3.85	3.19	3.18	3.05	2.88
MnO	0.04	0.04	0.05	0.07	0.04	0.08	0.04
MgO	0.95	0.97	1.29	1.38	1.35	1.47	1.06
CaO	2.05	2.13	2.60	3.53	2.64	2.64	3.21
Na2O	3.18	3.04	2.57	2.71	2.80	2.81	2.49
K2O	4.10	4.05	3.95	3.15	3.90	3.75	3.81
P2O5	0.07	0.06	0.08	0.08	0.08	0.07	0.08
L.O.I.	2.49	2.19	2.75	3.95	3.06	3.64	8.64
TOTAL	100.06	99.75	99.17	99.47	98.87	99.30	103.45
INAA							
FeO*	-----	2.33	2.90	-----	3.16	-----	-----
Na2O	-----	3.31	2.86	-----	3.08	-----	-----
Recalculated to 100%							
SiO2	72.30	72.27	71.23	70.08	70.04	70.28	70.41
TiO2	0.34	0.35	0.41	0.45	0.45	0.42	0.44
Al2O3	14.28	14.44	14.48	14.71	14.90	14.80	14.83
FeO*	2.44	2.39	2.96	3.34	3.32	3.19	3.04
MnO	0.04	0.04	0.05	0.07	0.04	0.08	0.04
MgO	0.97	0.99	1.34	1.44	1.41	1.54	1.12
CaO	2.10	2.18	2.70	3.70	2.76	2.76	3.39
Na2O	3.26	3.17	2.67	2.84	2.92	2.94	2.69
K2O	4.20	4.15	4.10	3.30	4.07	3.92	4.02
P2O5	0.07	0.06	0.08	0.08	0.08	0.07	0.08
Rock type	HKR	HKR	HKR	HKVD	HKVD	HKVD	HKVD

*- All Fe is calculated as FeO

Table A1: Major element analysis from the White Apron Ridge section of the Butcher Ridge Igneous Complex.

Sample	79038	79040	79042	80314	80313	79043	80315
Height(m)	1803	1804	1805	1806	1807	1808	1809
Field unit	Rg	Rg	Rg	Rg	Rg	Rg	Rg
SiO2	79.86	70.00	69.69	61.50	69.51	70.52	69.82
TiO2	0.33	0.32	0.33	0.33	0.35	0.32	0.32
Al2O3	13.91	14.36	14.23	15.59	14.01	14.18	14.04
FeO*	2.31	2.20	2.36	2.51	2.29	2.28	2.20
MnO	0.03	0.03	0.05	0.02	0.04	0.05	0.02
MgO	0.87	0.80	0.84	1.25	0.81	0.84	0.77
CaO	2.05	1.92	2.44	4.16	2.39	1.92	1.90
Na2O	3.16	3.31	3.73	3.06	3.59	3.28	3.12
K2O	4.09	4.62	3.05	2.05	2.88	4.53	4.41
P2O5	0.07	0.08	0.07	0.06	0.05	0.06	0.06
L.O.I.	2.05	2.57	2.92	10.00	2.96	2.01	1.93
TOTAL	99.73	100.21	99.71	100.55	98.85	99.99	98.59
INAA							
FeO*	-----	-----	-----	2.54	2.26	2.19	2.21
Na2O	-----	-----	-----	3.07	3.84	3.27	3.34
Recalculated to 100%							
SiO2	72.54	71.69	72.00	67.93	72.48	71.97	72.23
TiO2	0.34	0.33	0.34	0.39	0.33	0.33	0.33
Al2O3	14.24	14.71	14.70	17.22	14.61	14.47	14.53
FeO*	2.36	2.25	2.44	2.77	2.39	2.33	2.28
MnO	0.03	0.03	0.05	0.02	0.04	0.05	0.02
MgO	0.89	0.82	0.87	0.38	0.84	0.86	0.80
CaO	2.10	1.97	2.52	4.59	2.49	1.96	1.97
Na2O	3.24	3.39	3.85	3.38	3.74	3.35	3.23
K2O	4.19	4.73	3.15	2.26	3.00	4.62	4.56
P2O5	0.07	0.08	0.07	0.07	0.05	0.06	0.06
Rock type	HKR	HKR	VR	HYVR	VR	HKR	HKR

*- All Fe is calculated as FeO

Table A1: Major element analysis from the White Apron Ridge section of the Butcher Ridge Igneous Complex.

Sample	80663	80664	80665	79058	79056	80668	80669
Height(m)	1871	1872	1875	1878	1884	1885	1886
Field unit	Rg	Rg	Rg	Rg	Rg	Rg	Rg
SiO2	67.22	66.66	66.82	68.41	66.64	65.07	66.38
TiO2	0.45	0.45	0.46	0.42	0.44	0.46	0.47
Al2O3	14.40	14.09	14.22	13.94	14.12	13.93	14.06
FeO*	3.29	3.53	3.56	3.17	3.32	3.75	3.68
MnO	0.05	0.06	0.05	0.06	0.07	0.07	0.05
MgO	1.54	1.51	1.62	1.41	1.68	1.70	1.77
CaO	2.79	3.64	2.98	2.85	2.82	4.20	3.19
Na2O	2.71	2.77	2.77	2.84	2.75	2.50	2.88
K2O	3.59	3.16	3.54	3.76	3.59	2.79	3.43
P2O5	0.08	0.08	0.07	0.08	0.08	0.07	0.09
L.O.I.	3.70	3.62	3.14	2.73	4.02	4.62	3.13
TOTAL	99.82	99.57	99.23	99.67	99.53	99.16	99.13
INAA							
FeO*	3.25	-----	3.59	3.14	3.32	-----	3.73
Na2O	2.94	-----	3.14	3.01	2.97	-----	3.10
Recalculated to 100%							
SiO2	69.43	69.48	69.55	70.57	69.77	68.81	69.15
TiO2	0.47	0.47	0.48	0.43	0.46	0.49	0.49
Al2O3	14.98	14.69	14.80	14.38	14.78	14.73	14.65
FeO*	3.42	3.68	3.71	3.27	3.48	3.97	3.83
MnO	0.05	0.06	0.05	0.06	0.07	0.07	0.05
MgO	1.60	1.57	1.69	1.45	1.76	1.80	1.84
CaO	2.90	3.79	3.10	2.94	2.95	4.44	3.32
Na2O	2.82	2.89	2.88	2.93	2.88	2.64	3.00
K2O	3.73	3.29	3.68	3.88	3.76	2.95	3.57
P2O5	0.08	0.08	0.07	0.08	0.08	0.07	0.09
Rock type	HKD	HKVD	HKD	HKD	HKD	HKVD	HKD

*- All Fe is calculated as FeO

Table A1: Major element analysis from the White Apron Ridge section of the Butcher Ridge Igneous Complex.

Sample	80671	79055	80672	80673	80675	79014	79021
Height(m)	1899	1900	1900	1927	1957	-----	-----
Field unit	DaA	DaA	DaA	DaA	DaA	La	Lag
SiO2	64.32	66.45	65.18	64.75	55.60	58.81	65.22
TiO2	0.49	0.44	0.49	0.52	0.64	0.64	0.50
Al2O3	14.16	14.11	14.13	14.03	14.56	14.65	14.44
FeO*	4.07	3.44	3.99	4.57	7.99	7.02	4.38
MnO	0.06	0.09	0.05	0.07	0.13	0.14	0.09
MgO	1.97	1.57	2.10	2.23	5.13	3.86	1.81
CaO	4.61	3.00	3.33	4.67	8.65	7.74	3.95
Na2O	2.50	2.83	2.72	2.56	2.02	2.63	2.89
K2O	2.52	3.67	3.31	3.07	1.41	2.01	3.45
P2O5	0.08	0.08	0.08	0.09	0.07	0.10	0.08
L.O.I.	4.61	3.67	3.88	2.30	2.14	1.70	2.72
TOTAL	99.39	99.35	99.26	98.46	99.34	99.30	99.53
INAA							
FeO*	-----	3.45	4.01	4.57	7.87	-----	-----
Na2O	-----	3.02	2.96	2.82	2.25	-----	-----
Recalculated to 100%							
SiO2	67.86	69.45	68.34	65.76	57.80	59.22	65.53
TiO2	0.52	0.46	0.51	0.53	0.67	0.64	0.50
Al2O3	14.94	14.75	14.81	14.25	15.14	14.75	14.51
FeO*	4.29	3.60	4.18	4.64	8.31	7.07	4.40
MnO	0.06	0.09	0.05	0.07	0.14	0.14	0.09
MgO	2.08	1.64	2.20	2.26	5.33	3.89	1.82
CaO	4.86	3.14	3.49	4.34	8.99	7.79	3.97
Na2O	2.64	2.96	2.85	2.60	2.10	2.65	2.90
K2O	2.66	3.84	3.47	3.11	1.47	2.02	3.47
P2O5	0.08	0.08	0.08	0.09	0.07	1.71	0.08
Rock type	HKVD	HKD	HKD	HKA	B	HKBA	HKA

*- All Fe is calculated as FeO

Table A2: CIPW norms calculated from the mean major element analysis of each rock group of the B.R.I.C., Antarctica.

Rock Type	B	HKBA	HKA	HKD	HKVD	HKR	VR
N	3	1	3	10	7	18	5
SiO2	55.42	60.18	66.22	69.22	69.45	72.00	72.23
TiO2	0.64	0.66	0.56	0.49	0.46	0.34	0.34
Al2O3	15.52	14.99	14.86	14.72	14.77	14.43	14.71
FeO*	8.41	7.02	4.83	3.66	3.41	2.43	2.36
MnO	0.15	0.14	0.09	0.06	0.07	0.04	0.04
MgO	6.14	3.95	2.38	1.78	1.59	0.94	0.86
CaO	10.32	7.92	4.78	3.11	3.82	2.16	2.66
Na2O	1.94	2.69	2.85	3.01	2.76	3.28	3.77
K2O	1.04	2.06	3.10	3.67	3.36	4.21	2.82
P2O5	0.07	0.10	0.09	0.09	0.08	0.06	0.07
	CIPW Norms (Weight Percent)						
Q	8.24	13.25	22.35	26.46	28.29	29.54	31.34
C	0.00	0.00	0.00	0.34	0.00	0.69	0.78
Or	6.15	12.15	18.32	21.69	19.83	24.88	16.65
Ab	16.43	22.77	24.11	25.47	23.36	27.79	31.94
An	30.57	22.75	18.62	14.87	18.01	10.31	12.75
Di	16.50	13.11	3.72	0.00	0.34	0.00	0.00
Hy	18.61	12.71	10.39	9.11	8.22	5.37	5.13
Mt	2.12	1.76	1.23	0.93	0.88	0.61	0.60
Il	1.22	1.24	1.06	0.93	0.88	0.65	0.65
Ap	0.17	0.24	0.21	0.20	0.19	0.14	0.16

*- Analyses were normalized using a Fe2O3/FeO ratio of 0.2 and calculated so that the totals equal 100%.

Appendix 3

Trace Element Analyses

The trace elements Sc, Cr, Rb, Sr, Cs, Ba, Hf, Ta, and Th including rare earth elements La, Ce, Sm, Eu, Tb, Yb, and Lu were determined at the Ohio State Nuclear Reactor Laboratory (NRL) using an INAA method similar to that of Laul (1977) and Jacob et al., (1977). Na2O and FeO data were also calculated for comparison with major element analyses and are listed accordingly. The analytical procedure was as follows.

Thirty-five unknown powder samples and eight standards, approximately 100 milligrams each, were sealed in separate ultra high purity silica glass vials and divided into two packages of equal size. The packages were irradiated in the University of Michigan Phoenix Memorial Reactor Laboratory for approximately forty hours at a flux of 1.0×10^{13} $ncm^{-2}s^{-1}$. Gamma rays emitted from the samples were counted using a Ge(Li) detector and a multichannel analyzer at the NRL for 2000 and 10,000 seconds, 7 days and 40 days after being irradiated respectively.

Accuracy of Results

Analytical accuracy can be assessed by comparing analyses of rock standards with analyses from other laboratories. Table 1 of Appendix 3 compares an average of data of 14 analyses of USGS granite standard G-2 made at

Ohio State University with two compilations on G-2. USGS standard basalt BCR was used for calibration, the assumed values are listed in Table A3. The agreements are generally within analytical precision.

Analytical Results

Table A4 lists the concentrations of rare earth elements and other trace elements analyzed for by neutron activation analysis.

Table A3: USGS standard BCR values assumed for calibration and comparison of concentrations of USGS standard (G-2).

	1	2		3	4
ppm	BCR	OSU-INAA	+%	Abbey	G+R(1977)
Sc	32.0	3.41	1.44	3.5	3.25
Cr	17.6	11	16.98	8	6.5
Rb	47.0	141	13.5	170	167
Sr	330	413	5.55	480	467
Sb	0.70	0.07	18.0	0.06?	0.07
Cs	0.95	1.30	6.78	1.4	1.34
Ba	675.0	1732	5.07	1900	1813
La	25.0	87.08	1.07	92	81.5
Ce	54.0	162	2.93	160	156
Sm	6.60	7.22	1.15	7.2	6.73
Eu	1.95	1.35	1.72	1.4	1.41
Tb	1.10	0.53	10.94	0.5?	0.43
Yb	3.40	0.76	14.46	0.86	0.77
Lu	0.50	0.10	15.4	------	0.11
Hf	5.20	8.43	3.27	8?	8.1
Ta	0.90	0.96	2.93	0.8?	0.90
Th	6.00	24.26	1.60	25	24.9
wt. %					
Na2O	3.27	4.07	1.41	4.06	------
FeO*	12.00	2.38	1.84	2.42	------

*- All Fe as FeO

1. USGS standard BCR values assumed for calibration.
2. USGS standard granite (G-2) determined at the Nuclear Research Laboratory, Ohio State University based on 14 separate analyses by numerous independent operators. Precision is indicated by the coefficient of variation at one standard deviation.
3. USGS standard granite (G-2) values recommended by Abbey (1980).
4. USGS standard granite (G-2) values recommended by Govindaraju and Roelandts (1977).

Table A4: Trace element analysis from the White Apron Ridge section of the Butcher Ridge Igneous Complex.

Sample	80631	80394	80399	80404	80401	80326	80403
Height(m)	1545	1607	1685	1690	1719	1760	1772
Field unit	Dac	Dac	Dac	La	La	Lag	Lag
Sc	40.5	39.0	19.8	16.0	12.9	13.1	11.4
Cr	217	157	60	40	32	30	35
Rb	36	42	110	115	130	152	132
Sr	129	172	274	238	272	212	220
Cs	0.77	0.87	3.39	3.46	4.24	4.36	3.47
Ba	196	269	484	568	618	608	630
La	10.2	11.6	25.9	29.7	31.8	32.1	33.1
Ce	23.5	26.0	53.7	61.0	66.9	66.8	66.6
Sm	2.74	3.00	4.81	5.32	5.70	5.60	5.78
Eu	0.78	0.80	0.93	0.97	0.97	0.98	0.97
Tb	0.58	0.63	0.75	0.88	0.87	0.88	0.92
Yb	2.22	2.45	2.91	2.95	2.99	2.96	2.95
Lu	0.50	0.52	0.44	0.40	0.42	0.46	0.43
Hf	2.56	2.87	4.58	5.19	5.53	5.57	5.53
Ta	0.53	0.64	1.24	1.34	1.40	1.52	1.21
Th	3.10	3.49	9.43	11.15	12.03	12.03	12.39
Rock type	B	B	HKA	HKA	HKD	HKD	HKD

Table A4: Trace element analysis from the White Apron Ridge section of the Butcher Ridge Igneous Complex.

Sample	80306	80307	79033	80308	79036	80314	80313
Height(m)	1778	1782	1786	1787	1797	1806	1807
Field unit	Rg	Rg	Rg	Rg	Rg	Rg	Rg
Sc	6.0	5.5	5.6	5.6	5.8	6.0	5.5
Cr	18	13.2	15.3	13.7	14.2	15.9	13.6
Rb	142	157	145	151	162	54	228
Sr	258	244	262	246	258	921	275
Cs	3.21	3.41	3.03	3.53	3.41	12.92	21.72
Ba	676	710	713	702	702	896	710
La	32.3	30.8	31.4	33.2	34.8	31.6	31.2
Ce	70.1	62.4	59.7	62.5	70.5	64.7	62.4
Sm	5.34	5.07	5.06	5.32	6.18	4.86	4.97
Eu	0.76	0.73	0.71	0.73	0.74	0.79	0.71
Tb	0.76	0.78	0.78	0.78	0.96	0.71	0.74
Yb	2.75	2.76	2.66	2.82	3.13	2.53	2.61
Lu	0.32	0.32	0.31	0.32	0.35	0.28	0.31
Hf	5.25	5.08	5.22	5.16	5.37	5.70	5.19
Ta	1.51	1.61	1.17	1.42	1.23	1.39	1.62
Th	12.90	12.58	13.00	12.96	13.38	14.48	13.28
Rock type	HKR	HKR	HKR	HKR	HKR	HYHKR	VR

Table A4: Trace element analysis from the White Apron Ridge section of the Butcher Ridge Igneous Complex.

Sample	79043	80315	80323	80324	80325	80410	80419
Height(m)	1808	1809	1830	1832	1834	1844	1864
Field unit	Rg	Rg	Rg	Rg	Rg	Rg	Rg
Sc	5.3	5.4	5.8	5.9	6.0	8.0	9.1
Cr	14.5	12.4	15.6	15.2	16.4	24.2	24.8
Rb	169	161	238	162	157	147	163
Sr	236	231	306	256	251	266	254
Cs	2.79	2.90	29.68	3.29	2.16	2.21	2.40
Ba	691	689	682	717	698	655	725
La	32.2	30.7	31.5	33.4	34.1	32.0	35.2
Ce	61.1	59.1	63.1	64.2	67.3	65.1	72.8
Sm	5.58	4.87	5.11	5.49	6.21	5.51	6.02
Eu	0.74	0.70	0.73	0.77	0.81	0.82	0.88
Tb	0.88	0.70	0.78	0.85	0.91	0.84	0.88
Yb	2.88	2.62	2.68	2.89	3.10	2.80	2.91
Lu	0.33	0.31	0.31	0.34	0.37	0.43	0.42
Hf	5.26	5.15	5.21	5.21	5.20	5.33	5.44
Ta	1.16	1.55	1.52	1.44	1.47	1.37	1.27
Th	13.17	13.19	13.24	13.33	13.14	12.64	12.77
Rock type	HKR	HKR	VR	HKR	HKR	HKR	HKD

Table A4: Trace element analysis from the White Apron Ridge section of the Butcher Ridge Igneous Complex.

Sample	80663	80665	79058	79056	80669	79055	80672
Height(m)	1871	1875	1878	1884	1886	1900	1900
Field unit	Rg	Rg	Rg	Rg	Rg	DaA	DaA
Sc	9.8	10.4	9.1	9.9	11.4	10.0	12.6
Cr	28.5	28.5	27.7	28	34	29	40
Rb	156	160	148	146	130	162	138
Sr	267	251	278	251	260	272	201
Cs	2.91	2.95	2.47	3.51	1.63	2.40	2.15
Ba	715	633	649	692	662	677	607
La	33.1	32.4	31.7	32.6	31.8	32.6	31.0
Ce	69.2	67.8	66.0	66.8	64.9	66.8	63.9
Sm	5.58	5.58	5.34	5.54	5.54	5.48	5.39
Eu	0.92	0.91	0.87	0.90	0.91	0.88	0.92
Tb	0.88	0.87	0.79	0.82	0.84	0.80	0.81
Yb	2.95	2.83	2.87	2.93	2.88	2.83	2.90
Lu	0.39	0.39	0.43	0.39	0.44	0.48	0.41
Hf	5.56	5.61	5.38	5.43	5.40	5.51	5.26
Ta	1.32	1.36	1.25	1.19	1.32	1.20	1.28
Th	12.99	12.88	12.51	12.90	12.32	13.08	11.74
Rock type	HKD	HKD	HKD	HKD	HKD	HKD	HKD

Table A4: Trace element analysis from the White Apron Ridge section of the Butcher Ridge Igneous Complex.

Sample	80673	80675
Height(m)	1927	1957
Field unit	DaA	DaA
Sc	15.4	33.1
Cr	46	141
Rb	126	64
Sr	276	197
Cs	2.45	1.57
Ba	583	345
La	29.6	17.0
Ce	60.6	36.9
Sm	5.23	3.74
Eu	0.93	0.86
Tb	0.82	0.68
Yb	2.90	2.59
Lu	0.42	0.46
Hf	5.01	3.48
Ta	1.30	0.79
Th	11.09	5.85
Rock type	HKA	B

Appendix 4

Rb-Sr Isotope Analyses

Procedure

Rb, Sr contents and $^{87}Sr/^{86}Sr$ ratios were determined by Dr. R. J. Pankhurst at the Institute of Geological Sciences, London, England. Rb and Sr contents were measured by x-ray fluorescence spectrometry. The Sr isotopic ratios were determined on a micromass 30 mass spectrometer. All errors were quoted as + 2 sigma. Initial $^{87}Sr/^{86}Sr$ ratios were calculated assuming a +0.5% eror in the $^{87}Rb/^{86}Sr$ ratio, a decay constant for ^{87}Rb of 1.42×10^{-11} yr^{-1}, and an age of 179+3.5 Ma.

Analytical Results

Results are listed in Table 4 (Chapter 4).

Oxygen Isotope Analyses

Procedure

Extraction of oxygen from silicates for oxygen isotope analyses were performed at the University of Utah Stable Isotope Laboratory using the oxidation reaction method (Baertschi and Silverman, 1950; Silverman, 1951; Clayton and Mayeda, 1963), with bromine pentafluoride (BrF_5) used as the oxidizing agent. The sample size range from 5 to 20 milligrams, but average about 10 milligrams. Grain size was between 140 and 120 mesh. To insure sample purity mineral samples were cleaned using acetone and doubly distilled water, and then hand picked with a camel hair brush, under a binocular microscope.

Following the cleaning of each sample, an accurately measured aliquot was placed in one of six solid nickel reaction vessels. After all six vessels had been loaded they were connected by adjustable valves to a common manifold. Each vessel was then individually opened to a vacuum created by a roughing pump to allow sealing of the teflon fittings which cover the connection between the reaction vessels and the manifold. Leak tests on each reaction vessel are performed every two to three hours along with periodic tightening of the vessel-manifold connection. This procedure was performed until the leak rate for each vessel was less than 10 millitorr per hour, and was usually established in twelve to sixteen hours.

After all six vessels had obtained a sufficient vacuum, approximately equal amounts of oxidizer was loaded into each vessel. This was acheived by placing a cold bath of liquid nitrogen about the vessel prior to opening each vessel to the common manifold containing the reagent. A pressure-temperature gradient created by the cold baths caused reagent transfer into the vessel, and was usually completed in three to five minutes. After each vessel had been loaded with reagent and the liquid nitrogen baths removed, the vessels were heated at 800 degrees centigrade for 16 to 18 hours with ceramic furnaces. After heating, the vessels were cooled and then individually opened to a glass extraction line under pressures of 10^{-5} to 10^{-7} millitorr. A small amount of the liberated O_2 gas, and usually a small amount of incondensible phases were able to expand into the glass line. The gases then passed through a series of U-shaped tubes suspended in liquid nitrogen cold baths in which condensible phases were removed.

After the O_2 gas filtered through the cold traps, it was passed over a group of carbon rods which were surrounded by a small ceramic furnace and heated to 800 degrees centigrade. The rate at which the O_2 gas was passed over the heated carbon was controlled by a valve located in front of the furnace, and was adjusted so as to keep the pressure of the O_2 gas in the line between 0.3 and 0.5 millitorrs. A glass finger immersed in liquid nitrogen helped draw the O_2 gas through the furnace to react with the heated carbon to

produce CO_2 which was subsequently frozen out in the cold finger. When the reaction of O_2 and the heated carbon was terminated the furnace temperature was reduced to 600 degrees centigrade. Reaction time usually lasted about fifteen minutes unless a large amount of incondensible phases were present. The liquid nitrogen bath was removed from the CO_2 cold finger allowing the gas to expand back through the ceramic furnace and into an isolated cold finger. A mercury filled manometer was used to measure the gas pressure, which was then compared to theoretical yields calculated from major element analyses. Experimental yields less than 94% of the calculated yields may be affected by fractionation and should be considered with speculation.

The CO_2 gas was transferred to a sample bottle and promptly sealed. The procedure was repeated for all six samples. The oxygen isotope analyses of the CO_2 gas was measured on a Micromass mass spectrometer relative to CO_2 from a standard. Results were reported as deviations permil relative to Standard Mean Ocean Water (SMOW). Deviations relative to SMOW were calculated using the following equation:

$$\delta^{18}O = \left[\frac{\left(^{18}O/^{16}O\right)_{sample} - \left(^{18}O/^{16}O\right)_{SMOW}}{\left(^{18}O/^{16}O\right)_{SMOW}} \right] \times 10^3 ‰$$

Analytical Accuracy

Accuracy of the results can be assessed by comparing several analyses of a standard with the accepted value for that standard. Comparison of 9 analyses of Tintic Quartzite are compared with the accepted value from a separate laboratory in Table A5.

Analytical Results

Table 7 (Chapter 4) lists the delta ^{18}O values calculated from the extracted O_2 gases.

Table A5: Comparison of 9 analyses of Tintic Quartzite with an accepted value determined from another laboratory. All values reported as per mil.

Date Analyzed	Delta-18	Accepted Value
6-29-81	+11.2	+11.9
6-29-81	+11.6	+11.9
7-8-81	+11.9	+11.9
12-18-81	+11.7	+11.9
1-22-82	+11.8	+11.9
2-28-82	+12.1	+11.9
4-23-82	+11.9	+11.9
4-23-82	+12.1	+11.9
4-23-82	+11.7	+11.9

Mean of analyses - 11.8.
Standard deviation - 0.2774.
Coefficient variation - 2.36%.

Appendix 5

Rb-Sr Mixing Theory in Two Component Systems

Two component mixing models can be used to evaluate the role of assimilation in the petrogenesis of suites of igneous rocks. The model has been appled to variation diagrams of ratio-ratio, ratio-element, and element-element types in an attempt to test for mixing and place constaraints on probable end members (Langmuir et al., 1977).

The general form of the mixing equation is a hyperbola: $Ax + Bxy + Cy + D = 0$, where x,y = general variables along the abscissa and ordinate respectively (Langmuir et al., 1977). The coefficients A,B,C, and D are a function of the type of plot used. The appropiate coefficients of the general mixing hyperbola for the three types of plots described above are derived in Vollmer (1976) and will not be presented here.

Applying these principles to Rb-Sr systematics, mixing between two components having different concentrations of strontium and different $^{87}Sr/^{86}Sr$ ratios can be expressed as a hyperbola. In coordinates of $(^{87}Sr/^{86}Sr)_M$ and Sr_M, the hyperbolic equation is of the form:

$$\left(\frac{^{87}Sr}{^{86}Sr}\right)_M = \frac{Sr_A Sr_B\left[\left(\frac{^{87}Sr}{^{86}Sr}\right)_B - \left(\frac{^{87}Sr}{^{86}Sr}\right)_A\right]}{Sr_M(Sr_A - Sr_B)} + \frac{Sr_A\left(\frac{^{87}Sr}{^{86}Sr}\right)_A - Sr_B\left(\frac{^{87}Sr}{^{86}Sr}\right)_B}{Sr_A - Sr_B}$$

where A and B represent the two end members and M represents

the mixture (Faure, 1977). This mixing hyperbola can be transformed into a straight line by plotting $(^{87}Sr/^{86}Sr)_M$ versus $^1/Sr_M$. As mixing of two components will produce a linear trend on such a plot, the goodness of fit of the data points is a test of the validity of the mixing hypothesis (Faure, 1977).

Calculation of the end members from such a plot requires that either the initial $^{87}Sr/^{86}Sr$ ratios or the Sr concentrations of each be known or assumed. As defined by Faure (1977), the mixture of two components in differing proportions can be specified by a parameter (f) defined as f=A/(A+B) where A and B represent the weights of the two components. The concentraton of any element X contaned in a mixture of two components A and B can then be expressed as a linear function:

$$X_M = f(X_A - X_B) + X_B$$

where X_M is a linear function of f (Faure, 1977). Using this relation and the concentrations of the end members, whether they be assumed or calculated from initial $^{87}Sr/^{86}Sr$ ratios on a mixing test plot, the percentage of each end member of a mixture can be derived.

Determination of end members and the mixing hypothesis can be tested further if major and trace element analyses are available. Compositions of the end members can be calculated to see if they are plausible. Mixing produces

straight lines on element-element plots (Langmuir et al., 1977), subsequently the X concentrations defined earlier can be plotted against major and trace element analyses. Likewise, a goodness of fit of the data points is an additonal test to the validity of the mixing hypothesis. Thus, if simple mixing is present, linear relationships will result on Sr-element plots. The end members compositions can be derived from regression analysis by solving for the elemental concentrations using the Sr concentrations of each end member.

REFERENCES

Abbey, S., 1980. Studies in standard samples for use in the general analysis of silicate rocks and minerals. Geostandards Newsletter 4, 163-190

Anderson, A.T., Clayton, R.N., & Mayeda, T.K., 1971. Oxygen isotope thermometry of igneous rocks. Journal of Geology 79, 715-729

Aramaki, S., & Lipman, P., 1965. Possible leaching of Na2O during hydration of volcanic glasses. Proceedings of the Japanese Academy 41, 467-470

Askin, R.A., Barrett, P.J., Cureen, S., & Young, G., 1971. Stratigraphic sequences of the Beacon Supergroup (Devonian and older (?) to Jurassic) in the Darwin Mountains, Antarctica. New Zealand Antarctic Research Programme (working group in geology). Victoria University of Wellington

Baertschi, P., & Silverman, S. R., 1950. The determination of the relative abundances of the oxygen isotopes in silicate rocks. Geochimica et Cosmochimica Acta 1, 317-328

Behrendt, J. C., Drewry, D. J., Jankowski, E., & Grim, M. S., 1981. Aeromagnetic and radio echo ice-sounding measurments over the Dufek Intrusion, Antarctica. Journal of Geophysical Research 86, 3014-3020

Brooks, C., & Hart, S. R., 1978. Rb-Sr mantle isochrons and variations in the chemistry of Gondwanaland's Lithosphere. Nature 271, 220-223

----- James, D. E., & Hart, S. R., 1976. Ancient Lithosphere: its role in young continental volcanism. Science 193, 1086-1094

Boyd, F. R., 1961. Welded tuffs and flows in the rhyolite plateau of Yellowstone Park, Wyoming. Geological Society of America Bulletin 72, 387-426

Clayton, R. N., & Mayeda, T. K., 1963. The use of bromine pentafluoride in the extraction of oxygen from oxides and silicates for isotope analysis. Geochimica et Cosmochimica Acta 27, 43-52

Compston, W., McDougall, I., & Heier, K. S., 1968. Geochemical comparison of the Mesozoic basalt rocks of Antarctica, South Africa, South America, and Tasmania. Geochimica et Cosmochimica Acta 32, 129-149

Coryell, C. D., Chase, J. W., & Winchester, J. W., 1963. A procedure for geochemical interpretation of terrestial rare-earth abundance patterns. Journal of Geophysical Research 68, 559

Cox, K. G., Bell, J. D., & Pankhurst, R. J., 1980. The Interpretation of the Igneous Rocks. London: Allen and Unwin, 450p

Craig, H., 1961. Standard for reporting concentrations of deuterium and oxygen-18 in natural waters. Science 133, 1833-1834

DePaolo, D. J., 1981. Trace elements and isotopic effects of combined wallrock assimilation and fractional crystallization. Earth and Planetary Science Letters 53, 189-202

Dowty, E., 1980. Synneusis reconsidered. Contributions to Mineralogy and Petrology 74, 75-84

Ehlers, E. G., 1972. The Interpretation of Geological Phase Diagrams. San Francisco: Freeman, 220p

Elliot, D. H., 1972. Major oxide chemistry of the Kirkpatrick Basalt, Central Transantarctic Mountains. International Union of Geological Sciences, Series B, (1), 413-418

---- 1974. The tectonic setting of the Jurassic Ferrar Group, Antarctica. International Association of Volcanology and Chemistry of the Earth's Interior, Proceedings of the Symposium on Andean and Antarctic Volcanology Problems, 1-16

Epstein, S., 1959. The variations of the 18O/16O ratio in nature and some geologic applications, in Researches in Geochemistry. (ed. P. H. Abelson), New York: Wiley and Sons, 217-240

---- & Taylor, H. P., 1967. Variation of 18O/16O in minerals and rocks in Researches in Geochemistry. (ed. P. H. Abelson) New York: Wiley and Sons 1, 217-240

Ewart, A., 1979. A review of the mineralogy and chemistry of Tertiary-Recent dacitic, latitic, rhyolitic, and related salic volcanics, in Trondhjemites, Dacites, and Related Rocks. (ed. F. Barker), Amsterdam: Elsevier, 13-121

Faure, G., 1977. Principles of Istope Geology. New York: Springer Verlag, 446p

---- 1981. Strontium isotope composition of volcanic rock: Evidence for contamination of the Kirkpatrick Basalt, Antarctica, in Geophysical-Geochemical Evolution of the Earth. (ed. W. S. Fyfe), 75-81

---- & Elliot, D. H., 1971. Isotope composition of strontium in Mesozoic basalt and dolerite from Dronning Maud Land. British Antarctic Survey Bulletin 25, 23-27

---- Hill, R. L., Jones, L. M., & Elliot, D. H., 1972. Isotope composition of strontium and silica content of Mesozoic basalt and dolerite from Antarctica, in Antarctica Geology and Geophysics. (ed. R. J. Adie), Oslo: Universitetsforlaget, 617-624

---- Bowman, J. R., Elliot, D. H., & Jones, L. M., 1974. Strontium isotope composition and petrogenesis of the Kirkpatrick Basalt, Queen Alexandra Range, Antarctica. Contribution to Mineralogy and Petrology 48, 153-169

---- Bowman, J. R., & Elliot, D. H., 1979. The initial 87Sr/86Sr ratios of the Kirwan Volcanics of Dronning Maud Land: comparison with the Kirkpatrick Basalt, Transantarctic Mountains. Chemical Geology 26, 77-90

---- Pace, K. K., & Elliot, D. H., 1982. Systematic variations of 87Sr/86Sr ratios and major element concentrations in the Kirkpatrick Basalt of Mt. Falla, Queen Alexandra Range, Transantarctic Mountains, in Antarctica Geology and Geophysics (Proceedings Volume, SCAR Symposium, Madison, Wisconsin). (ed. C. Craddock), 1172p

Felder, R. P., 1980. Geochronology of the Brown Hills, Antarctica. Ohio State University M.S. Thesis, 105p

Ford, A. B., 1976. Stratigraphy of the Dufek Intrusion, Antarctica. United States Geological Survey Bulletin 1405-D, 1-36

Friedman, I., & Smith, R. L., 1958. The deteurium content of water in some volcanic glasses. Geochimica et Cosmochimica Acta 15, 218-228

Garlick, G. D., 1966. Oxygen isotope fractionation in igneous rocks. Earth and Planetary Science Letters 1, 361-368

Govindaraju, K., & Roelandts, I., 1977. Neutron activation analysis of two USGS rock reference samples (Granite G-2, Andesite AGV-1) and discussion in light of compiled data. Geostandards Newsletter 1, 163-179

Grindley, G. W., & Laird, M. G., 1969. Geology of the Shackelton Coast, in Geologic Maps of Antarctica, Antarctic Map Folio Series, Folio 12, Plate 14. (ed. V. C. Bushnell & C. Craddock), New York: American Geographical Society

Gunn, B. M., & Warren, G., 1962. The geology of Victoria Land between the Mawson and Mulock Glaciers, Ross Dependency, Antarctica. New Zealand Geological Bulletin 71

Gunn, B. M., 1966. Modal and elemental variations in Antarctic tholeiites. Geochimica et Cosmochimica Acta 30, 881-920

Hamilton, W., 1965. Diabase sheets of the Taylor Glacier region, Victoria Land, Antarctica. United States Geological Survey Professional Paper 456-B, 1-72

Harker, A., 1909. The natural history of igneous rocks. New York: Macmillan, 312p

Harrington, H. J., 1958. Nomenclature of rock units in the Ross Sea, Antarctica. Nature 182, 105-121

Haskell, T. R., Kennett, J. P., & Prebble, W. A., 1965. Geology of the Brown Hills and Darwin Mountains, Southern Victoria Land, Antarctica. Transantarctic Royal Society of New Zealand 2, 231-248

Hibbard, M. J., 1981. The magma mixing origin of mantled feldspars. Contributions to Mineralogy and Petrology 76, 158-170

Hoefs, J., 1973. Stable Isotope Geochemistry. New York: Springer-Verlag, 140p

----- 1980. Stable Isotope Geochemistry. (2nd ed.) New York: Springer Verlag, 203p

---- Faure, G., & Elliot, D. H., 1980. Positive correlations of 18O and initial 87Sr/86Sr ratios of Kirkpatrick Basalt, Mt. Falla, Transantarctic Mountains. Contributions to Mineralogy and Petrology 75, 199-203

Jacobs, J. W., Korotev, R. L., Blanchard, D. P., & Haskin, L. A., 1977. A well-tested procedure for instrumental neutron activation analysis if silicate rocks and minerals. Journal of Radioanalytical Chemistry 40, 93-114

Krauskopf, K. B., 1979. Introduction to Geochemistry. (2nd ed.) New York: McGraw-Hill, 617p

Kyle, P. R., 1980. Development of heterogeneities in the subcontinental mantle: evidence from the Ferrar Group, Antarctica. Contributions to Mineralogy and Petrology 73, 89-104

---- Elliot, D. H., & Sutter, J. F., 1981. Jurassic Ferrar Supergroup tholeiites from the Transantarctic Mountains, Antarctica, and their relation to the initial Fragmentation of Gondwana. Gondwana V (ed. Cresswell, M., Vella, P.), 283-287

---- Pankhurst, R. J., & Bowman, J. R., 1982. Isotopic and chemical variations in Kirkpatrick Basalt Group rocks from South Victoria Land., unpublished, 15p

Langmuir, C. H., Vocke, R. D., Hanson, G. N., & Hart, S. R., 1977. A general mixing equation with application to Icelandic basalts. Earth and Planetary Science Letters 37, 380-392

Laul, J. C., 1979. Neutron activation analysis in geologic materials. Atomic Energy Review

Lipman, P. W., 1965. Chemical comparison of glassy and crystalline volcanic rocks. United States Geological Survey Bulletin 1201-D, D1-D24

---- Christiansen, R. L., & VanAlstine, R. E., 1969. Retention of alkalis by calc-alkalic rhyolites during crystallization and hydration. American Mineralogist 54, 286-291

Lofgren, G. E., 1971. Spherulitic textures in glassy and crystalline rocks. Journal of Geophysical Research 76, 5635-5648

---- 1974. An experimental study of plagioclase crystal morphology: isothermal crystallization. American Journal of Science 274, 243-273

---- 1980. Experimental studies on the dynamic crystallization of silicate melts, in Physics of Magmatic Processes. (ed. R. B. Hargraves), New Jersey: Princeton, 487-551

---- & Gooley, R., 1977. Similtaneous crystallization of feldspar intergrowths from a melt. American Mineralogist 62, 217-228

Manson, V., 1967. Geochemistry of basaltic rocks: major elements, in The Poldervaart Treatise on Rocks of Basaltic Composition. (ed. H. H. Hess & A. Poldervaart), New York: Interscience, 1, 215-269

Marshak, M., Kyle, P. R., McIntosh, W., Samansov, V., & Shellhorn M., 1980. The Butcher Ridge Igneous Complex: Part 1. Field Studies, Antarctic Journal of the United States 16, 54-55

Masuda, A., 1962. Regularities in variation of relative abundances of lanthanide elements and an attempt to analyze separation-index patterns of some minerals. Journal of Earth Sciences, Nagoya University 10, p173

McBirney, A. R., 1979. Effects of assimilation, in The Evolution of the Igneous Rocks, Fifthieth Anniversary Perspectives. (ed. H. S. Yoder), Princeton Press, 588p

Noble, D. C., 1965. Ground water leaching of sodium from quickly cooled rocks. (abstract) American Mineralogist 50, p289

----- 1967. Sodium, potassium, and ferrous iron contents of some secondarily hydrated natural silicic glasses. American Mineralogist 52, 280-286

Norrish, K., & Hutton, J. T., 1969. An accurate x-ray spectrographic method for the analysis of a wide range of geologic samples. Geochimica et Cosmochimica Acta 33, 431-453

Pecerillo, A., & Taylor, S. R., 1976. Geochemistry of some calk-alkaline volcanic rocks from the Kastamonu area, Northern Turkey. Contributions to Mineralogy and Petrology 58, 63-81

Ross, C. S., & Smith, R. L., 1955. Water and other volatiles in volcanic glass. American Mineralogist 40, 1071-1089

Silverman, S. R., 1951. The isotope geology of oxygen. Geochimica et Cosmochimica Acta 1, 26-42

Stull, R. J., 1979. Mantled feldspars and synneusis. American Mineralogist 64, 514-518

Sun, S. S., & Hanson, G. N., 1976. Rare earth element evidence for differentiation of McMurdo volcanics, Ross Island, Antarctica. Contributions to Mineralogy and Petrology 54, p139

Swanson, S. E., 1977. Relation of nucleation and crystal growth to the development of granitic textures. American Mineralogist 62, 966-978

Taylor, H. P., 1968. The oxygen isotope geochemistry of igneous rocks. Contributions to Mineralogy and Petrology 19, 1-71

---- 1971. Oxygen isotope evidence for large scale interaction between meteoric ground water and Tertiary granodiorite intrusions, Western Canada Range, Oregon. Journal of Geophysical Research 76, 7855-7872

---- 1974. Oxygen and hydrogen isotope evidence for large scale interaction between ground waters and igneous intrusions with particular interest to the San Juan volcanic field, Colorado, in Geochemical Transport and Kinetics, Carnegie Institute of Washington. Publication 634, p299

---- 1977. Water/rock interactions and the origin of H2O in granitic batholiths. Journal of Geological Science 133, p509

---- 1978. Oxygen and hydrogen isotope studies of plutonic granitic rocks. Earth and Planetary Science Letters 38, 177-210

---- 1980. The effects of assimilation of country rocks by magmas on 18O/16O and 87Sr/86Sr systematics in igneous rocks. Earth and Planetary Science Letters 47, 243-254

---- & Epstein, S., 1962. Relationship between 18O/16O ratios in coexisting minerals of igneous and metamorphic rocks. Geological Society of America Bulletin 73, 675-694

---- & Epstein, S., 1963. 18O/16O ratios in rocks and coexisting minerals of the Skaergaard Intrusion, East Greenland. Journal of Petrology 4, 51-74

Thompson, R. N., Morrison, M. A., Mattey, D. P., Dickin, A. P., & Moorbath, S., 1980. An assessment of the Th-Hf-Ta diagram as a discriminant for tectonomagmatic classifications and in the deyection of crustal contamination of magmas. Earth and Planetary Science Letters 50, 1-10

---- Dickin, A. P., Gibson, I. L., & Morrison, M. A., 1982. Elemental fingerprints of isotopic contamination of Hebridean Palaeocene mantle-derived magmas by Archaean sial. Contributions to Mineralogy and Petrology 79, 159-168

Vollmer, R., 1976. Rb-Sr and U-Th-Pb systematics of alkaline rocks: the alkaline rocks from Italy. Geochimica et Cosmochimica Acta 40, 283-295

Wood, D. A., 1980. The application of a Th-Hf-Ta diagram to problems of tectonomagmatic classification and to establishing the nature of crustal contamination of basaltic lavas of the British Tertiary Volcanic Province. Earth and Planetary Science Letters 50, 11-30

---- Joron, J-L., & Trevil, M., 1979. A re-appraisal of the use of trace elements to classify and discriminate between magma series erupted in different tectonic settings. Earth and Planetary Science Letters 45, 326 -336

York, D., 1969. Least squares fitting of a straight line with calculated errors. Earth and Planetary Science Letters 5, 320-324

This thesis is accepted on behalf of the faculty of the Institute by the following committee:

Philip K. Kyle

Adviser

David T. Norman

Glenn R. Osburn

Date

LATEAU

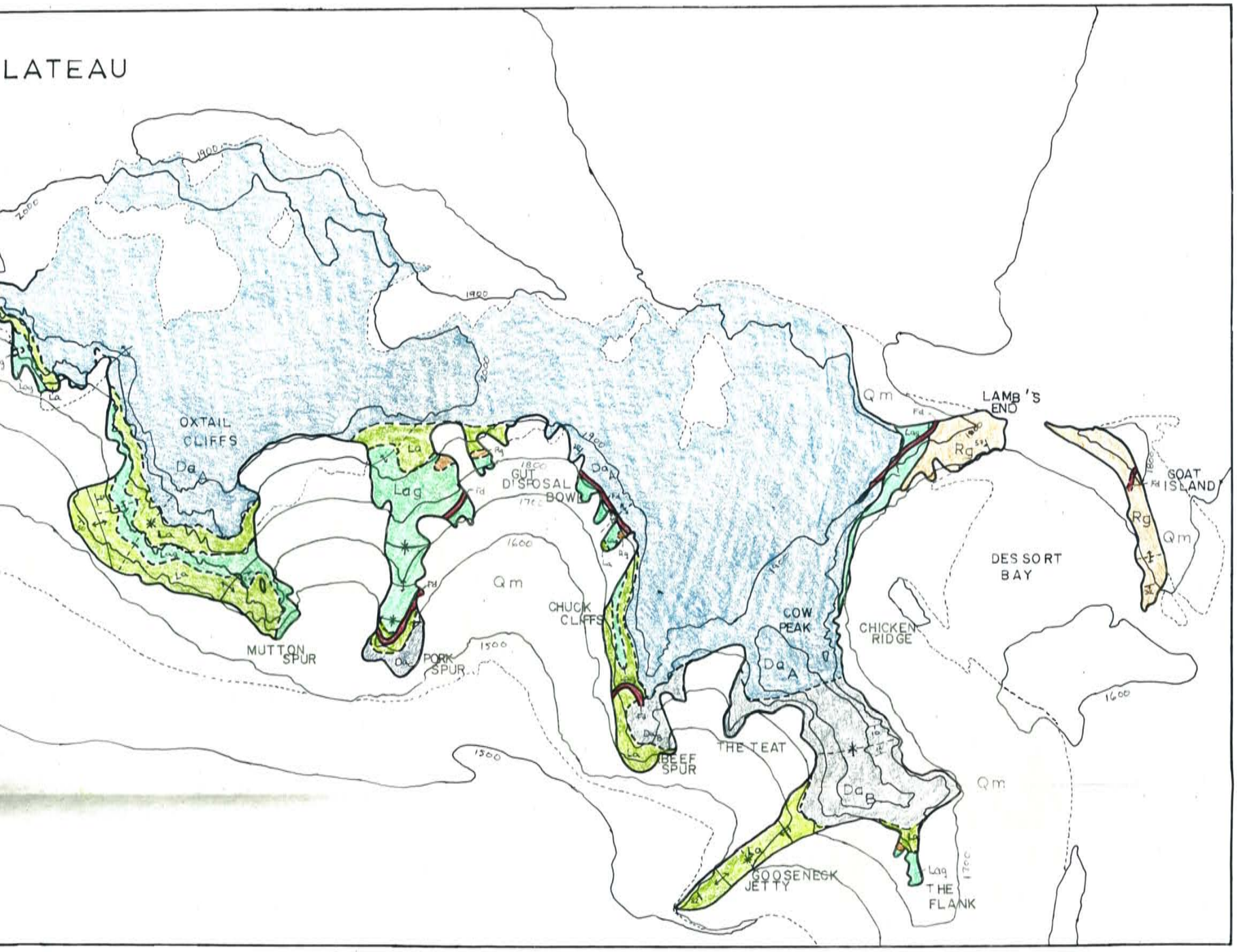

000

C.I.= 100 METERS

2 KILOMETERS

RIDGE IGNEOUS COMPLEX, ANTARCTICA

Shellhorn, and Philip R. Kyle

TION

STRUCTURAL FEATURES

Strike and dip of layering. Many are approximated

Contact; dashed where approximated

Anticlinal hinge. Dashed where approximated

Hinge of flexure. Arrow points towards steepening dip.

Synclinal hinge. Dashed where approximated

Snow, ice – rock contact

ure 5

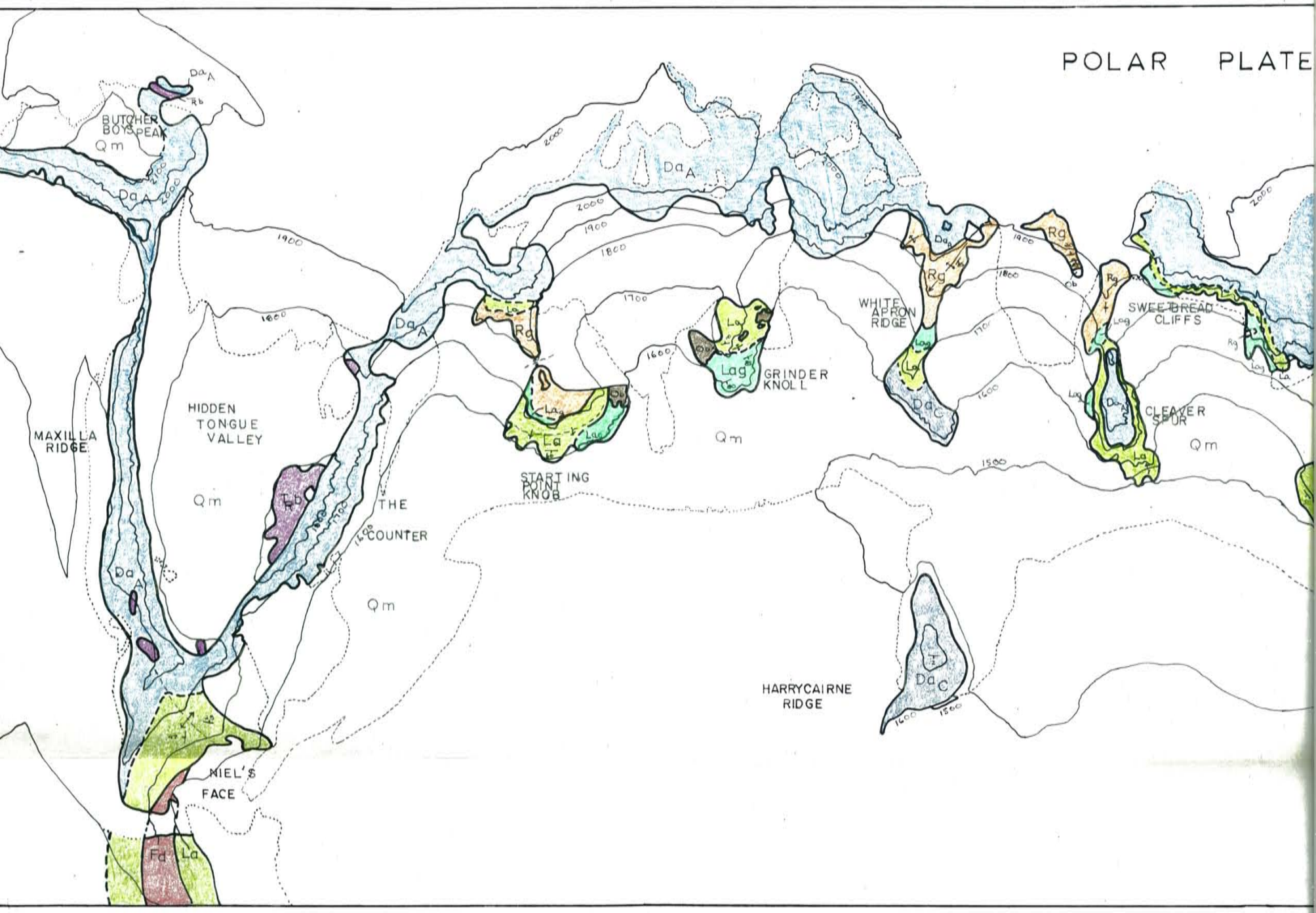

N

SCALE 1:5000

0 1

PRELIMINARY GEOLOGIC MAP OF THE BUTCHER RIDGE

By

Stephen Marshak, William C. McIntosh, Mark Shellhorn,

1980

EXPLANATION

GEOLOGIC UNITS

Qm	Undiffentiated overburden; moraine, ice-cored moraine, and talus.	Lag	Layered andesite with glass. Crystalline layers are 2-3 meters thick. Glass layers 0.3-0.5 thick have sharp contacts.
Fd	Fine-medium grained Ferrar Dolerite as cross cutting dikes and sills.	Rg	Layered rhyolite with glass. Glass layers are usually bordered by light weathering devitrified zones.
Da_A	Diffusely layered to massive andesite or dacite. Layered units are usually 2-3 meters thick.	Ob	Black glass or pitchstone. Locally bodies are cryptically layered.
Da_B	Diffusely layered andesite. Layering is lighter in color and more distinct than Da_A.	Da_C	Diffusely layered andesite. Possible basal unit of La.
La	Layered andesite. Layers are of equivalent thickness with the darker layers defined by concentrations of glass.	Rb	Xenoliths and rafts of Beacon Supergroup sandstone, shale, and coal.

Strike
are a

Antic
appr

Syncl
appr

Figure 5

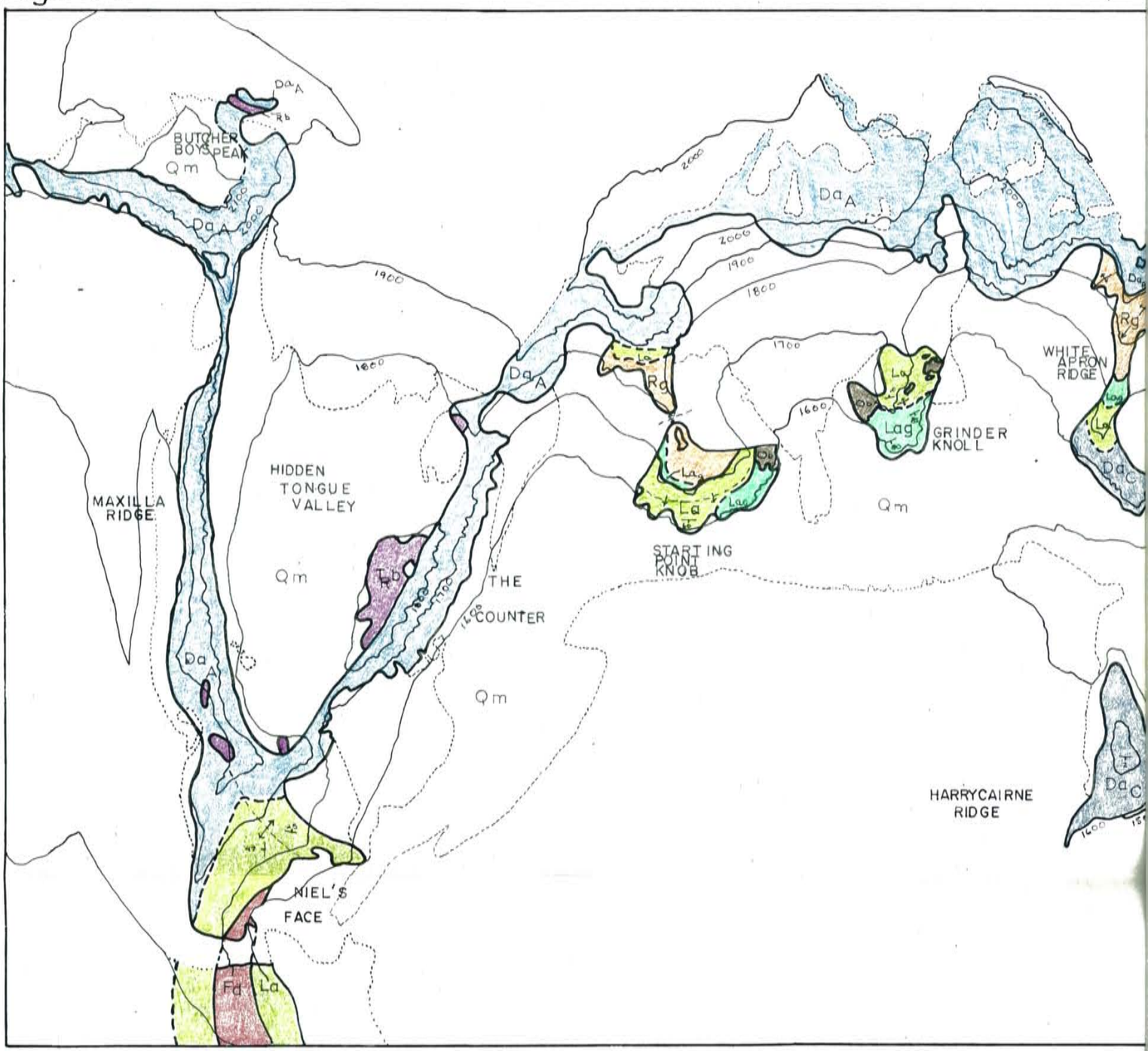

PRELIMINARY GEOLOGIC M

Stephen

GEOLOGIC UNITS

Qm	Undiffentiated overburden; moraine, ice-cored moraine, and talus.	Lag	Layered a layers are 0.3-0.5 thic
Fd	Fine-medium grained Ferrar Dolerite as cross cutting dikes and sills.	Rg	Layered r are usual ing devit
Da_A	Diffusely layered to massive andesite or dacite. Layered units are usually 2-3 meters thick.	Ob	Black glas are crypti
Da_B	Diffusely layered andesite. Layering is lighter in color and more distinct than $Da_{A'}$	Da_C	Diffusely basal uni
La	Layered andesite. Layers are of equivalent thickness with the darker layers defined by concentrations of glass.	Rb	Xenoliths group san